FINAL REPORT

RDU 140319

IMPROVEMENT OF DISPERSION OF DIFFERENT CARBON NANOTUBES (CNTS) IN LIQUID POLYMER RESIN FOR COMPOSITES

MOHAMMAD DALOUR HOSSEN BEG
PROFESSOR DATO DR. ROSLI MOHD YUNUS
DR. BIJARIMI BIN MAT PIAH

FACULTY OF CHEMCIAL AND NATURAL RESOURCES ENGINEERING, UMP

2017

ABSTRACT

This research presents a non-destructive modification of multi-walled carbon nanotube (MWCNT) and fabrication of MWCNT reinforced unsaturated polyester resin (UPR) nanocomposite. In this work, pre-dispersion of MWCNTs was performed in the tetra hydro furan (THF) solvent. In addition, pre-dispersion and post- dispersion time was optimized as 1.5 hour and 2 hour, respectively. The pre-dispersed MWCNT reinforced UPR (THF-MWCNT-UPR) nanocomposite exhibited better properties as compared to directly dispersed MWCNT reinforced UPR (MWCNT-UPR) nanocomposite. The optimum amount of MWCNT was evaluated through mechanical properties of nanocomposites contained 0.05 to 0.5 wt% MWCNT. The experimental tensile modulus (TM) of 0.3 wt% MWCNT reinforced 0.3CNT-UPR nanocomposite linearly fitted with Halpin –Tsai equation. Therefore, 0.3 wt% MWCNT was suggested as the optimum quantity. The nondefect modification of MWCNT was carried out with hyper branched polyester (HBP) and shellac (SL) functional polymers. The structural and thermal properties of 10 wt% HBP and SL coated HBCNT and SLCNT was noticeably improved as compared to pristine MWCNT. Moreover, 10 wt% HBP and SL coated HBCNT and SLCNT nanotubes remarkably reduced the curing temperature of nanosuspensions. Therefore, 10 wt% was considered as the optimum amount of HBP and SL to modify MWCNT. Optimum HBP coated MWCNT incorporated (OHBPCNT-UPR) nanocomposite became stiff. Conversely, optimum SL coated MWCNT incorporated (OSLCNT-UPR) nanocomposite became tough as compared to MWCNT reinforced nanocomposite. Different ratios of HBCNT and hydroxyl (OH) functionalized MWCNT (OHCNT) were incorporated in UPR to fabricate hybrid (HBOHCNT-UPR) nanocomposites. The ratio of HBCNT and OHCNT was optimized as 2:1 through the curing behavior of hybrid nanosuspensions. The comparative study was carried out among non-covalent and covalent functionalized as well as hybrid MWCNT reinforced UPR nanocomposites. Hybrid MWCNT incorporated nanosuspension exhibited the lowest curing temperature as compared to non-covalent and covalent functionalized MWCNT incorporated nanosuspensions. The hybrid nanocomposite exhibited the highest stiffness among nanocomposites which was individually fabricated with HBCNT and OHCNT. The mixture of non-covalent functionalized and covalent functionalized MWCNT jointly reinforced the properties of UPR. From this research 5 journal and 3 conference papers has been published.

TABLE OF CONTENTS

CHAPTER 1

INTRODUCTION

1.1 BACKGROUND

Polyesters (PEs) are one of the most versatile synthetic copolymers. They are hetero chain macromolecules that possess carboxylate ester groups as an integral component of their polymer backbones. PEs are extensively used as fibres, plastics, composites and for coatings applications as well (Goodman and Rhys, 1965; Goodman, 1968; Morgan, 1965; Wen et al., 2011; Albdiry and Yousif, 2013).

Unsaturated polyester resins (UPRs) are more readily processable than metals and ceramics. They are widely used as thermosetting resins in various sectors. Usually, UPRs are solidified with cross-linking agents to produce cross-linked UPRs, which have limited structural reliability for engineering applications. Therefore, they are frequently reinforced with macro, micro and nanofillers to boost up their desired properties. Successful incorporation of fillers in UPR composite has enabled new combinations of mechanical, electrical, magnetic, optical, chemical and surface properties. As a result, they are found in wide applications in the arena of construction, marine, automotive, aerospace, packaging, electronics, information, pharmaceuticals, biomedical, energy, sports goods and personal care sectors (Genhua et al., 2004; Gojny et al., 2005; Marco et al. 2011; Wen et al., 2011; Albdiry and Yousif, 2013).

At the beginning, blending of different polymers was conducted to fabricate composite materials for unique properties. However, blending lead to marginal improvement in properties which were not suitable as engineering materials. Therefore to improve the strength and stiffness of polymer materials different kinds of organic and inorganic silicate, carbon and metal compound were blended as filler with polymer matrix (Barrau et al. 2003). Moreover to achieve desired mechanical and other properties, it was necessary to load high amount of filler which increase cost and

processing become difficult. Therefore, currently nanofillers are very popular to get high mechanical as well as other properties at lower concentration of filler. The nanofiller reinforced polymer matrix is known as polymer nanocomposite (Bellayer et al., 2005).

Polymer nanocomposite is a new arena of composite materials, which is receiving significant attention both in academia and industry. The nano filler can provide ultra-large interfacial area per volume between the nano-element and polymer matrix. As a result, the reinforced composites exhibited superior toughness without giving up stiffness or optical clarity. It also possesses greater thermal and oxidative stability, better barrier, mechanical properties and self-extinguishing behavior as unique properties. Carbon nanotubes (CNTs) are emerged as the most promising nanofiller for polymer nanocomposites because of their outstanding properties compared to other fillers. The fantastic properties of individual CNT make an ideal reinforcing agent in the arena of polymer nanocomposites (Iijima, 1991; Kayatin and Davis, 2009; Spitalsky et al., 2010).

Besides, CNT is geometrically distinctive due to its structure as well as surface area which provides vast opportunity for interaction with any continuous phase (Gojny et al., 2004). Moreover, a small amount of CNTs with sound dispersion in polymer matrix exhibits abundant enhancement of different properties (Kota et al., 2007). Therefore, incorporation of carbon nanotubes (CNTs) is an attractive alternative filler to reinforce polymer matrix.

However, CNT reinforced nanocomposite properties are dependent on the degree of dispersion, interfacial adhesion with matrix in the composite system (Singh et al. 2013). The curing process of filler incorporated UPR is delayed due to free radical scavenging nature of carbon nano materials (Monti et al., 20011). Additionally several phenomena limit the promising application of CNT in nano composite technology. For instance, the main drawbacks of CNT are dispersion and compatibility with polymer matrices, their morphology and Van der Waal's forces are aggregated them into bundles as like as ropes which are stabilized by numerous $\pi-\pi$ interactions (Gryshchuk et al., 2006). Moreover, not only potential energy but also the aspect ratio and flexibilities of

CNTs are responsible for their entanglements as a consequence difficult to separate into individual nanotube (Breton et al., 2004; Quanxiang et al., 2014). Therefore they are restricted to homogeneous dispersion in polymer matrix.

Extensive effort has been applied to break the nanotube bundles for using individual nanotube as potential reinforcing filler. For this reason, destructive and nondestructive modification techniques are employed to overcome these drawbacks. Nondestructive technique such as non-covalent functionalization attracts attention to modify the nanotube side wall without any defect which can be carried out by physical and chemical methods (Chen et al., 2001; Britz and Khlobystov, 2006; Nanda Gopal Sahoo et al., 2010). Physical method involves shear mixing of CNTs in matrix. These have been carried out at room temperature with different non hydrogen bonding Lewis base solvents to take away the nanotube surface interaction (Ausman et al. 2000; Lau et al., 2005; Liu and Choi, 2012).

Chemical methods are carried out by action of surfactants, surface modification and polymer wrapping technology (Barber et al. 2003; Myung et al. 2012, Kim et al., 2012). This modification can be carried out with synthetic and natural polymers which contain functional end groups (Xu et al., 2004; Singh et al., 2004; Pan et al., 2009; Soradech et al., 2013).

Multi functional hyper branched polyesters are emerged as incredible Dendron for functionalization of CNT. Hyper branched polymers are highly branched macromolecules with three-dimensional dendritic architecture. Because of their high solubility, and abundance of functional groups, hyper branched polymers have potential applications in wide range of fields from drug delivery to material coatings (Bifeng Pan et al., 2009; Caminade and Majoral, 2010; Siqueira Jr et al., 2012). Besides the large number of reactive end-groups of hyperbranched polymer capable for rapid cross-linking, therefore, they are potential to design thermosetting network (Gao and Yan 2004; Voit 2005; Carlmark et al., 2009).

Wide ranges of naturally occurring polymers derived from renewable resources are available for various material applications. They are potentially used in coatings,

gels, foams, films, thermoplastics and thermoset resins (Long Yu et al., 2006). Shellac is one of the thermosetting resin of animal origin secreted by the lac insect *Kerria lacca* . The resin is secreted as a covering for the insect larvae. It is a hard, tough, amorphous resin, which is nontoxic and produces films of good water resistance and exceptional gloss. Shellac is generally believed to be a physical mixture of two resins secreted simultaneously by the lac insect (*Kerria lacca*). These resins are composed of a number of aliphatic polyhydroxy acids present in the form of lactones, lactides and inter-esters. The major components of shellac include aleuritic acid, shellolic acid and jalaric acid. Besides, it contains waxiness, pigments and other water-soluble substances. Nonetheless, it has macromolecular like properties due to its extreme hydrogen bonding (Hagenmaier and Baker, 1993). It has been used as thermoplastics, adhesives, sealants, insulating materials, and coating materials in various fields such as industrial materials, medicine, and food ingredients due to its various unique properties such as thermoplasticity, oil resistibility, cohesiveness, and insulating ability along with its nonpoisonous nature. Shellac has been extensively used for water, gas, lipid and microbial spoilage protection to extend the shelf-life of products in food and agro industries (Hagenmaier and Baker, 1993; McGuire and Hagenmaier, 1996; Phan The et al., 2008; Valencia-Chamorro et al., 2009). It has also been used for the moisture protection of drugs, controlled drug delivery system and enteric coating for drugs and probiotics in the pharmaceutical industry (Limmatvapirat et al., 2004; Stummer et al., 2010; Soradech et al., 2013).

These studies reveal that shellac is a potential functional coating material. Researchers have used shellac to coat nanoparticles. In the case of coating application it serves desired purposes due to availability and easy processability, from this point of view it has been considering to coat MWCNT.

Among various CNTs, multi-walled carbon nanotubes (MWCNTs) are frequently incorporated with varieties of polymers as an important reinforcement to find superior properties of the resulting materials (Logakis et al., 2011; Hemmati et al., 2008; Ritter et al., 2010; Mina et al., 2010; Mina et al., 2014). However, there have been limited investigations on MWCNT reinforced UPR composites because of stated drawbacks (Battisti et al., 2009; Seyhan et al., 2007).

1.2 PROBLEM STATEMENT

The background study reveals that UPR is a popular thermosetting resin. Several types of research have done to overcome the drawbacks of UPR. Numerous researchers incorporated different types of filler to reinforce this matrix. To date, nanofillers are more attractive as compared to macro and micro fillers. Among nanofillers CNT attract attention to reinforce polymer matrix. However, in the case of CNT there are some limitations which discourage for fabrication of CNT- reinforced polymer nanocomposites. The specific problems are stated below:

- The mechanical properties of commercially available unsaturated polyester resin (UPR) are relatively weak. Due to these poor properties, UPR cannot be fully exploited in industrial applications. Therefore, carbon nanotubes are used as nanofillers to reinforce the UPR matrix for fabrication of nanocomposites. However, the potential reinforcing efficiency of these nanofillers is not achieved due to their inhomogeneous dispersion in the matrix if they are directly incorporated without modification. Generally, better dispersion of CNTs in polymer matrix reportedly results in improved mechanical and thermal properties of the polymer nanocomposites.
- There are no controls on the concentration of carbon nanotubes (CNT) and dispersion time for fabrication of CNT- reinforced polymer nanocomposites. Usually, lower content of CNT is dispersed more easily than higher concentration. However, the addition of lower content of CNT which does not provide desired mechanical properties in one hand and the addition of higher content gives rise to aggregate formation on the other, enabling poor dispersibility and hence resulting in the poor mechanical performance of the nanocomposites. As a result, optimization of CNT concentration and dispersion time in UPR is essential for the enhancement of mechanical properties.
- Shellac used as a coating material which contains carboxylic and hydroxyl functional groups. These functional groups can functionalize the nanomaterials

through adhering to the surface. However there are no attempts have been found to functionalize multi-walled carbon nanotube with shellac.

- Carbon based nanofillers delay the curing process of the unsaturated polyester resin due to scavenging behavior. This delay involves energy loss for fabrication of nanocomposites. To overcome this problem, modification of CNTs is necessary to investigate the effect of CNT modification on curing process.
- CNT dispersion is affected by van der Waals force which exists among CNTs and helps them to form CNT bundles. Different techniques are followed to reduce the van der Waals force and to improve sound dispersion in the matrix. The defect functionalization, as well as covalent functionalization of CNT is very common to improve the dispersion quality. However, defective CNT is not appropriate to improve mechanical and other properties of CNT- based UPR nanocomposites.

1.3 OBJECTIVES

In the light of the aforesaid problems, this work has been undertaken to improve the dispersion of Multi-walled CNTs (MWCNTs) in UPR matrix by means of a method of solvent pre-dispersion. In this case, noncovalent functionalization of MWCNT has been performed with synthetic and natural functional polymers. The specific objectives of this work are:

(i) To improve dispersion of MWCNT in UPR matrix by using tetrahydrofuran (THF) as low-boiling point Lewis base solvent as a pre-dispersing agent.

(ii) To evaluate optimum sonication time and concentration of MWCNT for fabrication of MWCNT reinforced UPR nanocomposite.

(iii) To perform non-covalent functionalization of MWCNT with synthetic hyperbranched polyester (HBP) and natural shellac (SL) functional polymers and to evaluate the optimum concentration of those functional polymers.

1.4 SCOPE OF STUDY

(i) Dispersion of MWCNT at 0.5–1.5 hr sonication in Tetrahydrofuran (THF) as low-boiling point Lewis base solvent. Dispersion of MWCNT in UPR with mechanical stirring and ultra sonication technique at time 1–2 hr.

(ii) Optimization of different loaded MWCNTs (0.05–0.5 wt%). The optimum amount of MWCNT was evaluated by the application Halpin–Tsai model in observed mechanical properties of nanofiller loaded nanocomposites.

(iii) Non defect as well as Non covalent functionalization of MWCNT is performed with hyper branched polyester (HBP) and shellac (SL) functional polymers. Different amount (5–15 wt %) of these polymers were coated on the surface of MWCNT and then optimization of these polymers are performed.

1.5 SIGNIFICANCE OF STUDY

Solvent pre-dispersion method produces well dispersed MWCNT reinforced UPR nanocomposites. The properties of pre-dispersed MWCNT reinforced nanocomposites are greater compared to direct dispersed MWCNT reinforced nanocomposites. The thermal properties of noncovalent functionalized MWCNT are significantly improved as compared to pristine MWCNT. The curing performance, as well as structural properties of modified MWCNT incorporated nanocomposites, is also remarkably improved as compared to pristine MWCNT reinforced nanocomposite. HBP coated MWCNT increases the stiffness of nanocomposite whereas shellac cc MWCNT enhances the toughness of nanocomposite.

CHAPTER 2

LITERATURE REVIEW

2.1 INTRODUCTION

This chapter describes in detail on Carbon nano tube (CNT) reinforced polymer nanocomposites. Special emphasis is given on thermosetting polymer resins which were reinforced with different types of CNTs. In addition it briefly describes physics and chemistry of CNT. Moreover different dispersion methods of CNT have been reviewed here, special emphasis are given on ultra sonication as physical method, solvent and non covalent functionalization as chemical dispersion method. Reviews have been carried out on synthetic polymer and natural polymer as CNT coating materials. Finally multi walled carbon nanotube (MWCNT) reinforced different polymer nanocomposites thermo-mechanical properties, morphologies are represented in this literature.

2.2 UNSATURATED POLYESTER RESIN

Unsaturated polyester resins (UPRs) are short chain polyester containing polymerizable double bonds which are formed through condensation polymerization of saturated or unsaturated acids or acid anhydrides with difunctional alcohols or oxides. Generally UPR molecular weight range from 1,200-3,000 g/mol (Chanda and Roy, 1998). They are readily soluble in reactive styrene monomer because of their low crystallinity (Mona Malik et al., 2000).The styrene monomer serves as thinning agent for easy handling of viscose UPR, in addition to perform as a cross-linking agent between unsaturation sites on adjacent oligoimer chains. Therefore commercial resins contain styrene as high as 40% by weight. The organic peroxide or curing catalyst is added prior to the curing process. The Crosslinking reaction of UPR consists of a copolymerization of the vinyl monomer with the double bond of unsaturated polyester. During curing, a three-dimensional network is formed. Unsaturated polyester resins belong to the group of thermoset resins (Fink, 2005).

The difference between unsaturated polyester (UP) and unsaturated polyester resin (UPR) are as UP is the polyester as they emerge from the condensation vessel. It is rarely sold as such, because they are brittle at room temperature and difficult to handle. Whereas polyester is freshly synthesized in a plant, it is mixed with the vinyl monomer in the molten state. Thus materials those are viscous at room temperature, with an amount of styrene content. Such a mixture of unsaturated polyester with the vinyl monomer is referred to as an UPR.

At the manufacturing point of view, UPR is beneficial due to rapid crosslinking and cost effective. In addition, the thermal properties of UPR show better high-temperature performance as compared to epoxy resins. The continuous working temperature for an epoxy resin is typically 150°C or less whereas UPR shows heat deflection temperature as high as 205°C making it a better choice for high- temperature applications. Furthermore, the mechanical properties of UPR are generally not as encouraging as those of epoxy resins (Mallick, 1993). Additionally, the high cross-link density of UPR thermoset resins is generally hard and brittle as well as restraining their potential for load bearing applications. Therefore, the mechanical properties of UPR can be improved with filler as a composite material. Several researchers were incorporated different types of inorganic, organic and nanofiller to fabricate polyester composites (Mallick, 1993).

Generally, UPR is molded as compression and casting process. In addition, complex geometries can be molded by using resin transfer molding (RTM) which are allowed to cure before removal (Fried, 1995). In the state of molding, UPR is usually applied as a glass fiber (GF) reinforced composite (GFC). The high strength to weight ratio of GFC, microwave transparency, and corrosion resistance has led to use in many air transport applications (Chanda and Roy, 1998). The most familiar polyester composite goes by the trade name Fiberglas® (Owens Corning). Fiberglas® is a GFC material which became popular into 1940s and is widely used in the automotive, marine, construction, and aerospace industries. Fiberglas® found its way as an alternative to heavy porcelain shower stalls and bathtubs but made a memorable impact in the construction of automotive parts when in 1953 Chevrolet produced the first Corvette with a Fiberglas® body (Fried 1995; Leffingwell and Newhardt, 2002). The

consumption of UPR is double as compare to other thermoset resins which is stand as ranking 3rd among the thermoset polymers (Rodriguez et al., 2003).

2.3 UNSATURATED POLYESTER NANO COMPOSITES

In recent years, the development of nanocomposites has become an attractive new subject in materials science. They are consisted of two phases as like as traditional polymer composites which are fabricated by filler and matrix. A considerable number of researchers are demonstrating that nanoscopic dispersion of platelet-like structure in a polymer matrix results in remarkable enhancements in the strength, dimensional stability as well as resistance solvent, UV, flame and reduction in permeability to gases (Yu et al., 2000; Peigney et al., 2001; Li and Chou, 2003). Most notably, these properties improvement resulting from the fabrication of nanocomposite is taken place at extremely low concentration of nanofiller as compare to conventional filler material in a matrix. This "nano-size" yields a unique dependence on material properties and high surface areas which does not found in traditional composite systems (Thostenson et al., 2005). The enormously large surface area is available for interactions with a polymeric matrix coupled with high aspect ratio are mainly responsible for the observed enhancements. (Pinnavaia and Beall, 2000; Giannelis. 1995; Alexandre and Dubois, 2000; Byung-Wan Jo et al., 2008). For instance stiffness and fracture toughness of carbon nanotube-reinforced epoxy-composites was enhanced at low concentration of nanotube due to high aspect ratios and large interfacial surface area of multi-walled carbon (Gojny et al., 2004).

Recent studies reveal that UPR has been reinforced with different nano fillers to improve their properties (Oleksy and Galina, 2013; Albdiry and Yousif, 2013; Chirayil et al., 2014). The Wear resistance of UPR was improved by fabrication of hallo site nanotube reinforced nanocomposite. Surface morphology revealed a uniform dispersion of that nanotube in the UPR matrix (Albdiry and Yousif, 2013). Silsesquioxanes (POSS) modified bentonite improved the thermo-mechanical properties of UPR resin which provides unique properties including improved flame resistance and thermal stability of composite material (Oleksy and Galina, 2013; Yei et al., 2004). Plant based nano fibrils were incorporated in UPR matrix by simple mechanical stirring. The nano

fibril reinforced nanocomposite exhibited excellent mechanical properties due to high aspect ratio as well as formation of network structure with matrix. In addition, the interaction was developed between filler surface and matrix through strong hydrogen bonding. As a result, the glass transition temperature (T_g) of UPR matrix was noticeably increased (Chirayil et al., 2014). Fabrication of UPR nanocomposite using different type of nanofiller depends on the processing technique. For instance, UPR and layered silicate nanocomposite properties were significantly dependent on the fabrication technique in spite of existing there chemical reactions and physical interactions. X-ray scattering and thermo-mechanical analyses revealed that the crosslinking density and glass transition temperature were depending on the mixing time. In conclusion styrene molecules as a crosslinking agent were dispersed homogeneously inside and outside of that silicate layers with adequate mixing time. Therefore, the degree of crosslinking of that nanocomposite became almost similar to the neat crosslink UPR (Suh et al., 2000; Kornamann et al., 1998).

2.4 CARBON NANOTUBE AS REINFORCING AGENT

Generally nanoparticles are considered as high potential fillers to improve different properties of polymer matrices. According to the applied type of filler, nanoparticles can influence the electrical and thermal conductivity of the final nanocomposite (Oberlin and Endo, 1976). Carbon nanotubes (CNTs) are the interesting candidates with potential unique properties. They demonstrated an extraordinarily high stiffness and strength , a diameter dependent specific surface area up to 1300 m^2/g and an aspect ratio in the range of several thousands (Yu et al., 2000; Peigney et al., 2001;Li and Chou, 2003). According to their graphitic structure, CNTs possess a high thermo-mechanical and electrical properties which can be either semiconducting or metal-like. These properties attract researchers as highly desirable reinforcing candidates to improve the properties of polymers.

The outstanding specific surface area of CNTs is larger than conventional reinforcement fibres. This distinctive feature leads to special challenges for proper dispersion, adequate interfacial bonding and CNT-structure-property relationship as well as nano-micro- mechanical mechanisms. In addition the surface area of nanotubes

can act as desirable interface for stress transfer. The specific surface area of CNTs is dependent on the diameter and the number of sidewalls. The strong attractive forces between the CNTs lead themselves to extreme agglomeration. SWCNT provides the maximum specific surface area (Peigney et al., 2001). In order to minimize the specific surface area CNTs are aggregated and bonded as aligned bundles which are known as nano-ropes. These ropes, consisting of ten to hundreds of individual tubes, are difficult to separate and infiltrate with matrix. Figure 2.1 represents the graphene sheet (a), single walled carbon nanotube (b), double walled carbon nanotube (c) and multi walled carbon nanotube (d)

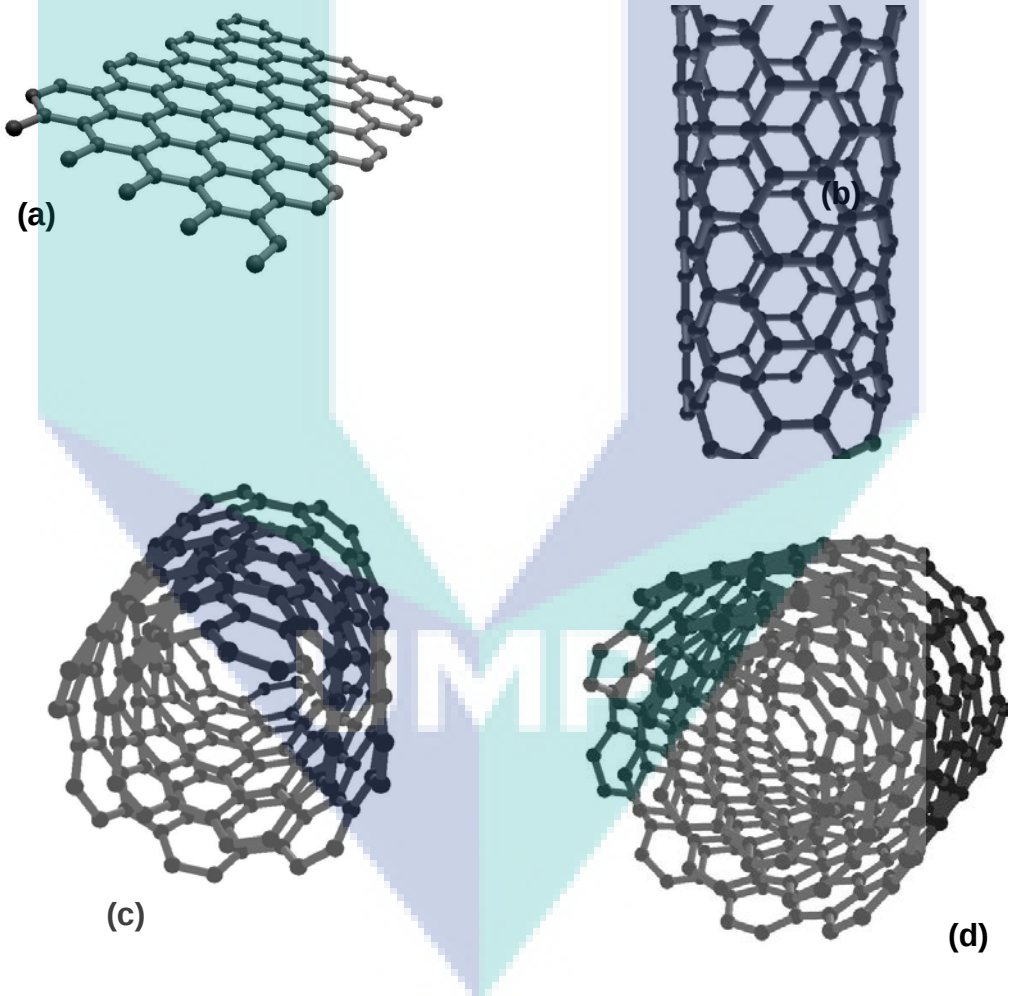

Figure 2.1: Grapheen Sheet (a), Single Walled Carbon Nanotube (b), Double Walled Carbon Nano Tube (c), Multi Walled Carbon Nano Tube (d)

On the contrary, MWCNTs have the lower aspect ratio as compare to SWCNTs. MWCNTs have a greater diameter and consisting of several concentric walls, which

provide smaller surface area as compare to SCNTs. Therefore, MWCNTs exhibit a much better dispersibility, but they provide smaller interface for stress transfer. Furthermore, the stress transfer between the concentric walls takes place via interlayer shearing to be transferred by van der Waals forces (Gojny et al., 2005).

Various methods are established to disperse nanotubes in polymer resins, such as stirring and sonication, have been reported as well known techniques in the literature. Most of these methods are either limited in capacity or not powerful enough to separate the agglomerates into individual nanotubes. One common technique to distribute CNTs in resin is the sonication technique (Gojny et al., 2005).

Development of interfacial adhesion between the CNTs and the matrix is essential. Sufficient stress transfer from the matrix to the nanotubes is required in order to efficiently utilize the potential of CNTs as structural reinforcement. The interfacial adhesion between the CNTs and the matrix can be improved by functionalizing of CNT-surface (Gojny et al., 2005).

A comprehensive knowledge is necessary about the quality of the CNTs to improve noticeable mechanical and physical properties of composite (Gojny et al., 2003; Allaoui et al., 2003). The nanotubes acquire variations of mechanical and physical properties according to the production methods, for instance chemical vapor deposition (CVD), electric arc-discharge method, laser ablation and other catalytic processes. There are many factors which influence those properties are defect-density and distribution (degree of graphitization), the curvature, the aspect ratio, the length and diameter distributions, the density and the purity. Moreover, one will find numerous variations in CNT length and diameter and a distribution of different chiralities in one batch as well. Bai et al. was fabricated nanocomposite with CVD-grown MWCNTs which was exhibited an increased elastic modulus, whereas the fracture strain was reduced due to the presence of agglomerates, leading to local defects enhancing early failure. Additionally a certain dependence of the mechanical behavior on the aggregate size could be found (Bai and Allaoui, 2003).

Finally, according to the research findings, currently CNT has been reinforced both thermoplastic and thermoset polymer matrices (Qian et al., 2000; Cooper et al., 2002; Safadi et al., 2002; Mina et al., 2014). Several researchers have been used CNT to reinforce polyester, epoxy, poly (methylmethacrylate) (PMMA), poly (vinyl alcohol), polypropylene, Polyethylene and poly (lactic) acid and so forth (Park et al., 2002; Biercuk et al., 2002; Cadek et al., 2004).

2.5 THERMAL ANALYSIS OF POLYMER NANOCOMPOSITES

The thermogravimetric analysis (TGA) reveals thermal stabilities of a material. The TGA and the derivative of thermogravimetric (DTG) thermograms of the MWCNTs are manifested dual weight losses in the DTG curve. The first DTG peak, appeared at lower temperature due to the degradation of the less stable amorphous carbon and the second weight loss peak appearing at higher temperature is attributable to the CNTs themselves stated elsewhere (Perez et al., 2009) . Additionally, Perez and coworkers have stated the thermal stability of CNTs-filled rubbers nanocomposites as a function of MWCNT content. The thermogram of MWCNT-styrene-butadiene rubber composite showed a single drop in the weight loss curve with the increasing temperature. Incorporation of nanotubes in the polymer matrix raises the onset of degradation as well as its maximum rate. The MWCNT- nitrilebutadiene rubber composites revealed dual drops in the weight loss curve. Moreover, the corresponding DTG thermograms showed two degradation peaks at low concentration of MWCNT. However, when the MWCNT content was increased only one degradation peak was detected in the thermograms of MWCNT- nitrilebutadiene nanocomposites (Perez et al., 2009).Therefore, MWCNT filler is capable to suppress thermal degradation of the elastomers may be attributed to barrier effects. For instance in case of clay fillers the pyrolysis rate declined due to the decrease of the polymer global mobility. It has shown that polymer chains confined in the mesoporous structures show greater thermal stabilities indeed (Perez et al., 2007).Thermogravimetric analysis of MWCNT incorporated polyvinyl butyral (PVB) composite a multi-stage decomposition was demonstrated, the decomposition temperature of this composite shifted toward a higher temperature as compared to matrix due to steric hindrance imposed on the thermal motion of the matrix chain segments (Alhazov and Zussman, 2012).

Differential scanning calorimetric (DSC) thermogram of polyurethane block polymers revealed dual melting endotherms. At low temperature ascribe due to dissociation of the urethane-soft segment hydrogen bonds whereas at high temperature endotherm is related to the breakup of inter-urethane hydrogen bonds and microcrystalline hard segments (Seymour and Cooper, 1973). Polyesters showed single, as well as multiple melting peaks. The multiple peaks originate in semi-crystalline polymers is due to several reasons. The study on the multiple melting peaks in Poly(ethylene succinate) (PES) have reported that the high temperature melting peak is primarily due to the melting of the re-crystallized crystals formed during the heating scan (Al-Raheil and Qudah, 1995; Qui et al., 2003). On the other hand low temperature melting peak is due to the melting of original crystals which forms during the initial crystallization process (Ichikawa et al., 2000; Gan et al., 2002).Similarly poly (butylenes succinate)(PBS) exhibits multiple melting peaks at lower and higher temperature (Yasuniwa and Satou, 2002). The appearance of a single melting peak in the thermograms of crystallized polyesters suggested melting of one type of crystal which is regarded as stable crystals (Rohindra et al., 2012).

Crystal formation includes nucleation and crystal growth. On the other hand, it is well established that nanometer-sized filler such as clay platelets are effective nucleating agents, different effects have been reported on the linear growth rate and the overall crystallization rate in nylon 1012 - clay nanocomposite (Wu et al., 2002). Di Maio and coauthors have studied the filler concentration effect on the crystallization of Poly caprolacton(PCL)-clay nanocomposites and mentioned that the dispersed clay platelets act as nucleating agents in the PCL matrix. Moreover they found a reduction of the melting temperature with the increase of clay content, demonstrating a reduced degree of crystals perfection and degree of crystallinity. This was attributed to the confinement of chains and segments in the presence of clay, hindering the segmental rearrangement during crystallization and restricting the formation of perfect crystals in the polymer matrix (Di Maio et al., 2004). In the case of montmorillonite clay reinforced polyethylene terpthalate (PET) nanocomposite, the glass transition temperature of composites decreased as compare to matrix due to plasticization effect of nanofiller, conversely at high concentration of filler glass transition temperature

increased again stated elsewhere (Ke and Yongping, 2005). Therefore, differential scanning calorimetry (DSC) provides information concerning intercalation. The many interactions the intercalated chains of the polymer form with the matrix greatly reduce their rotational and translational mobility. The situation is similar to that in a reticulated polymer, where restrictions on its mobility increase its glass transition temperature (T_g). A similar increase is anticipated to occur in a nanocomposite due to the elevation of the energy threshold needed for the transition. This effect is readily detected by DSC (Pavlidou and Papaspyrides, 2008).

2.6 DENDRITIC POLYMERS AND CARBON NANOTUBES

Functionalization of carbon nanotubes with dendrimers or dendrons can be either covalent or non covalent interaction. This type of functionalized CNT has led to use in various fields, such as biosensors and biology (Tomalia et al., 1985).

Dendritic polymers including dendrimers and hyper branched polymers (HBPs) are recognized as a fourth major class of macromolecular architecture. They are highly branched globular; according to their degree of structural control dendritic polymers are categories as (i) random hyper branched polymers, (ii) dendrigraft polymers and (iii) dendrimers (Fr´echet et al., 2001).

Hyper branched polymer (HBP) is a highly branched macromolecule with a large number of functional groups which can be prepared through a one-step polymerization process (Gao and Yan, 2004; Scholl et al., 2009). The structre of HBP is presented in Figure 2.2. The interest in HBP is growing rapidly due to their distinctive physical and chemical properties. They are potentially used in the arena of material coating, polymer additives, drug delivery, nanotechnology and supramolecular science (Daohong Zhang et al., 2011; Guo et al., 2009). HBP which contain unsaturation and epoxy groups has been successfully used in UV-cured flame retardant coatings and as additive for toughening and reinforcing thermosetting resin respectively (Huang and Shi,2007; Zhang et al., 2011). In addition, via free-radical copolymerization of HBP has also been applied as intermediate in the preparation of functionalized macro porous polymers (Daviset al., 1996). Moreover, huge number of end-groups in hyper branched

polymer has a great capacity for rapid crosslinking even at moderate molecular weights (Voit, 2005).

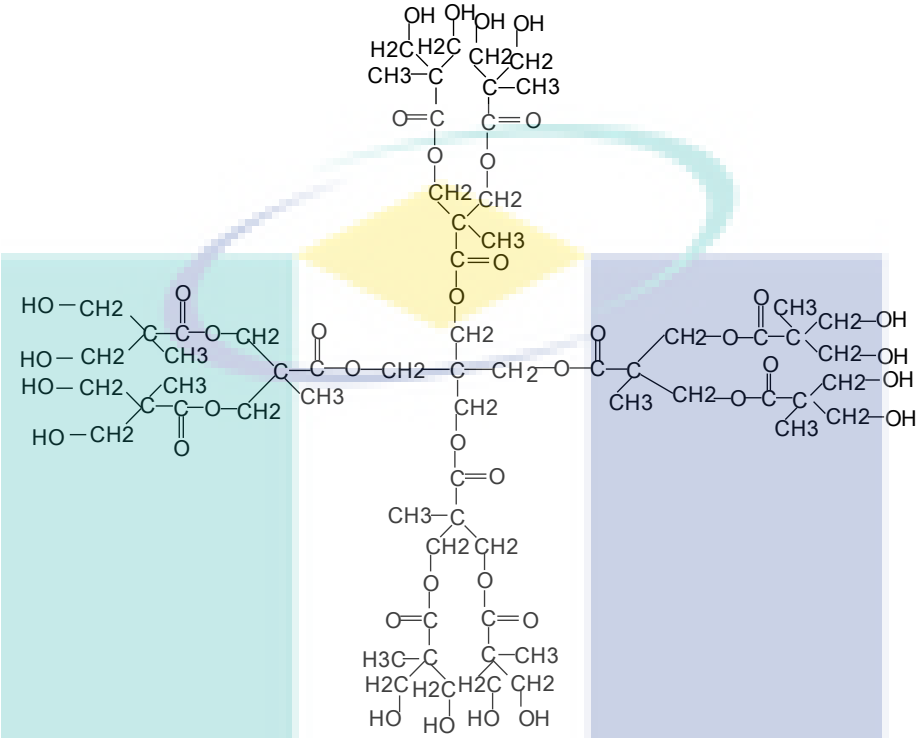

Figure 2. 2: Chemical structure of hyperbranched polymer (HBP)

Dendrigraft polymers may be regarded as semi-controlled branched polymer architectures intermediate in terms of structure control between dendrimers and hyper branched polymers (Teertstra and Gauthier, 2004).

Typically dendrimers is a special type of highly uniform, three dimensional, mono disperse polymer with a tree-like globular structure and consist a large number of functional groups. It consists of three distinct areas: the poly functional central core (dendrimer) or focal point (dendron), which represents the center of symmetry, various well-defined radial-symmetrical layers of repeating units known as generations. The end-standing groups are termed as peripheral or terminal groups as well (Matthias Seiler, 2006). They are synthesized by step-by-step, usually radially from a central core. Each level of branching units creates a new generation. They are different from all other types of polymers, because they are synthesized such a manner which control their whole architecture, a nano metric size, and a high level of mono disparity. Most of the

properties of dendrimers are related to the nature of their numerous terminal groups that might be varied according to the desired properties. A Dendron is a dendritic wedge, having one functional group at the core, and several functional terminal groups.

Several researchers reported that dendritic wedges are covalently or non-covalently attached with CNTs to induce dispersion quality (Hirsch and Vostrowsky, 2001; Davis et al., 2003). Particularly fullerodendron was attached on the side wall of CNT through non covalent interaction which has been induced the dispersion of CNT in solvent reported elsewhere (Takaguchi et al., 2005). Optical absorption spectroscopy and scanning electron microscopy (SEM) measurements provide evidence for well-dispersed CNTs via formation of fullerodendron-functionalized SWNTs. Additionally, in order to favor non-covalent interactions, hydrophobic functions such as conjugated aromatic groups appear as the most suitable. Generally poly(amidoamine) (PAMAM) dendron bearing anthracene as core and a generation 3 PAMAM dendrimer bearing naphthalene diimide terminal groups were able to strongly interact with CNTs (Sandanayaka et al., 2006; Valentini et al., 2006; Caminade and Majoral, 2010).

Therefore limited number of HBPs was used for wrapping the CNT. In addition, there is no literature available about 2-2-bis (methylol) propionic acid, generation 2 as hyper branched polyester (HBP) was used as MWCNT coating polymer. Moreover HBP coated MWCNT reinforced UPR nanocomposite did not fabricate elsewhere.

2.7 SHELLAC AS POLYMER COATING MATERIALS

There are numerous reasons for coating on materials. Usually coating is applied on materials to improve their mechanical stability and reduce abrasion of materials during manufacturing, shipping and storage (Okhamafe et al., 1986; Fell et al., 1979) Additionally materials are coated to protect them from light or humidity (Swarbrick et al., 1972). Moreover polymeric coatings can be applied on solid materials for decorative purposes to provide gloss (Porter and Felton, 2010). Furthermore it has become a routine process in the production of solid materials.

For each desired application a variety of different coating materials with specially made physicochemical properties is available. Most commonly used polymers are poly-acrylates, cellulose esters and ethers (Signorino et al., 2005; Edgar, 2005; Kokubo et al., 1997). Polyacrylates are synthetic polymers which are obtained by emulsion polymerization (Mast et al., 1945). Whereas cellulose derivatives are semi synthetic polymers gained either by esterification or etherification of natural cellulose. Degree of substitution and types of substituent represents the properties of the final polymer. Besides these coating polymers, there are few other materials used for coating applications. One of them is shellac.

2.8 MWCNT REINFORCED POLYMER NANOCOMPOSITES

The expansion of CNT/polymer nanocomposites opens new perspectives for multi-functional materials, such as conductive polymers with improved mechanical performance and with a perspective of damage sensing and ‘‘life’’-monitoring. In order to efficiently utilize the potential of CNTs to improve the mechanical performance of polymers, one has to be aware of aggravated challenges when comparing with conventional micro-scaled filler particles.

In recent times, the use of multi-walled carbon nanotube (MWCNT) as the filler in the polymer matrix is attractive due to its outstanding properties. Those properties have generated scientific and technical interest in the development of nanotube-reinforced polymer nanocomposites. Carbon nanotubes reinforced polymer nanocomposites were fabricated using different purification and dispersion processes (Gojny et al., 2003; Sandler et al., 1999). A small amount of MWCNT can significantly improve the material properties. For instance a certain amount of MWCNT notably increased the tensile strength and modulus of rubber epoxy matrix stated by Allaoui et al., (2002) (Allaoui et al., 2002). Likewise Montazeri et al., (2010) were noticeably improved the tensile strength and tensile modulus of MWCNT incorporated Epoxy nanocomposite by using only 0.5 wt% of MWCNT (Montazeri et al., 2010).

However, at the beginning of nanocomposite fabrication, the pure MWCNT did not reinforce the matrix due to lack of proper interaction between them; consequently

mechanical properties decreased significantly which has been reported by Lau and Shi as well (Lau and Shi, 2002). Likewise Yeh et al.,(2006) investigated the effect of MWCNT aspect ratio (*l*/d) on the mechanical properties of nanocomposite. They showed that the mechanical properties of nanocomposite with the higher aspect ratio (*l*/d) were better than the ones with the lower aspect ratio (Yeh et al., 2006).

In order to utilize nanotubes in multi-functional material systems, it is crucial to develop processing techniques that are amenable to scale-up for high volume, high rate production. Beside numerous researchers have been published different model equations to evaluate the optimum content of nano fillers in the polymer matrix.

Several models were proposed to evaluate the mechanical properties of the composites as a function of the volume fraction of the reinforcement. Most of these models were considered a homogeneous dispersion of the nanotubes in the matrix. However, it is frequently difficult to get a homogenous dispersion of CNT (Cox, 1952; Ogasawara et al., 2004). Therefore, Cox considered an orientation factor to take account of the randomness of the discontinuous fibers in composites (Cox 1952). Likewise, Bai used the orientation factor in the rule of mixture to find the randomly oriented CNTs in polymer matrix (Bai, 2003). Additionally, the in-plane randomly-oriented discontinuous fiber lamina model used for multi-walled carbon nanotube-phenylethynyl terminated polyimide composites (Ogasawara et al., 2004). The in-plane randomly oriented discontinuous fiber lamina model, and the Halpin–Tsai equation have also been used the experimental data (Gojny et al., 2004; Breton et al., 2004). The modified Cox model was used to study the mechanical properties of carbon nanofiber reinforced poly(methyl methacrylate) nano composites (Zeng et al., 2004). The Mori–Tanaka method was applied to calculate the modulus of nanocomposites which was fabricated with epoxy matrix and silicate clay particles. The model predictions were in well agreement with experimental results and the Halpin–Tsai equation were used to fit the experimental results (Luo and Daniel, 2003; Fornes and Paul, 2003). The modified Halpin–Tsai equation were suggested by Fornes and Paul to evaluate the optimum amount of nano clay in nylon 6-clay nanocomposites (Fornes and Paul, 2003). Yeh et al., (2006) have studied the mechanical behavior of MWCNT incorporated phenolic-based nanocomposites which were fabricated with different contents of MWNTs.The

modified Halpin–Tsai equation with orientation factor was fitted the experimental data successfully for evaluation of the optimum amount of MWCNT in the nanocomposite(Yeh et al., 2006). Montazeri et al.,(2010) were used orientation factor to modify Halpin-Tsai equation for optimization of MWCNT content in MWCNT-epoxy nanocomposites (Montazeri et al.,2010; Ayatollahi et al., 2011). In addition, they considered orientation factors, the effect of the filler aspect ratio into their expression. Moreover, they took into account the effect of nanotube discontinuity in composite sample. Montazeri and his co-researchers evaluated the mechanical properties of optimum amount of MWCNT reinforced epoxy nanocomposites system by using modified Halpin-Tsai equation. They incorporated different amount of MWCNT in that matrix by sonication technique. Halpin–Tasi equation was used to evaluate the optimum amount of MWCNT by using tensile modulus and tensile strength of those MWNT-epoxy nanocomposites and a good correlation between experimental data and the modified Halpin–Tsai theory was established (Montazeri et al., 2010). Therefore, modified Halpin-Tsai model can asses the optimum amount of randomly oriented nanoreinforcements in nanocomposites for getting maximum mechanical properties (Tai et al., 2008).

Ayatollahi et al., (2011) reported the effects of multi-walled carbon nanotubes (MWCNTs) concentration on the mechanical properties of epoxy/MWCNT nano-composites. They were emphasized on fracture toughness under bending and shear loading conditions. They found that the presence of MWCNTs had a greater effect on fracture toughness of nano-composites under shear loading compared with normal loading. The fracture mechanisms were studied with several scanning electron microscopy (SEM) pictures of fracture surfaces. They found a noticeable correlation between the characteristics of fracture surface and the mechanical behaviors. Generally the mechanical properties of polymers are supposed to be improved by incorporation of CNTs. The mechanical properties of the pure epoxy and the nano-composites are exhibited as higher filler loading resulted in higher Young's modulus of nano-composite. The modulus was increased with increasing the amount of MWCNT has been reported elsewhere as well (Montazeri et al., 2010; Yeh et al., 2006). They employed Halpin–Tsai theory to compare the results obtained for the Young's modulus with theoretical estimations (Mallick, 2008). According to this theory, the maximum

obtainable tensile modulus for a composite with a perfect distribution and impregnation with polymer is given by following equation,

$$E_c = \left(\frac{3}{8}\frac{1+2\left(\frac{l_f}{d_f}\right)\eta_l V_f}{1-\eta_l V_f} + \frac{5}{8}\frac{1+2\eta_T V_f}{1-\eta_T V_f}\right)E_m \qquad (2.1)$$

in which

$$\eta_l = \frac{\frac{E_f}{E_m}-1}{\frac{E_f}{E_m}+2\left(\frac{l_f}{d_f}\right)}, \quad \eta_T = \frac{\frac{E_f}{E_m}-1}{\frac{E_f}{E_m}+2} \qquad 2.2$$

Where E_c is the tensile modulus of the composite, l_f is the length of MWCNTs, d is the average outer diameter of nanotube, E_{NT} is the tensile modulus of the nanotubes, E_m is the tensile modulus of the matrix and V_f is the volume content of MWCNTs. The tensile modulus of nano-composites calculated using Esq. (2.1) and (2.2). The calculated tensile modulus is in good agreement with the experimental value only at low concentration of MWCNTs which advocates a sound dispersion and interfacial strength between filler and matrix (Song and Youn, 2005; Bal, 2010). This theory assumes a uniform dispersion of the filler in the matrix and a flawless bonding.

Whereas with increasing the MWCNTs content, the difference between the theoretically predicted and experimentally obtained modulus increased, due to agglomeration of MWCNT within the nano-composite (Gojny, 2004). In addition, the mechanical properties of nanocomposite were decreased due to presence of voids which were generated during mixing of filler-matrix with the hardener. Furthermore, at higher concentration of MWCNTs the viscosity of the mixture increases; as a consequence degassing of suspension becomes more difficult. Similar correlation between the dispersion status and the mechanical properties stated elsewhere (Fraczek and Blazewicz, 2009). Besides the elongation at break of nano-composites decreases relative to that of pure matrix, indicating a ductile to brittle trend in nano-composite with increasing the filler content. The similar finding has been reported in case of multiwalled carbon nanotube (MWCNT)/polycarbonate nanocomposites. It is notable

that different flaws like voids and impurities can also reduce the elongation at break were stated elsewhere (Satapathy et al., 2007; Ayatollahi et al., 2011).

A scalable calendaring approach with intense shear mixing was employed for manufacturing of cost effective nanocomposite as well as to achieve well dispersion of MWCNT in epoxy matrix. Electron microscopy was utilized to study the micro and nanoscale structure during the manufacturing process and optimize the processing conditions for producing highly-dispersed nanocomposites. In the light of this observation, MWCNT- Epoxy nano composites were processed with different amount of reinforcement and the thermo-mechanical properties were evaluated. The nano scale structure of those nanocomposites was demonstrated to evaluate the effect of shear mixing on dispersion. The nanocomposites fabricated by this process exhibited significantly enhanced fracture toughness at low nanotube concentrations. The fracture surfaces of nanotube-reinforced composites showed enhanced surface roughness as well as nanotube pullout. Agglomerated carbon nanotubes appeared to interact more effectively with the crack front and resulted in slightly higher overall fracture toughness. The high aspect ratios of the CNT in the processed composites facilitated the formation of a conductive percolating network at concentrations below 0.1% by weight. The thermal conductivity increased linearly with nanotube concentration to a maximum increase of 60% at 5 wt. % carbon nanotubes (Thostenson and Chou, 2006).

CHAPTER 3

MATERIALS AND EXPERIMENTAL METHODS

3.1 INTRODUCTION

In this research, multi walled carbon nanotube (MWCNT) was used to produce reinforced unsaturated polyester resin (UPR) nanocomposite (CNT-UPR nanocomposite). In addition non-covalent functionalized MWCNT was prepared as a means of well dispersion in matrix and to improve the property of nanocomposites as well. Different analysis including thermo-mechanical properties of nanocomposites was performed to understand the nanocomposite behavior and identifies the possible ways in which performance might be improved.

This chapter describes in brief the materials, CNT treatment methods and characterization techniques, nanocomposite processing and testing methods.

3.2 MATERIALS

Orthopthalic unsaturated polyester resin (Polymal) (UPR) was used as matrix materials. Tetra-hydro furan (THF) solvent was used as pre-dispersion media. Methyl ethyl keton peroxide (MEKP) was used as curing initiator. Multi-walled carbon nanotubes (MWCNTs) and hydroxyl functionalized MWCNT (OHCNT) was used as reinforcing nanofiller.

Hyper branched polyester (HBP)(2-2-bis (methylol) propionic acid) generation 2 was used as functional polymer to non covalent functionalization of MWCNT. In addition the natural polymer shellac (SL) was used as coating material for non covalent functionalization of MWCNT. Figure 3.1shows the commercial grade shellac solution

in THF solvent. Additionally the specification and origin of these materials are represented in Table 3.1.

Table 3. 1: Materials name, specification and origin of materials

Name	Properties	Manufacturer	Country of Origin
Unsaturated Polyester Resin	❖ Viscosity 700-800mPa.S at 25^0C ❖ Volatile content is 30–35%, ❖ Gel time is 8−15 min.	Luxchem Polymer Industries Snd.Bhd.	Malaysia
Multi walled Carbon nanotubes	❖ Produced by moving-bed catalysis technique ❖ Diameter <8nm, length between 10−30 µm ❖ Carbon purity of 95%	Timesnano	China
Curing agent(Peroxides)	❖ Colorless liquid	Sigma Aldrich	USA
HBP	❖ molecular weight 1749.79g/mol ❖ contained 16 hydroxyl groups	Sigma Aldrich	USA.
Shellac	❖ Solid ❖ Polish grade ❖ Light chocolate color ❖ Order less		Bangladesh
Tetrahydrofuran and Acetone		Merk	Germany
Mold releasing agent	Paste and Cream	John Burn & Co. (B'ham) Ltd	England

3.3 METHODS

Figure 3.1 illustrates the overall methodology flow chart. The pre-dispersion of MWCNT was carried out in THF solvent at different sonication time using Elma 37kHz sonicator (made in German), having device power capacity of 320 W. THF pre-dispersed MWCNT (THF-MWCNT) was dispersed in UPR at different time using same sonicator. Different concentration (0.05-0.5wt%) of pre-dispersed MWCNT were incorporated in UPR matrix and optimization was performed through different analysis. Optimum amount of MWCNTs was modified with different concentration (5-15 wt% with respect to MWCNT weight) of hyper branched polymer (HBP) and shellac (SL). HBP and SL coated MWCNT were subjected for different analysis to evaluate the optimum amount of HBP and SL. HBP and SL modified MWCNT were incorporated in UPR to fabricate nanocomposites. Different ratio of HBP coated MWCNT and OH functionalized MWCNT blend together then incorporated in UPR to fabricate hybrid nanocomposites.

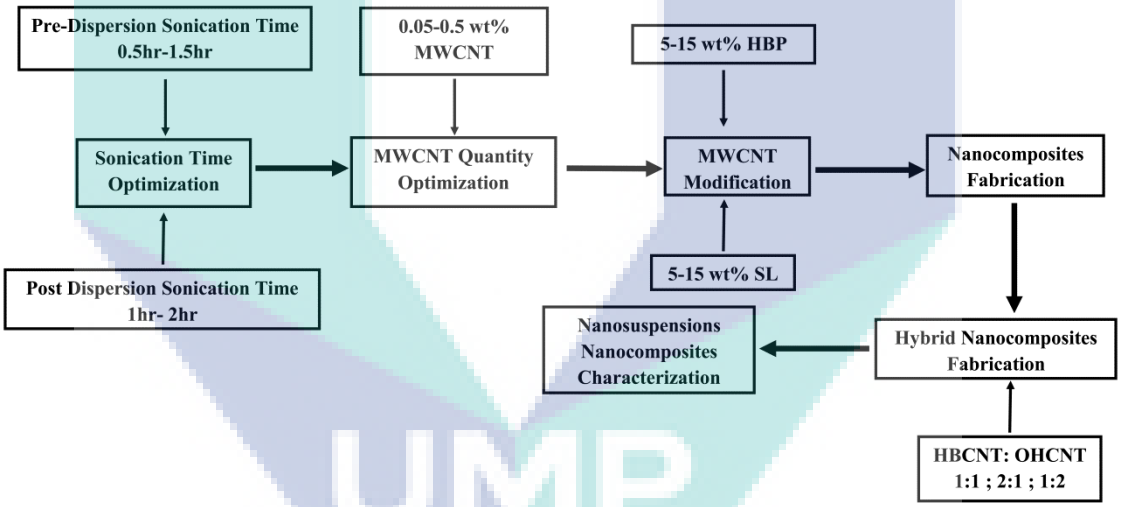

Figure 3.1: Overall methodology flow chart

3.3.1 Pre-Dispersion and Post Dispersion Time Optimization

MWCNT pre-dispersed suspensions were prepared in tetra hydro furan (THF) solvent. The ratio of MWCNTs and THF was 1:25. These suspensions were stirred by a magnetic stirrer for 15 minutes, followed by the sonication in an ultra-sound bath for 0.5, 1 and 1.5h as pre-dispersion time. The optimum pre-dispersion time was estimated

through physical sediment observation of nanosuspensions and scanning electron micrographs of MWCNT. Figure 3.2 (A) and (B) represents the pre-dispersion and post dispersion process flow chart respectively.

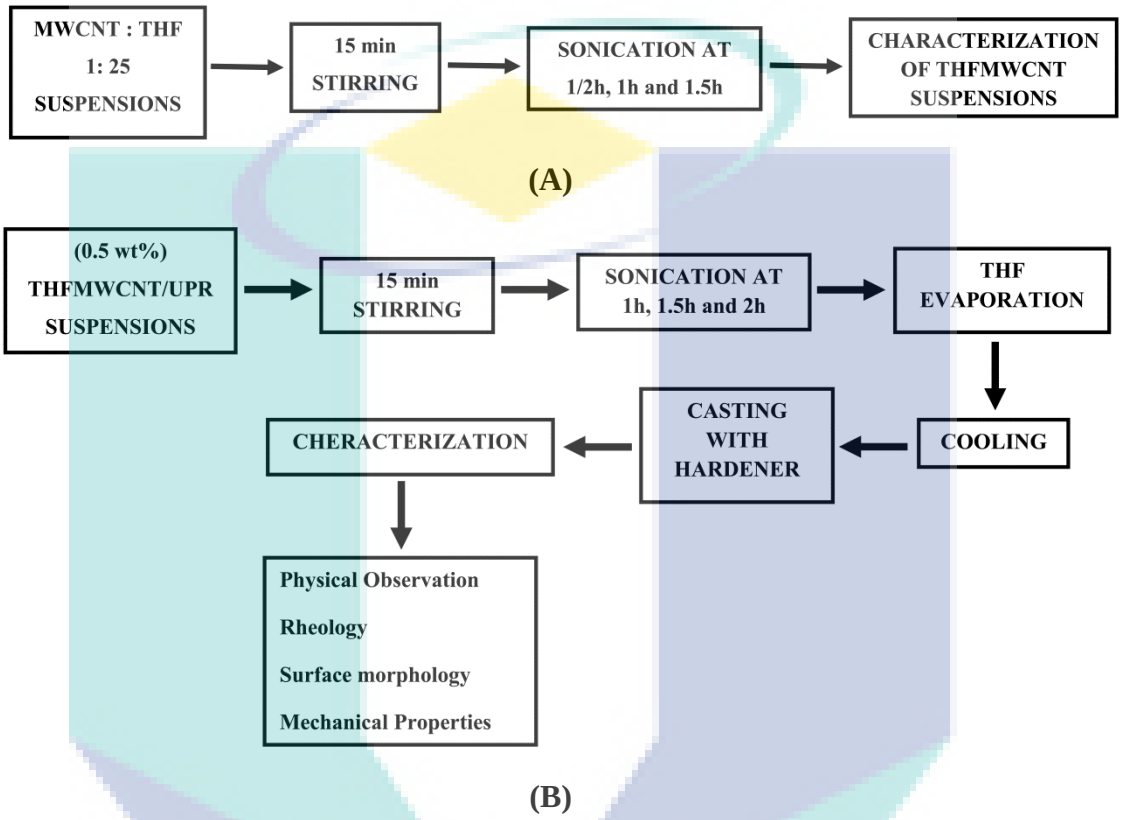

Figure 3.2: Pre-Dispersion (A) and Post Dispersion (B) Sonication Process Flow Chart

After that, pre-dispersed MWCNT (THF-MWCNT) was mixed with unsaturated polyester resin (UPR). There were three suspensions prepared, in addition to each suspension was contained 0.5wt% MWCNT with respect to UPR, these suspensions were stirred for 15 min and subsequently sonicated for 1h, 1.5h 2 h as post dispersion time. The MWCNT/UPR suspensions which contained THF as solvent were heated at around 5 minute to the boiling temperature (66^{o}C) of THF. The warm suspensions were placed in a cold water bath to cool them at room temperature. MEKP (1 wt %) was added to these suspensions as initiator and gently stirred for 3 minutes, then placed in vacuum to remove the bubbles. Finally, the bubble free mixture was poured on the

specimen mold and cured at room temperature. The post dispersion time was optimized by characterization of nano suspensions and nanocomposites.

Beside the nanocomposites of MWCNT and UPR were also prepared without THF solvent by the same technique as described earlier.

Thus the samples were subjected for comparative analysis was neat UPR, MWCNT reinforced UPR nanocomposite (MWCNT−UPR) and THF pre-dispersed MWCNT reinforced UPR nanocomposite (THF−MWCNT−UPR).

3.3.2 MWCNT Quantity Optimization

There were five sorts of MWCNT reinforced UPR nanocomposites fabricated with 0.05, 0.1, 0.2, 0.3, and 0.5wt% MWCNT. Pre and post dispersion was carried out according to the estimated optimum sonication time. The solvent evaporation, cooling and curing was conducted as like previous technique.

Therefore, the prepared samples were subjected to various measurements are neat UPR, 0.05CNT-UPR, 0.1CNT−UPR, 0.2CNT-UPR, 0.3CNT-UPR, 0.5CNT-UPR nanocomposites which were fabricated with 0.05, 0.1, 0.2, 0.3, 0.5 wt% MWCNT respectively. The optimum amount of MWCNT reinforced UPR (OPCNT-UPR) nanocomposites was illustrated from these specimens. The experimental flow chart is represented in Figure 3.3.

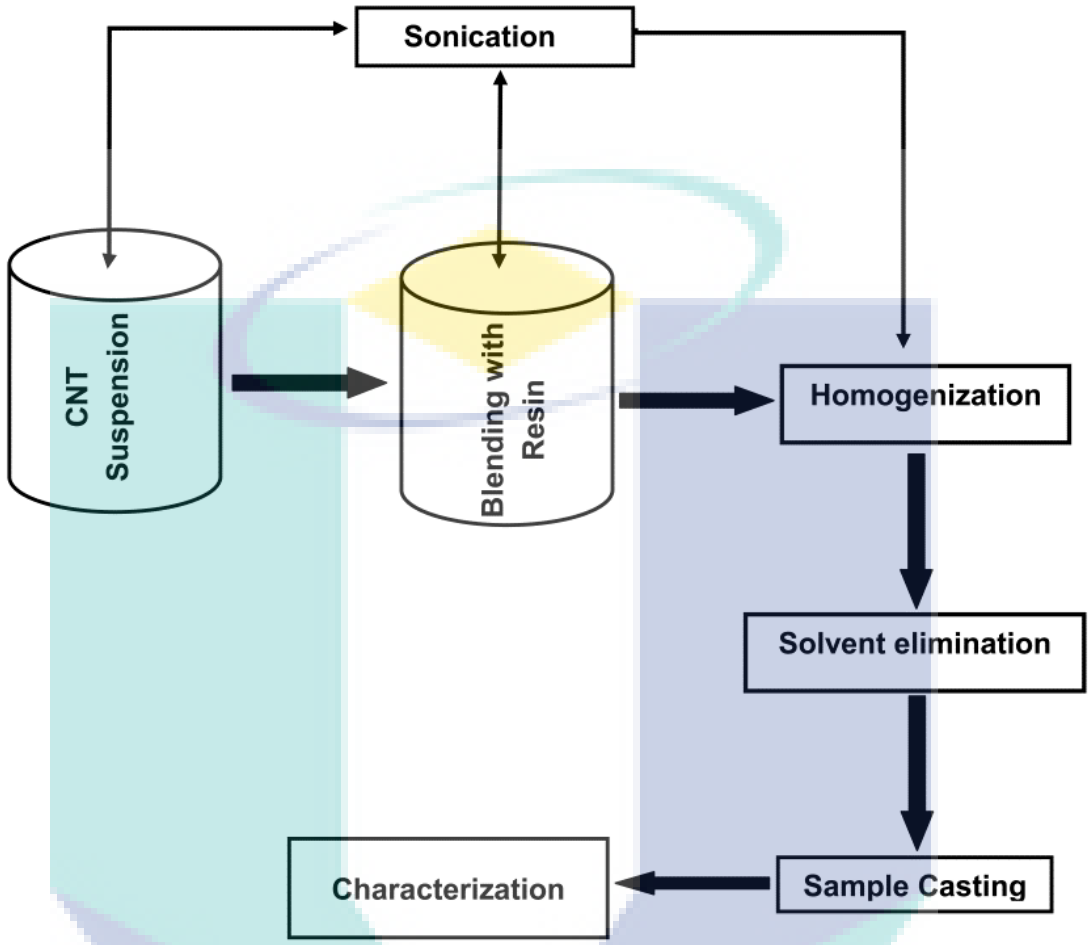

Figure 3.3: Composite Fabrication Process Flow Chart

3.3.3 MWCNT Coating Process

(i) Hyper Branched Polyester (HBP) Coating on MWCNT

HBP coated MWCNTs (HBCNT) was prepared by solution technique. The HBP concentrations were 5, 10 and 15wt% with respect to the weight of MWCNT. At first HBP was dissolved in THF solvent and prepared 0.002gm/ml dilute solution. Secondly, oven dried MWCNT was pre-dispersed in THF solvent, the ratio of MWCNT and THF was maintained as 1: 10. The suspension was sonicated for 1.5h in an ice cube filled ultrasound bath. Then pre-dispersed MWCNT suspension was added with HBP solution. The suspension of MWCNT and HBP solution was stirred by magnetic stirrer

at around 1500 rpm for 15 minute. In addition it was sonicated for another 1.5 hour for homogeneous dispersion of MWCNT in solution. Finally THF solvent was eliminated by evaporation at 66°C to get HBCNT which was dried in vacuum oven at 100°C. According to these process three types of HBP coated HBCNT1, HBCNT2 and HBCNT3 nanotubes were prepared which contain 5, 10 and 15wt% HBP respectively. These nanotubes were subjected for destructive and non destructive analysis to evaluate the optimum amount of HBP coated on OPHBCNT nanotube.

(ii) Shellac Coating on MWCNT

Shellac was coated on the surface of MWCNT to prepare SLCNT nanotube. The solid shellac was dissolved in THF solvent and prepared 0.002gm/ml dilute solution. Different concentrations of shellac were maintained with respect to the weight of MWCNT. According to the previous technique, oven dried MWCNT was pre-dispersed in THF solvent. Then pre-dispersed MWCNT suspension was added with that shellac solution. The suspension of MWCNT and shellac solution was stirred and sonicated as said by earlier section. THF was taken out by evaporation. Finally SLCNT was dried in vacuum oven at 100°C. In accordance with this process 5, 10 and 15 wt% shellac was used in SLCNT1, SLCNT2 and SLCNT3 nanotube correspondingly. The SLCNT were subjected for destructive and non destructive analysis to assess the optimum amount of Shellac coated on OPSLCNT nanotube. The following flow chart in Figure 3.4 represents the coating process of HBP and shellac on MWCNT.

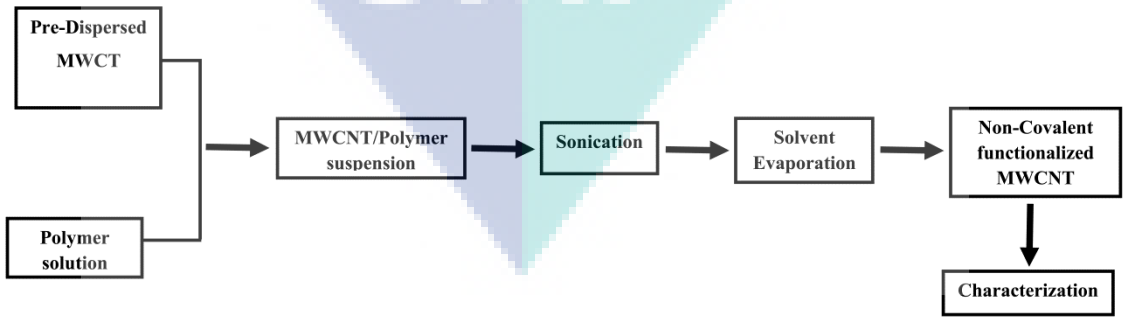

Figure 3. 4: MWCNT Coating process flow chart

3.3.4 Fabrication of Coated MWCNT Reinforced UPR nanocomposites

About 0.3wt% OPHBCNT and OPSLCNT nanotubes were independently dispersed in UPR. The suspension was vigorously stirred by homogenizer and followed sonication in ice cube filled ultrasound bath for 2 hr. About 1 wt% MEKP as initiator was added to these suspensions and gently stirred for 3 minute, then placed in vacuum to remove the bubbles. The bubble free suspension was poured in the specimen mold and cured at room temperature. Thus, the prepared samples subjected to analysis were UPR, OPCNT-UPR, OPHBCNT-UPR as well as OPSLCNT-UPR.

3.4 CHARACTERIZATION

3.4.1 Evaluation of Anti -Scavenging behavior of Modified MWCNT

In this work curing temperature of nanosuspension illustrates the scavenging behavior of different MWCNTs. Pristine and modified MWCNT incorporated UPR nanosuspensions were dynamically cured using differential scanning calorimetry (DSC) which was carried out at around 30-250^{0}C with the heating rate of 10^{0}C/min in the nitrogen atmosphere. A curing exotherm appeared at different temperature in the DSC thermograms with respect to different nanosuspension. The curing exotherm of neat UPR appears at the lowest temperature whereas pristine MWCNT incorporated UPR suspension exhibits curing temperature at the highest temperature due to scavenger behavior of pristine MWCNT. However, the curing exotherm of coated MWCNTs incorporated UPR nanosuspensions appear between the neat UPR and MWCNT-UPR nanosuspensions due to anti scavenger behavior of coated MWCNT. These exothermic pick temperatures illustrated the behavior of modified MWCNT as an anti-scavenger.

3.4.2 Viscosity

Viscosity measurement was carried out in the Faculty of Chemical and Nanural Resources Engineering, University of Malaysia Pahang. It was conducted according to ASTM D2983 using a Brookfield DV-III ULTRA, rotary viscometer. The standard capacity of sample holder is 9 ml and the container was mountain in water jacketed

block to maintain room temperature. The cylindrical spindle-31 was then rotated with different rpm ranges from 0.1 to 5.9, showing an individual share rate for each rpm, and the viscosity corresponding to share rate was recorded as mPa·s unit.

3.4.3 Fourier-Transform Infrared Spectroscopy

Fourier-transform infrared (FTIR) spectroscopy was performed in Faculty of Industrial Science and Technology, University of Malaysia Pahang, which detects the functional groups as well as bonding natures in the materials. The measurements were conducted by a Nicolet 6700 FT-IR spectrometer, Thermo Scientific, Germany, using standard KBr pellet technique in the range of 4000–500cm^{-1} wave number.

3.4.4 X-ray Diffractometry

X-ray diffraction (XRD) analysis was carried out in the Faculty of Industrial Science and Technology, University of Malaysia Pahang. The XRD data were collected by using a Rigaku Mini Flex II, Japan, operated at 30 kV, at 15mA and equipped with computer software to analyze the data. The specimens were step-wise scanned over the operational range of scattering angle (2θ) from 3 to 40°, with a step of 0.02°, using CuK$_\alpha$ radiation of wavelength λ=1.541Å. The data were recorded in terms of the diffracted X-ray intensities (I) versus 2θ. The degree of crystallinity (χ_c) was calculated using the equation (Zhang et al., 2011).

$$\chi_{XRD}(\%) = \frac{I_C}{I_C + I_A} \times 100 \quad ---------- (3.1)$$

Where, I_C and I_A are the integrated intensities of crystal and amorphous parts of the samples, respectively. The crystallographic spacing (*d*) was calculated by following Bragg's equation [Suh et al., 2000*]*.

$$\lambda = 2dSin\theta \quad ---------- (3.2)$$

The average size of the crystallites, D, was determined with the full width at half-maximum (FWHM) of XRD peak by using the following Scherer's equation [Inagaki et al., 2010]:

$$D = \frac{0.9\lambda}{\delta Cos\theta} \quad ---------- [3.3]$$

Where, δ is the FWHM (in radians) and θ is the diffraction angle. The δ value was determined by curve fitting after subtracting the amorphous background. The Gaussian curve was fitted at the top of the peak for determining δ and the position using an appropriate program.

3.4.5 Field Emission Scanning Electron Microscopy (FESEM)

Composites' non-fractured and fractured surfaces were investigated by using a (JOEL, JSM-7800F, Japan) field emission scanning electron microscope of Central laboratory , Universiti Malaysia Pahang. Samples were mounted on aluminium stubs with a carbon tape followed by a sputter coating with platinum to make them conductive prior to the field-emission scanning electron microscopy (FESEM).

3.4.6 Tensile Testing of Composites

Tensile testing was conducted according to ASTM 638-08, using a Shimadzu (Model: AG-1) Universal tensile testing machine fitted with a 5 kN load cell and operated at a cross-head speed of 1mm/min by keeping 65 mm gauge length was employed. Five samples of each category were tested for tensile strength (*TS*), tensile modulus (*TM*) and percentage of elongation-at-break (*EB*) measurements. This tesing was performed in the Faculty of Chemical and Nanural Resources Engineering, University of Malaysia Pahang.

3.4.7 Impact Testing

The impact testing was carried out according to the EN ISO 179 by a Ray-Ran Pendulum Charpy Impact System. The impact velocity was 3.5 m/s with the hammer weight of 0.163 kg. Dimensions of the samples were 80 mm × 8mm × 3.5 mm; five replicates were evaluated for each type of samples to obtain impact strength (*IS*). This tesing was performed in the Faculty of Chemical and Nanural Resources Engineering, University of Malaysia Pahang.

3.4.8 Differential Scanning Calorimetry

Differential scanning calorimetry (DSC) was conducted to determine the thermal transitions in the material, using a TA/Q1000 apparatus under nitrogen atmosphere and ramp method with a heating rate of 10°C min^{-1}.

During this analysis, the curing exotherm of nanosuspension was assessed in the temperature range of 30-250°C. Whereas the nanocomposites thermal transitions were evaluated in the temperature range of 30–400°C. This testing was performed in the Faculty of Chemical and Nanural Resources Engineering, University of Malaysia Pahang.

3.4.9 Thermogravimetric Analysis

Thermogravimetric analysis (TGA) conducted in the Faculty of Chemical and Natural Resources Engineering, University of Malaysia Pahang. It was performed by a TGA Q500 V6.4, Germany in a platinum crucible, ramping from room temperature to 700°C at 10°C/min in the Nitrogen atmosphere. The decomposition temperature has evaluated at 50% weight loss of materials and residue content was determined at the final stage of heating. Finally thermal stabilities of the materials were determined u weight loss by this ramping method.

CHAPTER 4

RESULTS AND DISCUSSION

4.1 INTRODUCTION

The results and discussions are divided in to five sections. These sections illustrate optimization of MWCNT pre-dispersion and post dispersion time and effect of pre-dispersion on nanocomposite properties, optimization of MWCNT concentration in UPR matrix, modification of MWCNT with synthetic hyper branched polyester (HBP) and shellac (SL) as natural functional polymers, optimization of those polymers concentration, characteristics of non covalent functionalized MWCNT reinforced nanocomposites, and characteristics of hybrid MWCNT reinforced nanocomposites. The final section illustrates the comparative analysis among non-covalent functionalized MWCNT reinforced UPR nanocomposite, covalent functionalized MWCNT reinforced UPR nanocomposite and mixture of non-covalent and covalent functionalized MWCNT reinforced UPR hybrid nanocomposite.

4.2 OPTIMIZATION OF PRE-DISPERSION AND POST DISPERSION TIME OF MWCNT IN SOLVENT AND MATRIX

4.2.1 Evaluation of Sonication Time for MWCNT Pre-dispersion

Figure 4.1 represents the physical observation of pre-dispersed MWCNT which was dispersed in low boiling point Lewis base (THF) solvent with different sonication time. The suspensions were observed after 18 hours. There were distinguishable MWCNT sediment observed in 0.5 hour and 1hour sonicated suspensions whereas 1.5 hour sonicated suspension was remained as homogeneous. Therefore, it is suggested that 1.5 hour sonication time is effective for pre-dispersion of MWCNT in low boiling point Lewis base solvent.

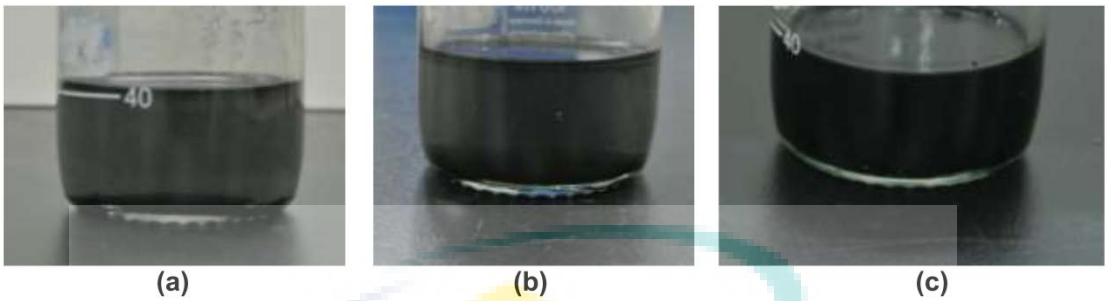

Figure 4.1: Photographs of (a) 0.5hr, (b) 1hr and (c) 1.5hr sonicated THF- MWCNT pre-dispersed suspensions

Figure 4.2 illustrates the micrographs of pristine MWCNT and pre-dispersed THF-MWCNT. The pristine MWCNT was existed as like as compact lump whereas the THF-MWCNT exist as small broken lump. In addition after 1.5 hour sonication they became free from entanglement. Many MWCNTs were separated as individual MWCNT from the compact bundles. This observation can be considered that 1.5 hour as an optimum sonication time for pre-dispersion of MWCNT.

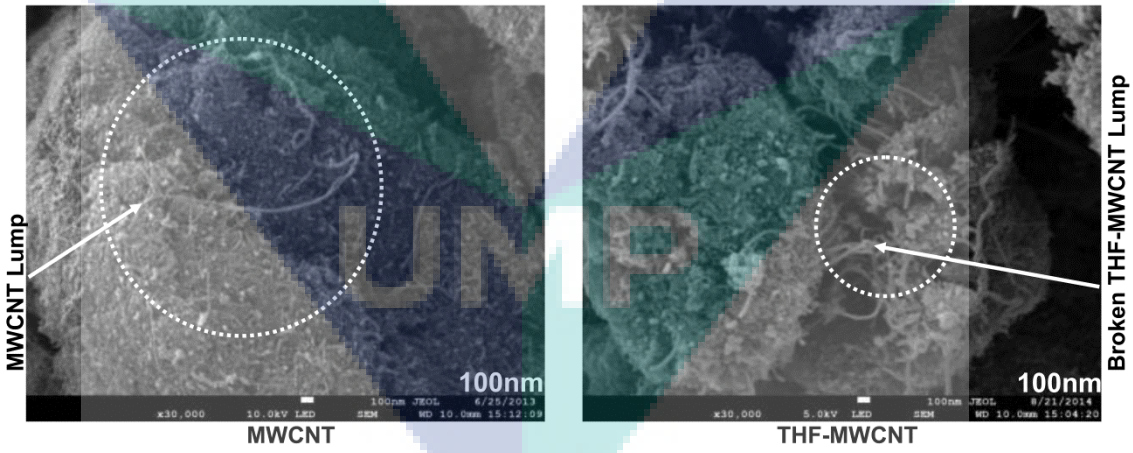

Figure 4.2: FESEM of MWCNT and THF-MWCNT

4.2.2 Evaluation of Sonication Time for Post dispersion of THF- MWCNT in UPR matrix: Effect of Pre-dispersion Technique on Nanocomposites Properties

(i) Physical observation of MWCNT sediment

Figure 4.3 illustrates the physical observation of MWCNT sediment in UPR matrix. Vial (a), (b) and (c) were sonicated for 1 hr, 1.5hr and 2 hr respectively, they contained THF-MWCNT in UPR. Vial (d) contained MWCNT-UPR suspension where MWCNT did not pre dispersed which was sonicated for 2hr as well.

In addition pictures (a)-(c) represent the effect of post-dispersion sonication time on dispersion of THF-MWCNT in nano suspensions. These samples were preserved at room temperature as well as convenient environment without hampering their sedimentation. The observation was carried out until 72 hours. MWCNTs were sediment at the bottom of vial (a) and (b) during that time. On the other hand there was no visible sediment in vial (c). Therefore 2 hr sonication can be considered as the most favorable time for post dispersion of THF-MWCNT.

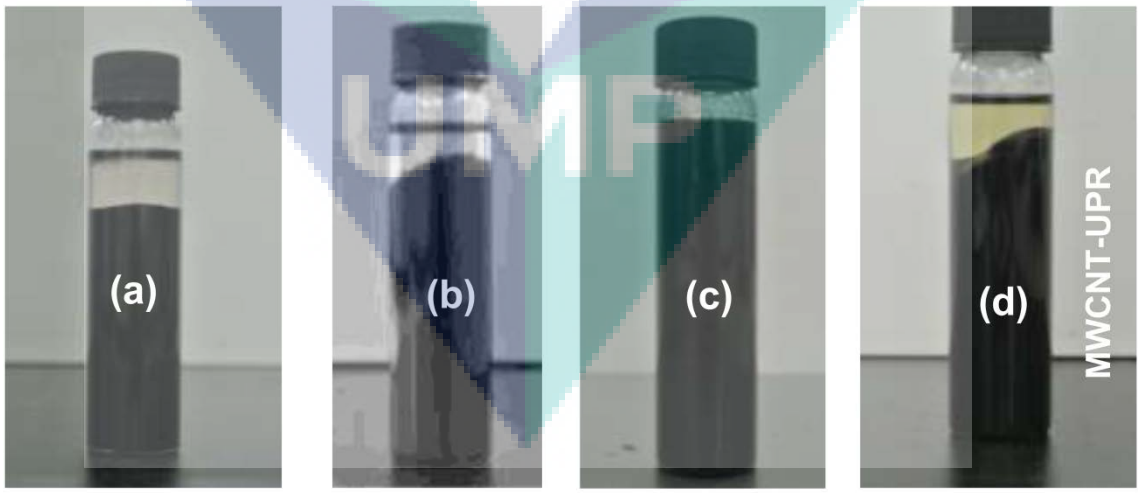

Figure 4.3: Photographs of (a) 1hr, (b) 1.5hr, and (c) 2hr sonicated MWCNT sediment in THF- MWCNT-UPR nanosuspension and (d) 2hr sonicated MWCNT-UPR nano suspensions

Furthermore, vial (c) and (d) represent the effect of pre-dispersion. The sedimentation of MWCNTs started after 18 hr in vial (d). Therefore observation notices that pre-dispersion technique is effective for homogeneous dispersion of MWCNT in UPR matrix.

(ii) Rheology of Nano suspensions at different sonication times

Figure 4.4(a) illustrates the effect of sonication time on the shear thinning behavior of nano suspensions. They exhibited non linear viscosity change at low shear rate as well as they behave like complex fluid. At low shear rate ($0.034S^{-1}$) 2 hour sonicated THF-MWCNT-UPR nano suspension exhibits 43491 mPaS as the highest viscosity, whereas 1 hr sonicated THF-MWCNT-UPR nano suspension exhibits the lowest viscosity 3798 mPaS. This result may be a notice of 2 hr sonication is the best time for dispersion of MWCNTs in UPR matrix.

Figure 4.4(b) shows the effect of pre-dispersion on the viscosity of nano suspensions. This graph represents the viscosity as a function of shear rate for UPR, MWCNT-UPR and pre-dispersed THF−MWCNT−UPR nano suspensions where the nano suspensions were sonicated for 2 hour. The viscosity of neat UPR was less dependent on shear rate which exhibited almost linear variation in the range of 0-1.7S¯1. The small change in viscosity at low shear rate was due to other ingredients which need for curing. This result implies that the liquid UPR reveals a Newtonian fluid. In case of Newtonian fluid viscosity is independent from the stress state and the shear rate (Abdalla et al., 2007).

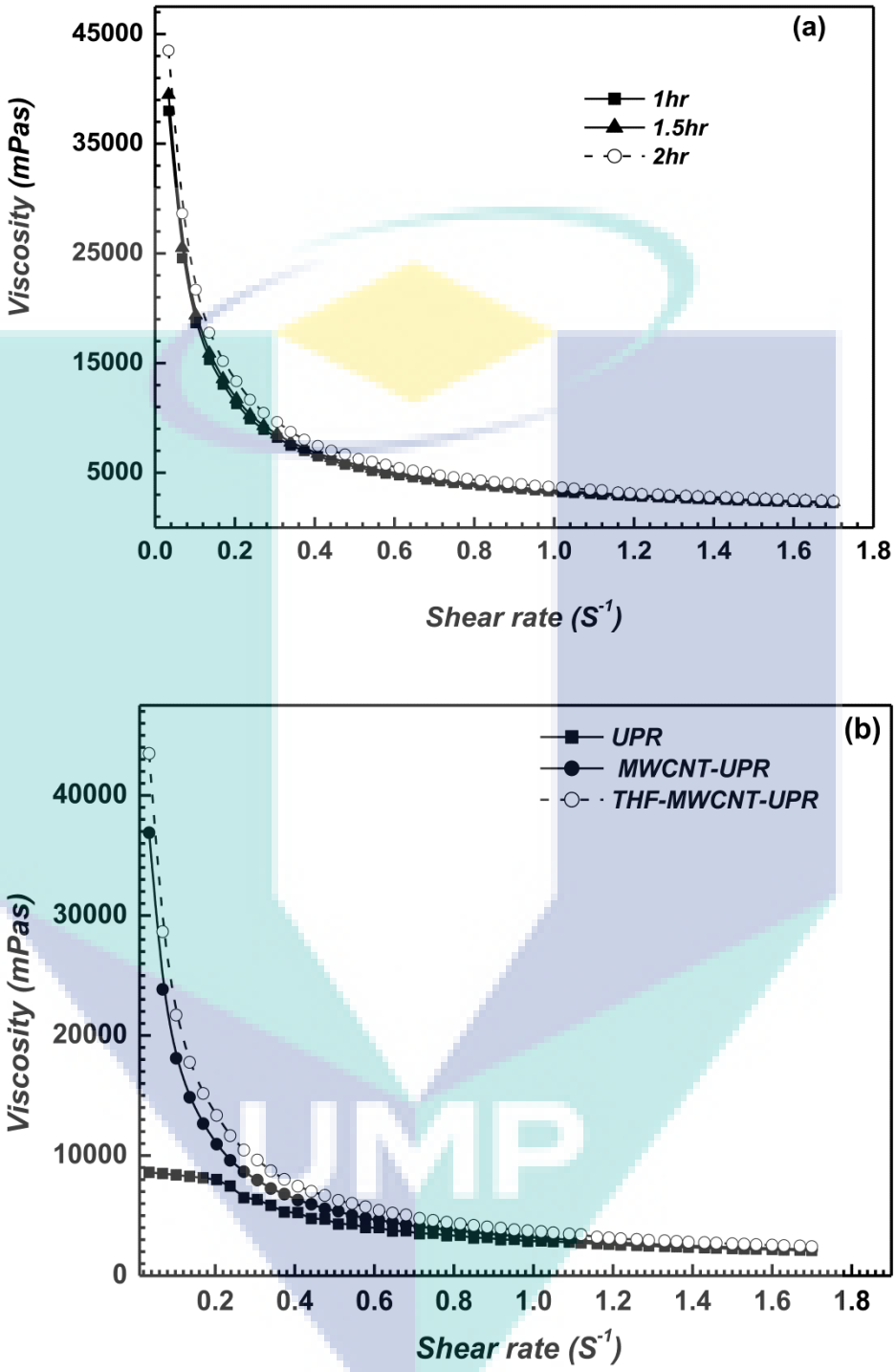

Figure 4.4: Shear thinning behavior of (a) THF-MWCNT-UPR nanosuspensions dispersed at different sonication time (b) UPR, MWCNT-UPR and THF-MWCNT-UPR nanosuspension

In contrast, the viscosity change is observed for nanocomposite suspensions with respect to shear rate is seemingly non-linear. So they behave like a complex fluid, the

fluid which shows non-linear viscosity behavior with shear rate is known as complex fluid. They are binary mixtures which have coexistence between two phases. Since at low shear rate less than $0.6S^{-1}$ the viscosity decreases quickly, they show shear thinning behavior at low shear rate, and such a behavior is absent in neat UPR. The low shear rate up to 0.6 S^{-1} is useful to differentiate the viscosity difference of neat resin and composites' suspensions. Both composites' suspensions demonstrate higher viscosities than the neat resin at low shear rate.

Moreover, the THF−MWCNT−UPR reveals a greater viscosity than MWCNT−UPR at low shear rate. This result may be an indication of a better dispersion of pre-dispersed MWCNTs in UPR matrix or a stronger interaction between resin and nanotubes. Similar results have been observed for carbon based nanoparticles which homogeneously dispersed in polyester resins (Kim et al., 2006). In another article, the higher viscosity of nanocomposites than neat resin has been reportedly attributed to strong interfacial interactions among MWCNT and UPR molecules as well as the formation of percolated structure by the carbon nanotubes (Abdalla et al., 2007). Their observations supported a strong interaction and well percolation between MWCTNs and resin molecules. It has also been reported that the percolated structure breaks down as the shear rate increases, resulting in decrease viscosities that are similar at high shear rates for all systems (Abdalla et al. 2007). Comparing the results of other reports and our findings, it is suggested that pre-dispersed MWCNT is well dispersed in UPR matrix; moreover UPR molecules were likely to wrap MWCNTs through uniform distribution and prevent them from the formation of agglomerates.

(iii) Plain surface morphology of nanocomposites

Figure 4.5 represents the plain surface morphology of (a) 1hr (b) 1.5 hr (c) 2 hr sonicated THF-MWCNT reinforced UPR nanocomposites (THF-MWCNT-UPR). The micrograph (d) represents the plain surface of MWCNT-UPR nanocomposite where the sonication time was as similar to (c)

In addition, micrographs (a), (b) and (c) illustrate the effect of sonication time for the dispersion of THF-MWCNT in nanocomposites. Twisted MWCNT and remarkable visible cracks are mentioned by dotted circle in the plain surface micrograph

(a). These types of surface morphology are sign of improper dispersion of MWCNT in UPR at that sonication time. Likewise, the micrograph (b) is 1.5 hr sonicated nanocomposite exhibits irregular dispersion. However the micrograph (c) of 2 hr sonicated THF-MWCNT-UPR nanocomposite represents homogeneously MWCNT dispersed plain surface. Therefore 2 hr sonication can be suggested as the optimum post dispersion time of MWCNT in UPR matrix.

Furthermore, the micrographs (c) and (d) represent the effect of pre-dispersion on the plain surface morphology of nanocomposites.

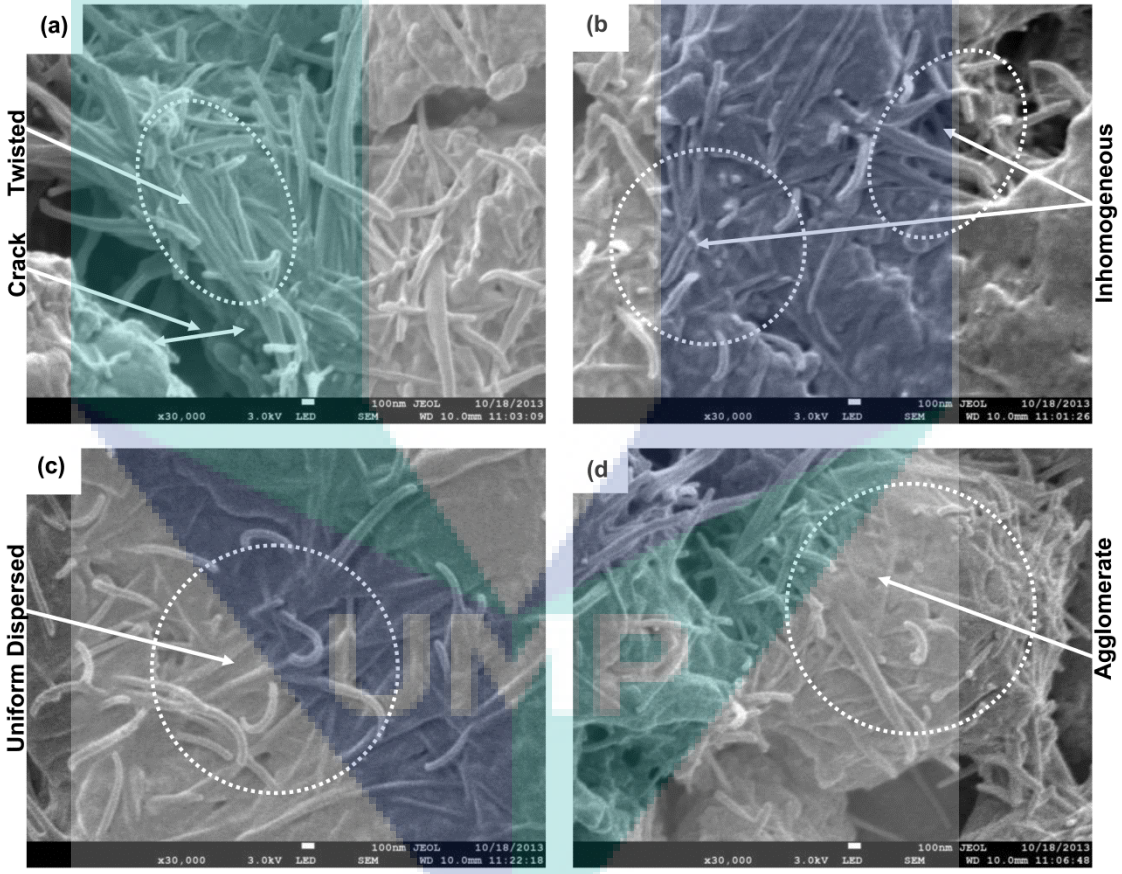

Figure 4.5: Plain surface of (a) 1hr, (b) 1.5hr, and (c) 2hr sonicated THF-MWCNT-UPR nanocomposites and (d) 2hr sonicated MWCNT-UPR nanocomposite

The MWCNT−UPR nanocomposite surface shows irregular dispersion of MWCNT with larger openings or voids, whereas THF−MWCNT−UPR surface comprises homogeneously dispersed MWCNT.

Agglomerates and homogeneous dispersion are indicated by dotted circles. The surface of THF−MWCNT−UPR in micrograph (c) shows quite well dispersion of nanotubes, whereas aggregates of MWCNTs are visible in the surface of MWCNT−UPR micrograph (d). THF−MWCNT−UPR nanocomposite surface exhibits individual nanotubes, being separated and embedded in the polymer matrix. In contrast, the clusters of nanotubes existed in the MWCNT−UPR nanocomposite system may be due to Van der Waals force among the MWCNTs is basically responsible for poor wetting of MWCNT by matrix (Hsu-Chiang Kuan et al. 2005).

These observations suggested that by means of pre-dispersion MWCNTs were homogeneously dispersed in UPR matrix, indicating a good distribution of nanotubes. The most striking observation in THF-MWCNT-UPR micrograph there were no cracks developed in the polymer-filler system, additionally the matrix was stacked to the surface of MWCNT. The micrograph (c) reveals that MWCNTs were sound wetted by resin which is an agreement of good wettability of pre-dispersed filler, also supported by viscosity analysis.

(iv) Mechanical properties of nanocomposites

Figure 4.6 (a) and (b) represent the plots for *TS*, *TM*, *IS* and *EB* as a function of sonication time. The corresponding values of *TS*, *TM*, *EB%* and *IS* for 1 hr sonicated THF-MWCNT-UPR nanocomposite are 30.16 MPa, 1.359 GPa, 8.97% and 3.79 kJ/m^2 and those for 1.5 hr sonicated THF- MWCNT-UPR are 33.6MPa, 1.421GPa, 8.83% and 3.9 kJ/m^2 respectively.

Thus, the corresponding *TS*, *TM*, and *IS* of 1.5hr sonicated THF-MWCNT−UPR nanocomposite was increased by an amount of 11.45, 4.5, 3%, whereas the EB was decreased by 1.5%. Likewise the values of *TS*, *TM*, *EB%* and *IS* for 2 hr sonicated THF-MWCNT−UPR nanocomposite are 35.13 MPa, 1.5 GPa, 8.93% and 4.6 kJ/m^2 correspondingly. Therefore, corresponding *TS*, *TM*, *IS* were increased by 16.5, 10, 21% as compare to 1 hr sonicated THF-MWCNT-UPR nanocomposite. Finally, after 2hr sonication suggested that most of the CNTs were disentangled as well as

homogeneously dispersed and soundly interacted with UPR matrix. These facts are illustrated repeatedly in surface morphology as well as in mechanical properties. Therefore, these results make obvious that 2hr is a good sonication time to improve the mechanical properties of nanocomposites.

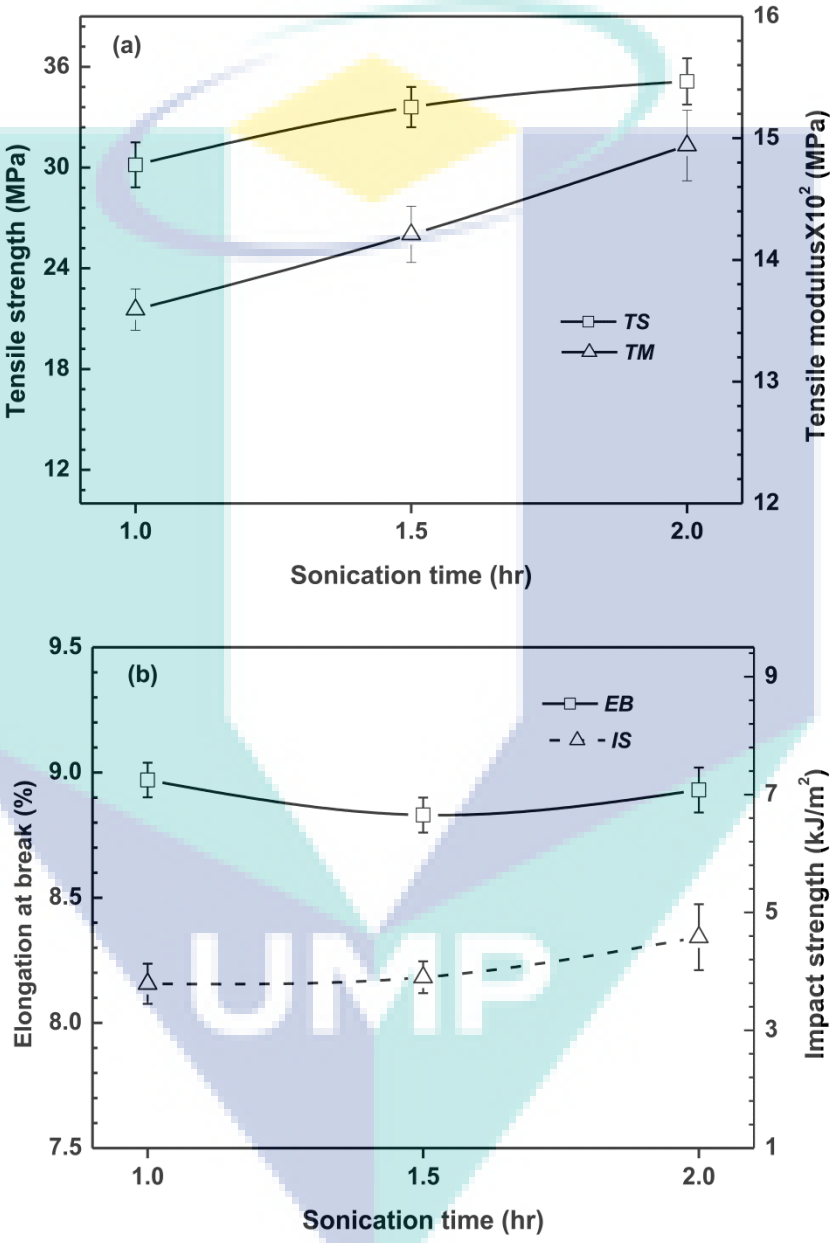

Figure 4.6: Tensile strength and tensile modulus (a), Elongation at break and impact strength (b) of THF-MWCNT-UPR nanocomposites as a function of sonication time

Figure 4.7 represents the effect of carbon nano tube pre-dispersion on the mechanical properties of nanocomposite. Figure 4.7(a) shoes the TS, TM and Figure 7(b) illustrates the IS and EB of UPR, MWCNT-UPR and THF-MWCNT-UPR

nanocomposites. The TS and TM of THF-MWCNT-UPR was increased 22.30% and 20.30% respectively compare to neat UPR whereas the TS and TM of MWCNT-UPR was increased 9.71% and 12% respectively. In addition the highest elongation at break and impact strength of THF-MWCNT-UPR nanocomposite suggests twisted MWCNT could exist in this nanocomposite, due to slip of the twisted nanotubes bundles EB was increased (Thess et al., 1996; Chaeichian et al., 2013).

The enhancement of mechanical properties of the THF−MWCNT−UPR nanocomposite over MWCNT−UPR nanocomposite and UPR are due to the good dispersion of MWNTs in the resin matrix as well as sound intercalation between filler and matrix. Whereas the dispersion was conducted in absence of THF, the MWCNTs undergo partial agglomeration which reduced the effectiveness of reinforcement. Such a phenomenon was disclosed by other researchers (Wang et al., 2012). The agglomerations of MWCNTs obviously narrow their active interfacial area and confine their performance. Therefore pre-dispersion in presence of THF reduces the MWCNTs agglomeration. In fact, the extraction of individual nanotube from MWCNTs bundles paves the way of affording both large surface area and strong interfacial interactions between the polymer and nanofiller inter phase, as declared elsewhere (Wang et al., 2012). These inherent advantages lead to efficient stress transfer between the MWCNTs and the UPR, as a result enhanced mechanical performances of nanocomposite. Moreover, higher elongations of nanocomposites indicate that MWCNTs are complimentary to more plastic deformation in the nanocomposites.

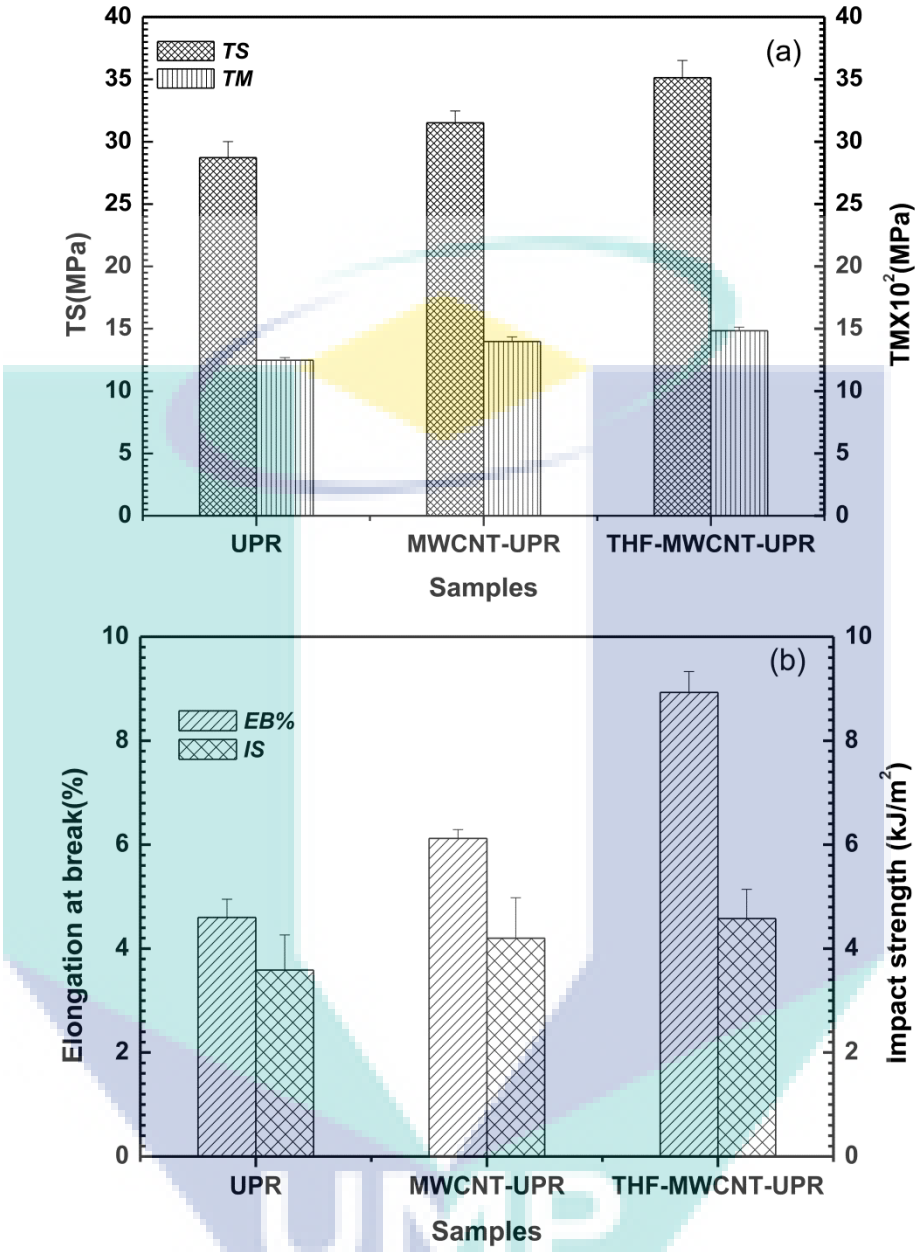

Figure 4.7: (a) Tensile strength and tensile modulus (b) Elongation at break and impact strength of UPR, MWCNT-UPR and THF-MWCNT-UPR nanocomposites

(v) Fracture morphology of nanocomposites

Figure 4.8 shows the fracture surface micrographs of THF-MWCNT-UPR and MWCNT-UPR nanocomposites. The micrographs a, b and c represent the effect of nanosuspension sonication time on the fracture morphology of THF-MWCNT–UPR nanocomposites. It is obvious that several nanotubes were pulled out when the composites were fabricated after 1 hour and 1.5 hour sonication. On the other hand

there were many fracture tips visible on the surface of THF-MWCNT-UPR nanocomposite which was prepared after 2 hour sonication. It seems that well dispersion and interaction between carbon nanotubes and UPR have existed in this nanocomposite.

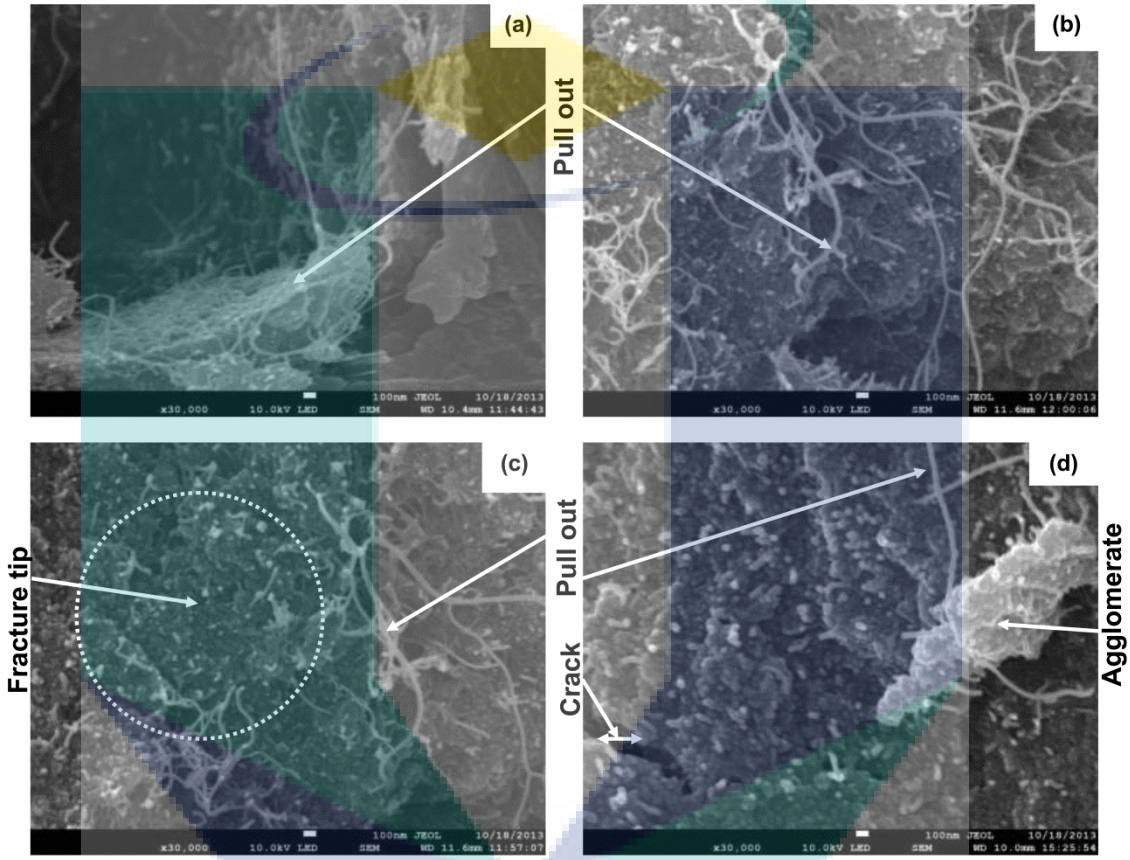

Figure 4.8: Fracture Micrographs of (a) 1hr, (b) 1.5hr, and (c) 2hr sonicated THF-MWCNT-UPR nanocomposites and (d) MWCNT-UPR nanocomposite

In addition, micrographs c and d of Figure 4.8 illustrate the effect of pre-dispersion on the fracture morphologies of THF-MWCNT-UPR and MWCNT-UPR nanocomposites respectively. Several bright tips of MWCNTs remain in the matrix and some of them pulled out during stretching of THF-MWCNT-UPR nanocomposite. There was no visible crack in the surface of THF−MWCNT−UPR nanocomposite, also support a better adhesion between pre-dispersed MWNTs and UPR molecules. On the contrary, small crack propagation region and agglomeration were noticeable on the surface of MWCNT−UPR nanocomposite. Thus, the pre-dispersion along with

sonication reveal a good avenue for good dispersion of MWCNTs in resin matrix. Not only that but also the increased interfacial area of nanotubes in composites can lead to the change of segmental morphology and influence the mechanical properties of nanocomposite as reported elsewhere (Desai and Haque, 2005; Kim et al., 2006).

Therefore, it can be suggested that appropriate dispersion time can be effective to wet the filler as well as increase the interaction between CNT and matrix. The pulling out of nanotubes was affected the mechanical properties of nanocomposites illustrated earlier.

Finally, sedimentation of MWCNT in THF and FESEM were noticed that 1.5 hr was the best as well as optimum sonication time for pre-dispersion of MWCNT in low boiling Lewis base (THF) solvent. Additionally, the dispersion quality of MWCNT in UPR was observed with sedimentation, rheology of nano suspensions, mechanical properties and surface morphologies of nanocomposites with different sonication times. These observations suggested that effective dispersion and potential interaction between MWCNT and UPR were obtained after 2 hr sonication of THF-MWCNT-UPR nanosuspension. Therefore, 2 hr can be considered as the optimum post dispersion sonication time. Moreover, pre-dispersed MWCNT reinforced nanocomposite was exhibited better properties than nanocomposite fabricated straight dispersion at the same sonication time. The distinguishable pre-dispersion effects have been predicted by comparing those properties at 2 hr sonicated THF-MWCNT-UPR and MWCNT-UPR nanocomposites. These sonication times have been employed for successive study.

4.3 EVALUATION OF OPTIMUM MWCNT QUANTITY

This section illustrates the optimum percentage of MWCNT, where different percentages of MWCNT had pre-dispersed in a Lewis base (THF) solvent at the optimum pre-dispersion sonication time. In addition, the pre-dispersed MWCNTs had dispersed in UPR at the optimum post-dispersion time. The MWCNT optimization processes were carried out through physical observation, rheology of nanosuspension, and tensile modulus of composites was fitted with Halpin –Tsai model equation. The qualitative dispersion was observed through surface morphology of different nanocomposites. XRD profiles of different CNT-UPR nanocomposites were studied to predict the optimum amount of MWCNT in OPCNT-UPR nanocomposite. The curing behavior of MWCNT filled UPR and the thermal properties were studied by using DSC and TGA thermograms of CNT-UPR nanocomposites.

4.3.1 Physical Observation of MWCNT Sediment in UPR with Different Concentration of MWCNT

The optical image of Figure 4.9 represents the sedimentation of MWCNT under the vial of 0.1CNT-UPR, 0.3CNT-UPR and 0.5CNT-UPR nanosuspensions. A relative dispersion quality was observed after 5 days settling time. It is obvious that there was no sediment in the vials of 0.1CNT-UPR and 0.3CNT-UPR suspensions. Whereas, MWCNT started to settle after 5 days in the vial of 0.5CNT-UPR suspension. Therefore, homogenety of MWCNTs in 0.1CNT-UPR and 0.3CNT-UPR indicated the qualitative dispersion as well as the sound interaction between MWCNT and UPR. It can be suggested that 0.3 wt% MWCNT did not form any visual aggregates after that holding period conversely, 0.5wt% MWCNT relatively may be re- aggregated after 5 days.

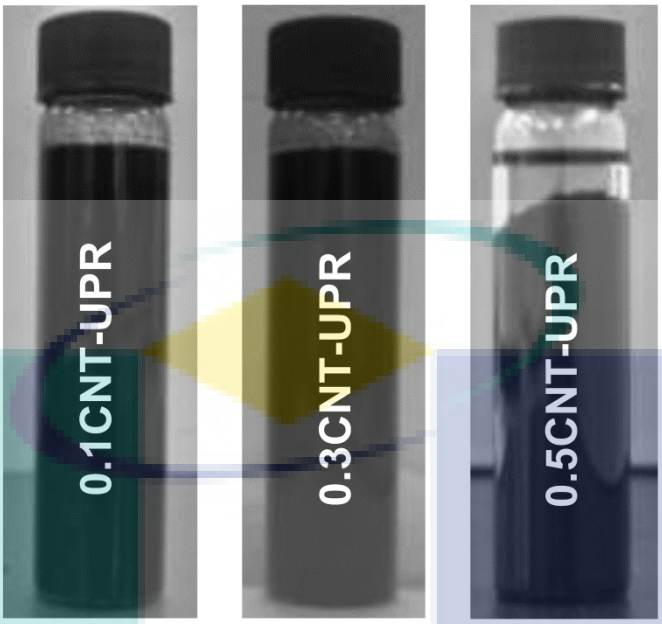

Figure 4.9: Photographs of MWCNT Sediment in CNT-UPR nanosuspensions contained 0.1, 0.3 and 0.5 wt% MWCNT

4.3.2 Rheology of CNT-UPR Nanosuspensions at Different Content of MWCNT

Figure 4.10 states the rheology of neat UPR, 0.1CNT-UPR, 0.3CNT-UPR and 0.5CNT-UPR nanosuspensions, where the viscosity change is a function of shear rate. The viscosity of neat UPR is less dependent on the shear rate, showing almost a linear variation in the range of 0–1.7S^{-1} .This result implies that UPR reveals a Newtonian fluid.

On the other hand, the change in viscosity of nanosuspensions with respect to shear rate is apparently non-linear. So they behave like a complex fluid, because they exhibit shear thinning behavior at low shear rate, and such a behavior is absent in neat UPR. The low shear rate up to 0.6 S^{-1} is significant to distinguish the viscosity difference of neat resin and nanosuspensions. The nanosuspensions were demonstrated higher viscosities than the neat resin at low shear rate. Moreover, 0.3CNT−UPR nanocomposite suspension reveals around 38000 mPas as the highest viscosity compares to other CNT−UPR nanosuspensions at that shear rate. This result may be a signature of a good dispersion, as well as the better interaction of MWCNTs and UPR matrix. The similar results demonstrated for carbon-based nanoparticles dispersed in

polyester resins, where the authors claimed a homogeneous dispersion of nanoparticles (Kim et al., 2006). In addition, the elevated viscosity of nanosuspensions than neat resin has been apparently attributed to strong interfacial interactions among MWCNT and UPR molecules in addition to the formation of percolation by the carbon nanotubes, reported elsewhere (Abdalla et al., 2007). Therefore, previous observations support a strong interaction of 0.3 wt% MWCNTs with UPR molecules and formation of sound percolation by MWCNTs in UPR. It has also been reported that the percolated structure breaks down as the shear rate increases, therefore the viscosity of all nanosuspensions was decreased at high shear rate (Abdalla et al., 2007). Comparing this result to other reports, it is suggested that 0.3 wt% MWCNT was well dispersed in UPR matrix through uniform distribution and prevented them from the formation of agglomerates (Kim et al., 2006; Abdalla et al., 2007). It has consisted with the plain surface morphology of 0.3CNT-UPR nanocomposite.

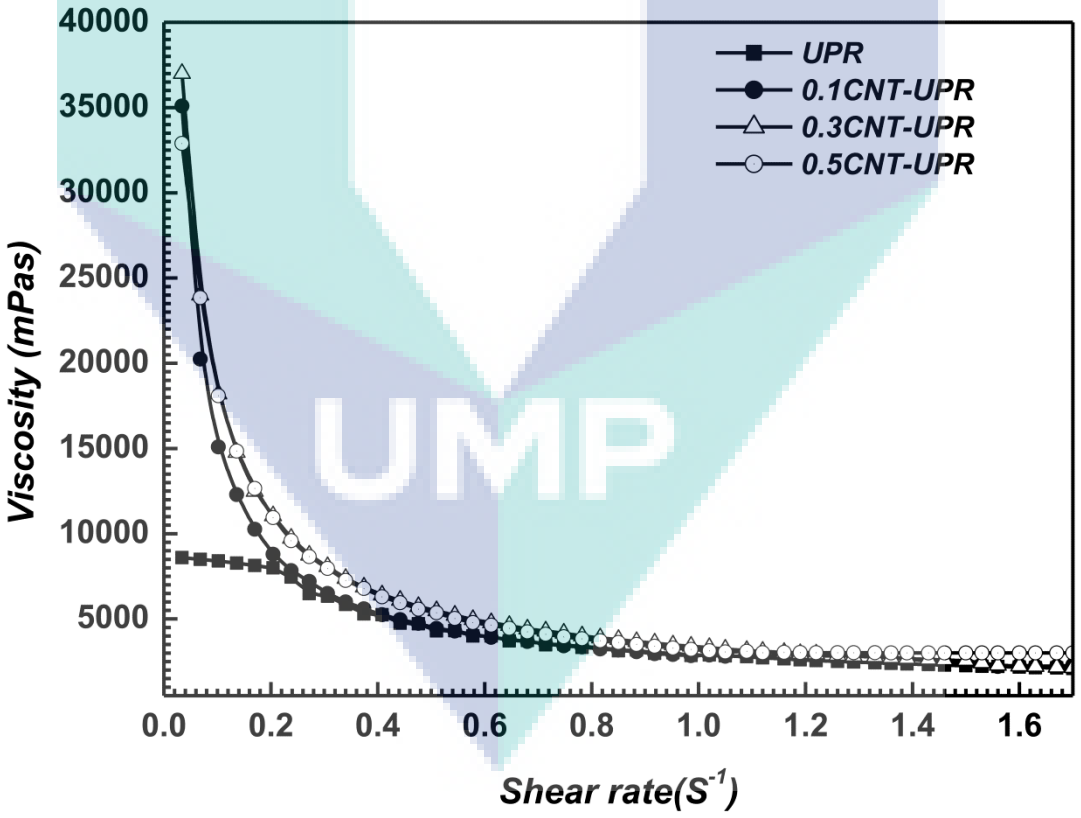

Figure 4.10: Viscosity of CNT-UPR nano suspensions as a function of shear rate

4.3.3 Mechanical Properties

(i) Tensile modulus

The relationship between the degree of MWCNTs dispersion and the mechanical properties of nanocomposites are discussed in this section. The experimental and calculated tensile moduli are plotted in Figure 4.11 as a function of MWCNT content. The mechanical properties of polymers are generally improved by the addition of CNTs. In addition modulus of the nanocomposite was increased with increasing the content of nanofiller has been stated elsewhere (Tai et al., 2004; Montazeri et al., 2010; Ayatollahi et al., 2011).

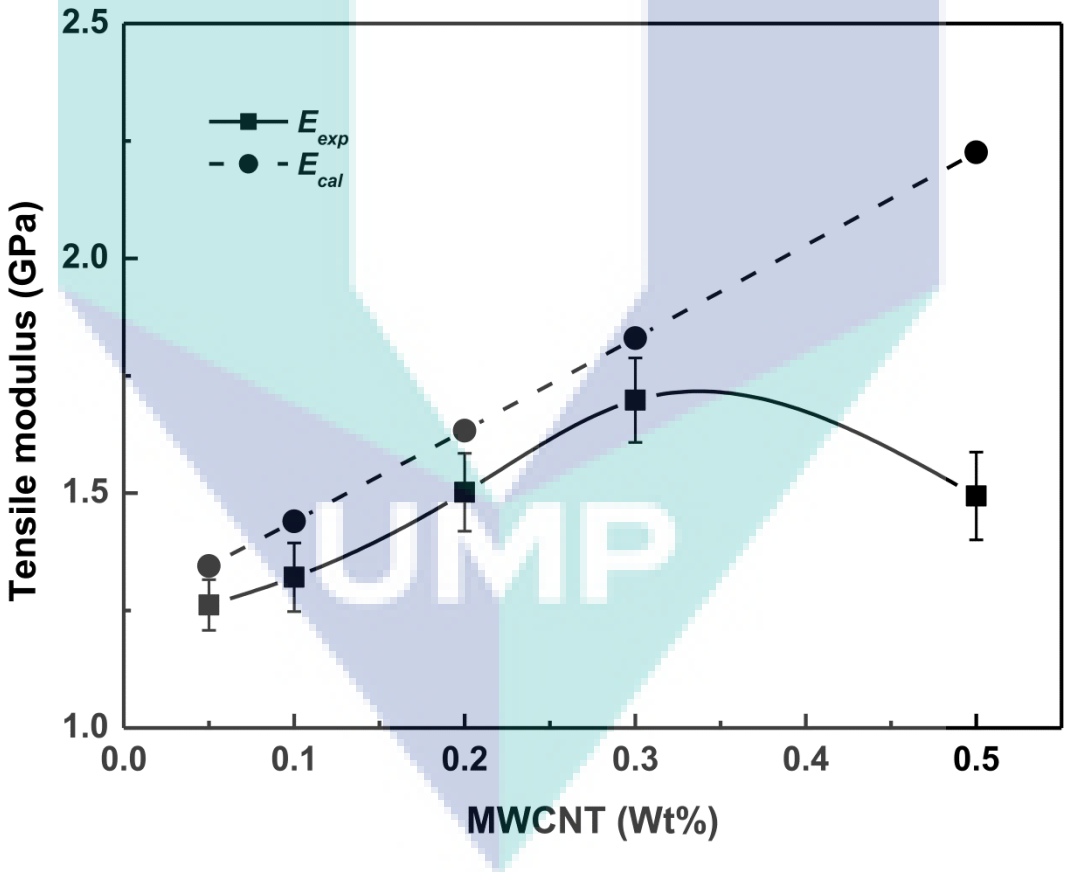

Figure 4.11: Tensile modulus of composites as a function of MWCNT content fitted with modified Halpin -Tsai equation

In this study, modified Halpin–Tsai equation has used to fit the experimental data (Halpin and Tsai, 1969; Halpin et al., 1976).

$$E_{comp} = \frac{1 + C\gamma\vartheta_{CNT}}{1 - \gamma\vartheta_{CNT}} E_{UPR} \ , \quad \gamma = \frac{\frac{E_{CNT}}{E_{UPR}} - 1}{\frac{E_{CNT}}{E_{UPR}} + C} \qquad (4.1)$$

Where, $C = (l/d)$ is aspect ratio as a constant shape factor of MWCNT filler, l , d length and outer diameter of MWCNT respectively. E_{UPR}, E_{CNT}, E_{comp} are the modulus of matrix, MWCNT and composites in that order, ϑ_{CNT} is the volume fraction of MWCNT which can be calculated with the density of UPR (ρ_{UPR}) , density of MWCNT (ρ_{CNT}) and the weight fraction of MWCNT (W_{CNT}) as

$$\vartheta_{CNT} = \frac{\rho_{UPR} W_{CNT}}{\rho_{CNT} - \rho_{CNT} W_{CNT} + \rho_{UPR} W_{CNT}} \qquad (4.2)$$

The numerical values of these properties are given by Times nano and present in Table 4. 1. Moreover, the measured values of E_{mat}, $V_{CNT,}$ and densities ($\rho_{UPR}$and ρ_{CNT}) of MWCNT and UPR are provided in this table as well.

The Halpin–Tsai equation was originally used for composites with unidirectional reinforcement. Cox found a parameter (α) known as orientation factor, to recount for the randomness of the discontinuous fibers (Cox, 1952). If the fiber length is greater than the specimen thickness, the fibers are assumed randomly oriented in two dimensions then orientation factor α = 1/3 is used for calculation of tensile modulus of the composite material. If the fiber length is excessively smaller than the thickness of the sample, the fibers are assumed randomly oriented in three dimensions; and the parameter α= 1/6 is used. In this study, the effective lengths of MWCNTs are less than 25 μm long, which is shorter than the thickness of specimens; therefore, three-dimensional MWCNTs distribution is assumed for MWCNT-UPR nanocomposites. The orientation factor α = 1/6 is chosen to modify the Halpin–Tsai equation (4.1) as below (Yeh et al., 2006; Tai et al., 2008; Ayatollahi et al., 2011)

$$E_{comp} = \frac{1 + C\gamma\vartheta_{CNT}}{1 - \gamma\vartheta_{CNT}} E_{UPR} \ , \quad \gamma = \frac{\frac{\alpha E_{CNT}}{E_{UPR}} - 1}{\frac{\alpha E_{CNT}}{E_{UPR}} + C} \qquad (4.3)$$

Figure 4.11 illustrates linear fits of Equation 4.3 for the nanocomposites which contained 0.05 to 0.3 wt% MWCNT. The linearly fitted TM suggested that these amounts of MWCNT dispersed uniformly in the matrix as well as formed flawless interaction between MWCNTs and UPR (Song and Youn et al., 2005). Therefore, the experimental tensile modulus at 0.3 wt% is highest as well as close to the calculated TM. However, the experimental tensile modulus is non-linear when the MWCNT concentration greater than 0.3 wt%. The TM of 0.5 CNT-UPR nanocomposite was decreased and the difference between calculated and experimental tensile modulus at 0.5 wt% MWCN was increased due to inhomogeneous dispersion, brutally tangled as well as aggregation of MWCNT at this concentration stated elsewhere (Gojny, 2004; Yeh et al., 2006; Ayatollahi et al., 2011) . Thus, it is concluded that the modified Halpin–Tsai equation can fit effectively the experimental results of tensile modulus. The plot also indicates that the optimum amount of MWCNT reinforcements in CNT-UPR nanocomposites for getting maximum mechanical properties is 0.3 wt% in this study.

Table 4. 1: Parameters for Halpin Tsai Equations (4.1) and (4.2)

Parameters of MWCNT and UPR							
MWCNT						**UPR**	
L_{CNT} **(μm)**	***D_{CNT}*** ***(nm)***	***E_{CNT}*** ***(TPa)***	***ρ_{CNT}*** **(g/cc)**	**W_{CNT} (wt %)**	***v_{CNT} (%)***	***E_{UPR}*** ***(GPa)***	***ρ_{UPR}*** ***(g/cc)***
24.5	6.36	1 (Montazeri et al., 2010)	2.3	0.05	0.033	1.248	1.53
				0.1	0.066		
				0.2	0.132		
				0.3	0.199		
				0.5	0.330		

(ii) Tensile strength and Elongation at break of nanocomposites

Figure 4.12 shows the effect of MWCNT content on the TS and EB of nanocomposites. The mechanical properties of nanocomposites were significantly improved in the range of 0.05 to 0.3 wt% of MWCNT. The TS of 0.3 wt% MWCNT incorporated nanocomposite revealed 40 MPa as the highest value among those nanocomposites. On the other hand, the EB of nanocomposites were decreased when the nanocomposites contained 0.05 to 0.3 wt% of MWCNT. Additionally, the lowest elongation at break (4.35%) was exhibited by the nanocomposite which contained 0.3 wt% MWCNT.

Finally, calculated and experimental values of TM in Figure 4.11 are suggested that 0.3 wt% MWCNT is the optimum quantity for fabrication of OPCNT-UPR nanocomposite. This suggestion is advocated by TS and EB of Figure 4.12. In addition it is suggested that UPR was wetted 0.3wt% MWCNT appropriately, therefore in 0.3CNT-UPR nanocomposite filler-matrix, a strong interface was developed, which played a significant role to reinforce the nanocomposite (Hull and Clyne, 1996). Moreover, poorly dispersed MWCNTs were twisted like a rope, as a result load transfer took place between adjacent MWCNT rather than filler and matrix, therefore, EB increased due to slip of the twisted nanotubes bundles (Thess et al., 1996).The successive effect of CNT concentration and dispersion on those mechanical properties can be illustrated by surface morphologies of nanocomposites.

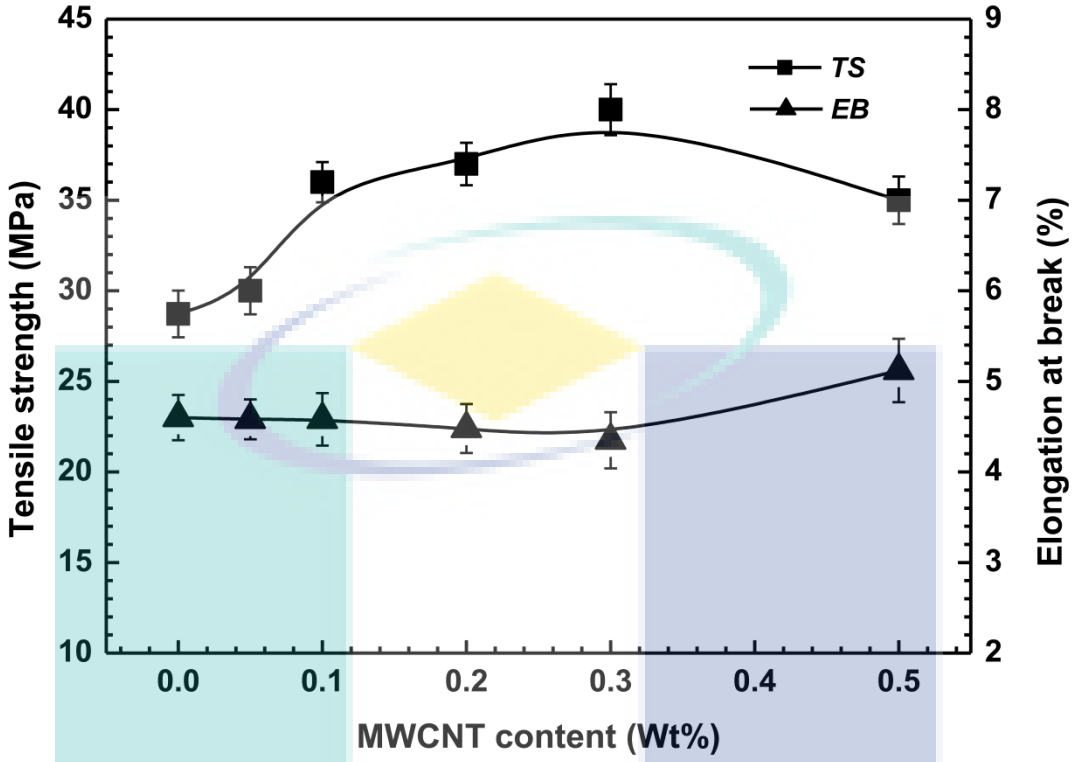

Figure 4.12: Tensile strength and Elongation at break of nanocomposites as a function of MWCNT content

4.3.4 Surface Morphology of Nanocomposites at Different Content of MWCNT

(i) Plain surface morphology

Figure 4.13 illustrates the plain surface morphology of Neat UPR (a), 0.1CNT-UPR (b), 0.3CNT-UPR (c), and 0.5CNT-UPR (d) nanocomposites. UPR surface exhibits visible wide crack and voids. Whereas the 0.1CNT-UPR plain surface shows narrow crack that was bridged by MWCNT. Besides, well-dispersed MWCNTs are visible on the plain surface of 0.3CNT-UPR nanocomposite. It is noticeable that crack was disappeared from this plain surface. However, the agglomerated MWCNT and widest crack near the aggregates are obvious on the plain surface of 0.5CNT-UPR nanocomposite. It is suggested that well dispersion and interaction between filler and matrix in 0.3CNT-UPR nanocomposite were shielded to build up the crack (Desai and Haque, 2005).

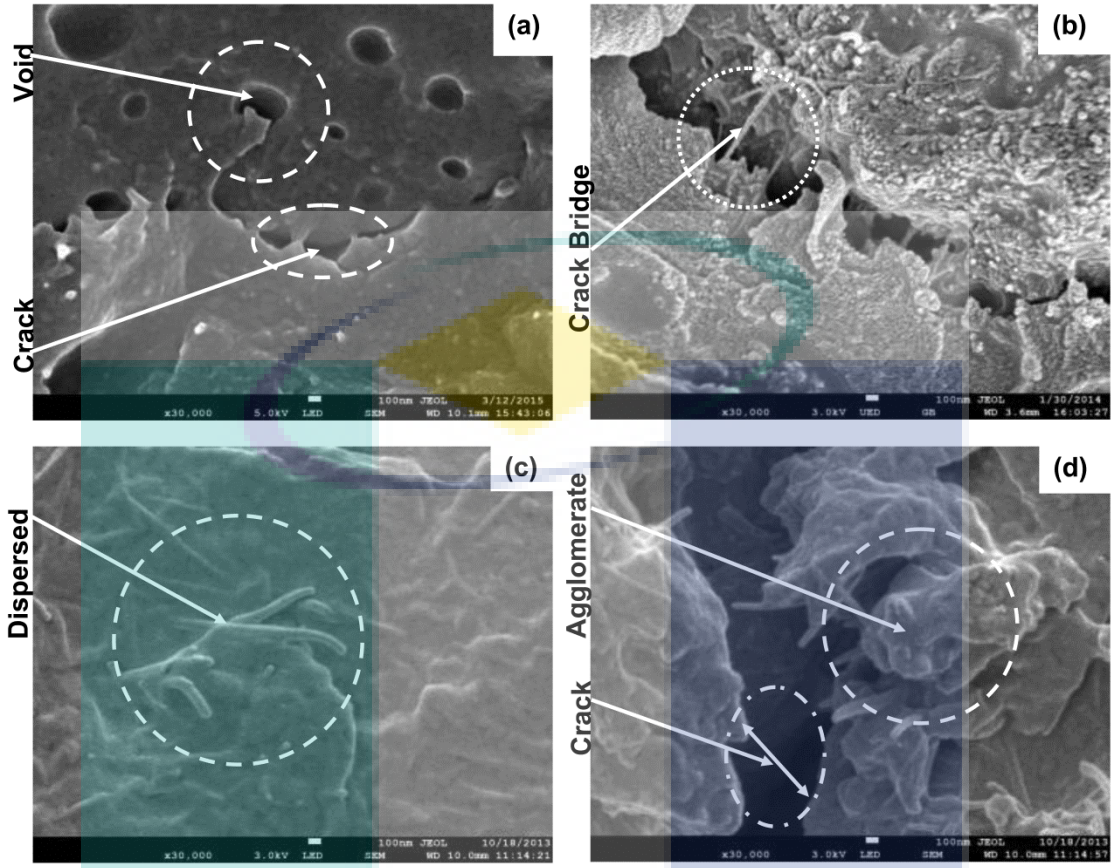

Figure 4.13: Plain surface micrographs of UPR (a), 0.1CNT-UPR (b), 0.3CNT-UPR (c), and 0.5CNT-UPR (d) nanocomposites

(ii) Fracture surface morphology

Figure 4.14 states the fracture morphologies of Neat UPR (a), 0.1CNT-UPR (b), 0.3CNT-UPR (c), and 0.5CNT-UPR (d) nanocomposites. The morphologies are distinguished by remarkable crack, failure of crack propagation, broken tips and CNT pull out on the surfaces UPR, 0.1CNT-UPR, 0.3CNT-UPR, and 0.5CNT-UPR respectively.

It seems that inadequate amount of MWCNT in 0.1CNT-UPR nanocomposite had failed to shield the crack initiation. In addition, the amount of MWCNT was not enough to shear the load of UPR, therefore, energy was dissipated by breaking most of the MWCNT, consequently crack was enlarged (Zhang et al., 2007). Moreover, a huge

number of broken tips of MWCNT are uniformly spread in the fractures surface of 0.3CNT-UPR nanocomposite.

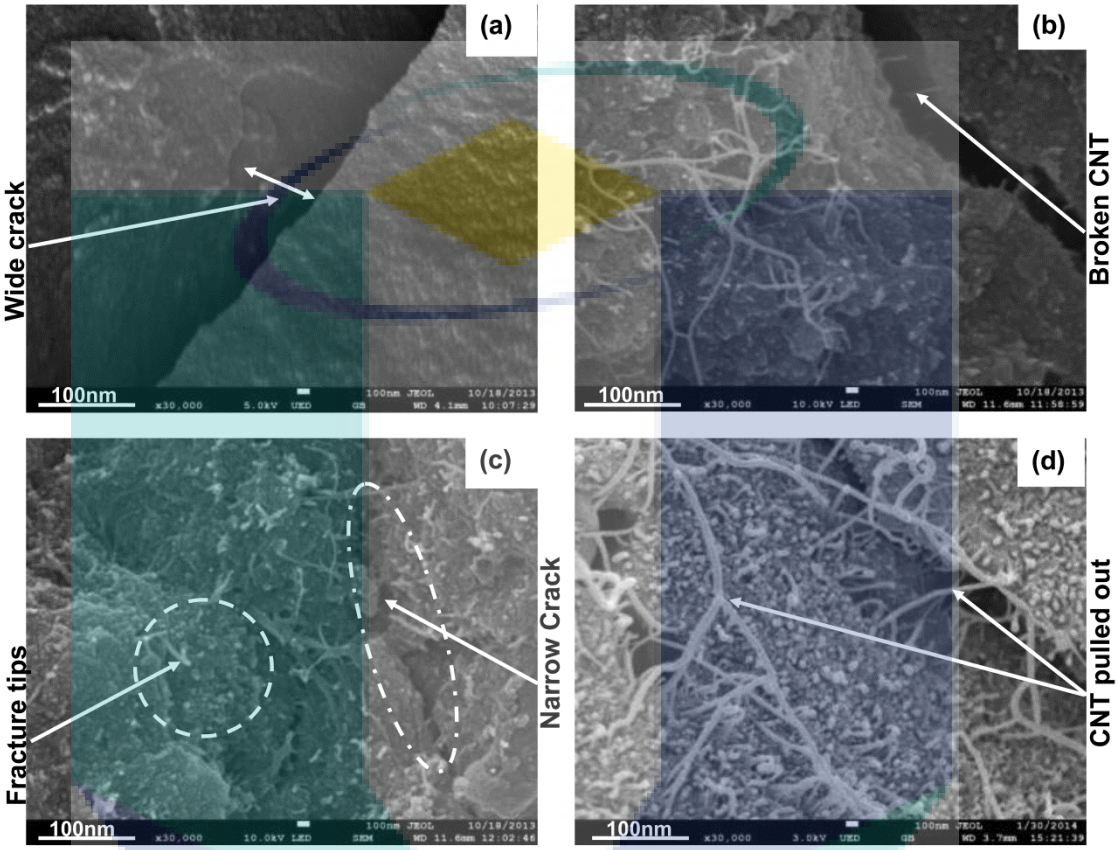

Figure 4.14: Fracture surfaces of neat UPR (a), 0.1CNT-UPR (b), 0.3CNT-UPR (c) and 0.5CNT-UPR (d) nanocomposites

Furthermore, the crack widening was shielded by several number of non-fractured MWCNT. It appears that 0.3 wt% MWCNT was sound dispersed and energy was dissipated equally as much as possible. Not only that, crack propagation of nanocomposite was declined with increasing the MWCNT platelets concentration in the 0.3CNT-UPR nanocomposites system. On the other hand, a knit like MWCNTs spread on the fracture surface of 0.5CNT-UPR nanocomposite. The Crack was deshielded in this surface. It materializes that aggregated MWCNT did not properly interact with UPR; therefore, CNTs were pulled out from the matrix during load transfer from matrix to filler in nanocomposite (Gryshchuk et al., 2006; Yueping et al., 2007).

Finally, it is an evident that, 0.3 wt% MWCNTs was well dispersed in the matrix as a consequence significantly declined crack initiation and form crack bridge in 0.3CNT-UPR nanocomposite. Therefore, it was withstanding high energy, able to shear load which obvious for the highest tensile strength, tensile modulus and the lowest elongation at break.

4.3.5 Structural Analysis of Nanocomposites as a Function of MWCNT Concentration

(i) X-ray Diffraction at different content of MWCNT

Figure 4.15 represents the XRD profiles of UPR and 0.1CNT-UPR, 0.3CNT-UPR and 0.5CNT-UPR nanocomposites. The UPR shows a broad peak at $2\theta = 23.43°$. The peak appearance is diffused as like a semi-crystal material. In addition, the corresponding peaks of 0.1CNT-UPR, 0.3CNT-UPR and 0.5CNT-UPR nanocomposites are at 20.87°, 18.91° and 20.13° respectively. These scattering angles attribute that MWCNT was contributed to removing the amorphousness of UPR as well as improve molecular arrangement in the nanocomposite system. Additionally, 0.3CNT-UPR nanocomposite exhibited a peak at the lowest scattering angle which suggested that 0.3 wt% MWCNT was efficiently performed as a nucleating agent. Moreover, a decrease in peak width and an increase in peak intensity for nanocomposites is also observed. The following discussion illustrates the effect of MWCNT content on peak width, crystallinity, lattice spacing and crystal size.

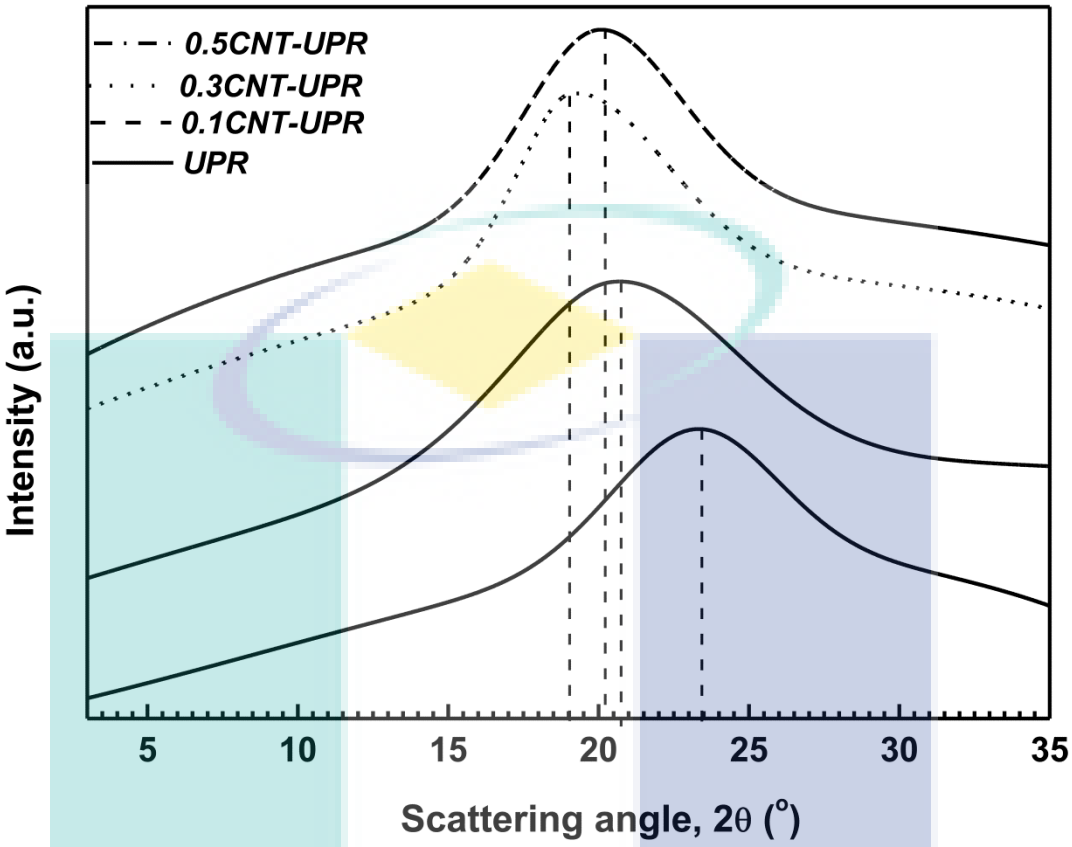

Figure 4.15: X-Ray scattering peaks of UPR and CNT-UPR nanocomposites

(ii) Correlation between the full width at half maximum and MWCNT content

Table 4.2 represents the full width at half maximum (FWHM) or $\Delta 2\theta$ of XRD peaks, crystallinity index (χ_{XRD}%), lattice spacing and crystal size of CNT-UPR nanocomposites as a function of MWCNT content.

The FWHM is expressed useful information of chain distortion, filler alignment as well as molecular dislocation in UPR and CNT-UPR nanocomposites (Vashista and Paul, 2012). It was declined with increasing the MWCNT content. The widest diffraction peak notices more molecular disorder in UPR (Jeong et al., 2003).On the other hand, relatively narrow as well as lower FWHM of nanocomposites advocated that MWCNT reduced the density of point defect in UPR. Furthermore, it corresponds to the degree of alignment of MWCNT. The FWHM of 5.2° as the lowest value for 0.3CNT-UPR nanocomposite notices that MWCNT was well aligned along UPR

molecules. On the other hand, FWHM of 0.5CNT-UPR nanocomposite was 7.19° as the highest value which was increased due to miss alignment of MWCNT with UPR (Minfang and Winey, 2007).

Table 4.2: FWHM, percentage of crystallinity, lattice spacing and crystal size as a function of MWCNT content

MWCNT (wt %)	2θ	FWHM (δ)(°)	Crystallinity (%) χ_{XRD}	Lattice spacing(*d* Å)	Crystal size (*D*)(Å)
0	23.43	9.44	14	3.73	8.4
0.1	20.87	6.14	17	4.20	12.96
0.3	18. 91	5.2	24	4.61	15.26
0.5	20.13	7.19	21	4.33	11.1

Besides, the degree of crystallinity (χ_{XRD}) was calculated by using the equation (4.3) (Zhang et al., 2011).

$$\chi_{XRD}(\%) = \frac{I_C}{I_C + I_A} \times 100 \quad (4.3)$$

Where, I_C and I_A are the integrated intensities of crystal and amorphous parts of the samples.

The estimated degrees of crystallinity of neat UPR, 0.1CNT-UPR, 0.3CNT-UPR and 0.5CNT-UPR nanocomposites are 14, 17, 24 and 21% respectively. The crystallinity of nanocomposites was increased due to the incorporation of MWCNT in UPR matrix. Additionally, the maximum crystallinity found in 0.3CNT-UPR nanocomposite. It seems that 0.3 wt% MWCNT properly dispersed and performed as a sound nucleating agent, similar nucleation effect of carbon nanotubes stated elsewhere (Lingyu Li et al., 2009; Avalos-Belmontes et al., 2012).

(iii) Lattice parameters as a function of MWCNT content

The crystallographic spacing (*d)* calculated with following Bragg's equation (Suhet al., 2000).

$$\lambda = 2dSin\theta \quad (4.4)$$

The average size of the crystallites, *D*, determined by the full width at half-maximum (FWHM) of XRD peak by using the following Scherer's equation (Inagaki et al., 2010):

$$D = \frac{0.9\lambda}{\delta Cos\theta} - - - - - - - - - - - - - - - - [4.5]$$

Where, δ is the FWHM (in radians) and θ is the diffraction angle. The δ value was determined by curve fitting after subtracting the amorphous background. The Gaussian curve was fitted at the top of the peak for determining δ and the position using an appropriate program.

The calculated lattice spacing (*d*) and crystal size (*D*) of UPR and CNT-UPR nanocomposites represent in Table 4.2. Both parameters had improved when 0.1, 0.3 and 0.5 wt% MWCNT incorporated in UPR matrix. The peak position shifted towards the lower scattering angle, therefore, the order of lattice constant is 0.3CNT-UPR>0.5CNT-UPR> 0.1CNT-UPR> UPR. In addition, increased lattice parameter may be attributed to the intercalation of nanoparticles into the matrix, providing a lattice distortion in UPR crystals. The 0.3CNT-UPR nanocomposite shows the highest lattice constant which leads to interfacial adhesion between filler and matrix. Therefore, it infers that 0.3 wt% MWCNT well dispersed in UPR matrix; the similar result obtained for carbon black reinforced epoxy resin (Sheng et al., 2004; Abdel-Aal et al., 2008). Furthermore, MWCNT content and peak width influenced crystal size which presents in Table 4. 2. The diffraction peak width decreased indicating the crystallite size of UPR increases. Therefore, due to the presence of MWCNTs more UPR molecules took part in crystallization. As a consequence, the order of crystal size is 0.3CNT-UPR>0.1CNT-UPR>0.5CNT-UPR>UPR.

4.3.6. Thermal Analysis of Nanocomposites as Function of MWCNT Concentration

(i) Effect of CNT concentration on curing temperature of nanosuspensions

The DSC thermogram in Figure 4.16 represents the curing behavior of UPR and CNT-UPR nanosuspensions. The curing process of UPR takes place by the free radical

mechanism. The strong exothermic peak of UPR thermogram is due to the copolymerization of UPR and styrene, whereas the peak like shoulder at high temperature is due to homopolymerization of UPR.

Additionally, the curing process of UPR is highly exothermic and it is poor thermal conductive. Moreover, the heat capacity of UPR is fair, as a consequence growing up the temperature in the curing process of UPR matrix (Rouison et al., 2004). Therefore, at elevated temperature UPR molecular coils acquired sufficient amount of thermal energy to overcome their hindrance and fascinate them to intramolecular polymerization, therefore, the shoulder like exotherm at high temperature in DSC thermogram appeared (Martin, 2007; Kosar and Gomzi, 2010; Monti et al., 2011). Furthermore, the thermograms of nanocomposite suspensions illustrate the existence of heat sinking filler in UPR matrix. The heat generated during curing process absorbed by MWCNT; as a result, Intra polymerization of UPR molecules prevents (Kubota, 1975; Avella et al., 1985).

The activation energy was calculated according to ASTM E-698-99 from equation [4.4] using the information of Figure 4.16 (Dodiuk et al., 2005).

$$E_a = 2.19R\frac{dlog\beta}{d(\frac{1}{T})} \dots\dots\dots\dots\dots\dots (4.4)$$

Where E_a is the activation energy (kJ/mol), R=8.314 (J/mol), β is the heating rate (K/min), and T is the peak temperature (°K).

The computed values present in Table 4.3. In addition, the activation energy of nanosuspensions frequently increased with increasing MWCNT content. It suggests that the free radical scavenging activity of MWCNT take part into increase the activation energy of nanocomposites. Additionally, this observation agrees to delay the curing reaction at a high concentration of MWCNT (Martınez and Galano, 2010; Monti et al., 2011).

Table 4.3: Curing temperature and activation energy of neat resin and CNT-UPR nanosuspension at different concentrations of MWCNT.

Samples	Curing Temperature (^{o}C)	E_a(kJ/mol)
UPR	93	16.4
0.1CNT-UPR	102	16.7
0.3CNT-UPR	109	17.05
0.5CNT-UPR	125	17.7

Finally, the DSC thermograms of liquid suspension mentioned that heat of reaction depend on the MWCNT content, moreover the exothermic peaks of suspension shift toward higher temperature when MWCNT content increased as shown in Figure 4.16.

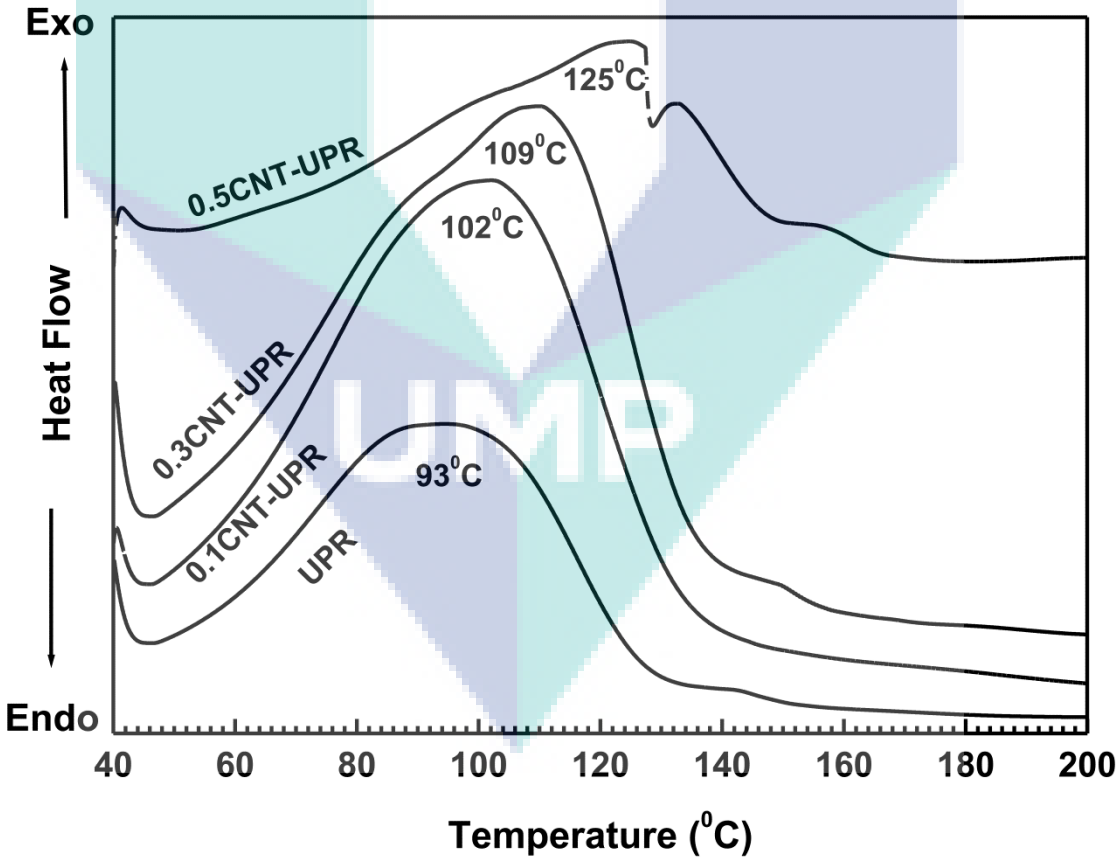

Figure 4.16: Curing exotherm of UPR and CNT-UPR nanosuspensions

(ii) Thermal transitions of neat UPR and CNT-UPR nanocomposites

Figure 4.17 illustrates the DSC thermograms of neat UPR, 0.1CNT-UPR, 0.3CNT-UPR and 0.5CNT-UPR nanocomposites. The information about intercalation of matrix and filler notice in these thermograms which influence both glass (T_g) and melting (T_m) transition of nanocomposites. The double peaks at high temperature (T_{m1}, T_{m2}) attribute to melting temperatures of nanocomposites. The transition temperatures were significantly enhanced by incorporation of the different amount of MWCNT in UPR as presented in Table 4.4. The wide melting peak at T_{m1} is due to original crystal growth in UPR whereas, the sharp melting peak at T_{m2} is the recrystallization temperature of CNT-UPR nanocomposites (David Rohindra et al., 2012).

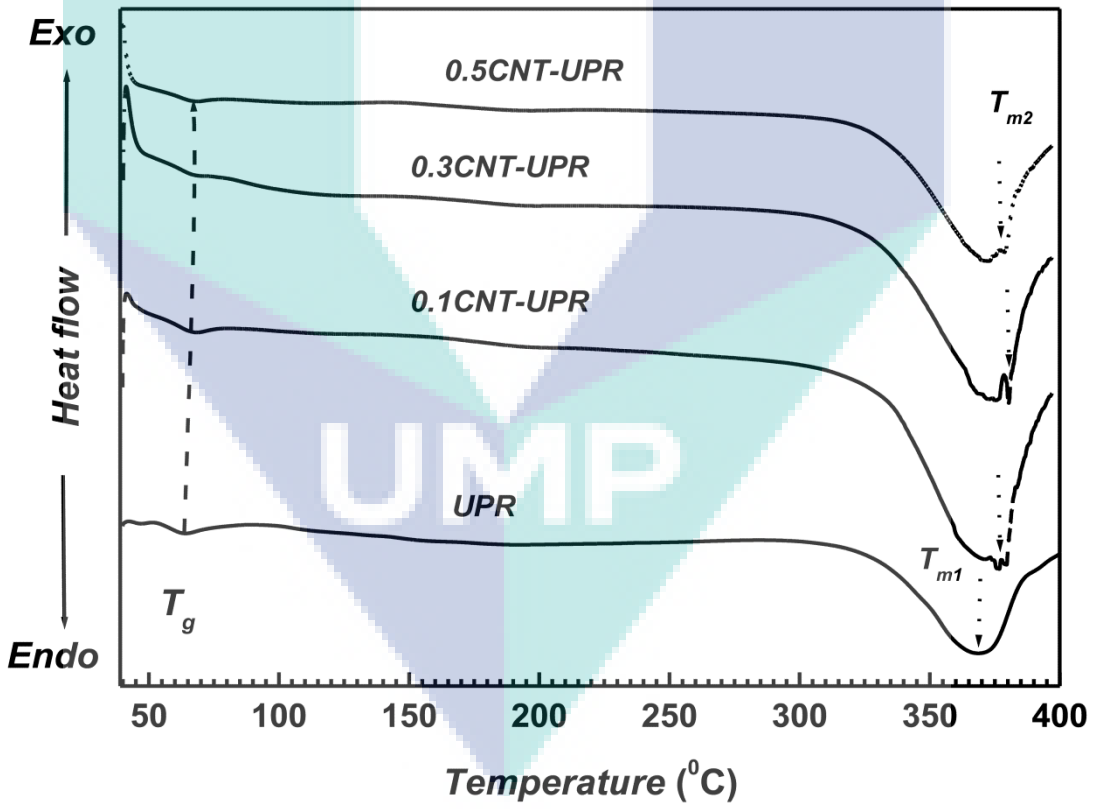

Figure 4.17: DSC thermograms of neat UPR, 0.1CNT-UPR, 0.3CNT-UPR and 0.5CNT-UPR nanocomposites

Lower glass transition and the recrystallization temperature of nanocomposites are due to lack of crystal perfection. Whereas high glass transition and melting temperature are due to segmental motion are stated elsewhere (Avella et al., 1985). Likewise 0.3CNT-UPR nanocomposite exhibited the highest glass transition and recrystallization temperature. It seems that 0.3 wt% MWCNT evenly dispersed in that nanocomposite, which effectively intercalated with UPR as well as performed as a nucleating agent (Pavlidou and Papaspyrides, 2008; Goffin et al., 2010).

(iii) Thermogravimetric analysis of nanocomposites

The thermogravimetric curves of UPR and CNT-UPR nanocomposites present in Figure 4.18. Matrix and nanocomposites disintegrated in some stages, related observation stated elsewhere (Seymour and Cooper, 1973; Dodiuk et al., 2005). Thermal decomposition of UPR took place at around 313°C and came to an end at around 446°C. In contrast, CNT-UPR nanocomposites' degradation began relatively at higher temperature than UPR matrix. The TGA traces of both UPR and nanocomposites appeared to fall at 150°C, because they associated with the discharge of volatile components such as residual solvent, polystyrene, Intra cross linked UPR which formed in nanocomposites due to scavenging effect of MWCNT (Cao and Lee, 2003; Martı´nez and Galano, 2010). The degradation of cross-linked resin has ascribed to the dissociation of C−C chain bonds and release of styrene at the site of dissociation (Manfredi et al., 2006; Inagaki et al., 2010).

While degradation temperature (T_d) can obtain from TGA traces, it is a common practice to consider the T_d at 50% weight loss of a sample as a sign of structural destabilization (Desai and Haque, 2005). Therefore, T_d values assessed for UPR, 0.1CNT-UPR, 0.3CNT-UPR and 0.5CNT-UPR from TGA curves and introduce in Table 4.4.

Table 4. 4: The T_g, and T_m values obtained from DSC thermograms of UPR and CNT-UPR nanocomposites together with their T_d, as evaluated from 50% weight loss from TGA thermograms.

Samples	T_g(°C)	T_m (°C)		T_d (°C)
		T_{m1}	T_{m2}	
UPR	62	370		378
0.1CNT-UPR	67	372	375	381
0.3CNT-UPR	68	375	380	395
0.5CNT-UPR	66	371	377	383

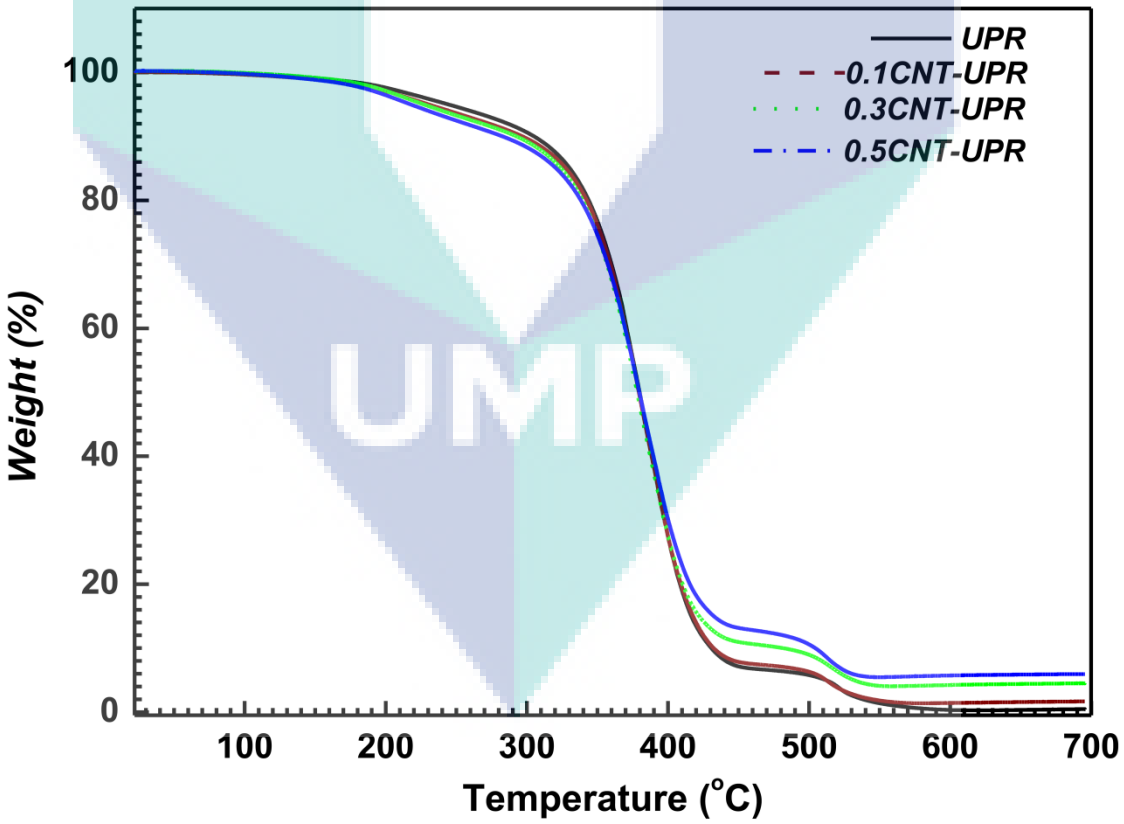

Figure 4.18: TGA thermograms of UPR and CNT-UPR nanocomposites

The DTG curves in Figure 4.19 illustrate the decomposition stages of UPR and CNT-UPR nanocomposites. Decomposition stages mentioned with dotted rectangle and circle. The shoulder like decomposition stage at around 200-245°C refers as the degradation temperature of unreacted styrene, polyester resin (Manfredi et al., 2006). The strong decomposition with splitting peaks at around 300−450°C referred as second stage decomposition of UPR and nanocomposites. In this temperature range, nanocomposites disintegrated at a higher temperature which is quite different from UPR.

It is most likely due to the interaction between MWCNT and UPR, as revealed by structural analysis, mechanical properties and fracture morphology. Besides, the splitting peak temperature of 0.3CNT-UPR nanocomposite was at around 410°C as the highest decomposition temperature among the nanocomposites. It recommends that in the case of 0.3CNT-UPR nanocomposite, either formation of bonding or strong interface between MWCNT and UPR which strictly shielded the UPR chains motion. The residue content at 600°C shows a significant difference between the UPR and nanocomposites, perhaps due to the MWCNT loading in resin (Martınez and Galano, 2010).

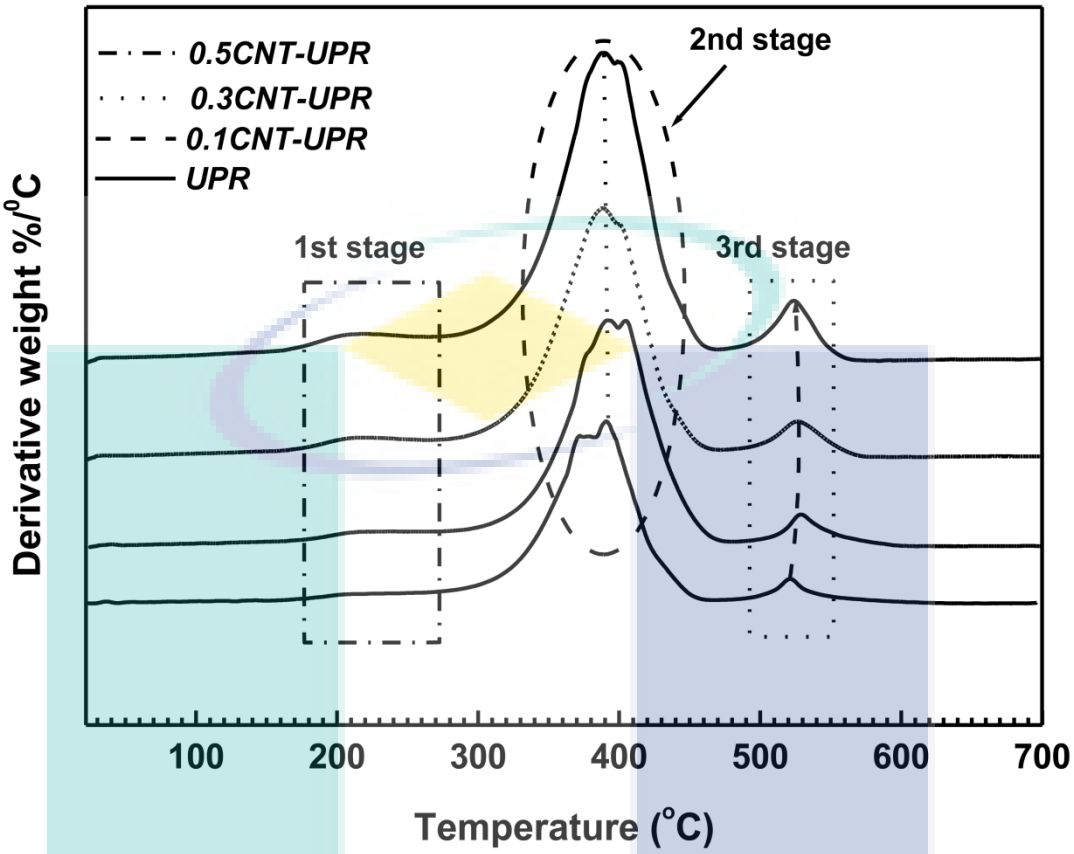

Figure 4.19: DTG thermograms of UPR and CNT-UPR nanocomposites

4.4 CHARACTERIZATION of HBP COATED MWCNT and NANOCOMPOSITES

4.4.1 Optimization of HBP Concentration

(i) Structural analysis of HBCNT as a function of HBP concentration

Figure 4.20 represents the X-ray diffraction profile of MWCNT, HBCNT1, HBCNT2 and HBCNT3. In the pattern of pristine MWCNT, a well-defined peak at around $2\theta = 25.71^{o}$ with a full- width-at-half-maximum (FWHM) of 2.92^{o} corresponds to the plane of hexagonal graphite-like structure of MWCNT (Nouralishahi et al., 2014). On the other hand, the corresponding diffraction peaks of HBCNT1, HBCNT2 and HBCNT3 are at around 25.80^{o}, 25.96^{o}, and 25.85^{o}. In addition, the FWHM of these HBCNT nanotubes are 2.87^{o}, 2.80^{o} and 3^{o} respectively. From these results, the average crystallite size (*D*) for pristine MWCNT, HBP coated MWCNTs has been estimated (Liu et al., 2014). Average *D* values for pristine MWCNT, and 5, 10 and 15 wt% HBP

coated CNT are estimated around 2.30nm, 2.7nm, 2.86 and 2.6 nm, respectively. These results strongly suggest that the surfaces of MWCNTs are coated by HBP, thereby increased the *D* values of HBCNT nanotubes. The relative high peak intensity of HBCNT2 reveals that 10 wt% HBP is an adequate to non-covalent functionalization of MWCNT.

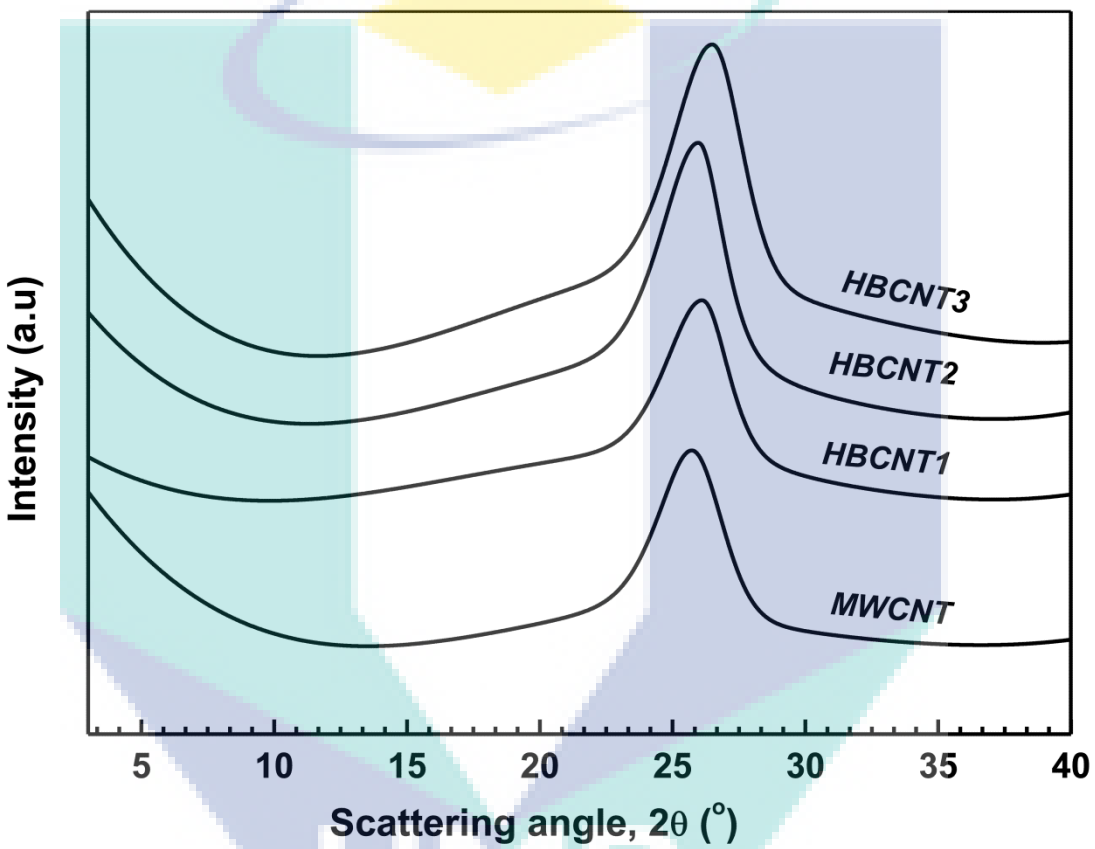

Figure 4.20: XRD profiles of MWCNT, HBCNT1, HBCNT2 and HBCNT3

(ii) DSC Analysis of HBCNT as a function of HBP concentration

Figure 4.21 represents the DSC thermograms of pristine MWCNT and HBP coated MWCNT. The MWCNT exhibits only one endothermic peak at around 103°C as glass transition (T_g), whereas, HBP coated MWCNTs showed distinguishable glass transition and melting transition at a higher temperature. The corresponding glass transition temperature peaks of HBCNT1, HBCNT2 and HBCNT3 appeared at around 108°C, 135°C, 118°C respectively. Additionally HBCNT2 exhibited the highest glass

transition temperature. It suggests that molecular motion was confined as well as plasticization effect was reduced as a result glass transition temperature was increased (Matthias Seiler, 2006; Pavlidou and Papaspyrides, 2008). Therefore, 10 wt% HBP is sufficient amount for potential non-covalent functionalization of MWCNT. Besides, the melting temperature of HBCNT suggested that HBP was melted on the surface of MWCNT. It is noticeable that there was no melting transition of pristine MWCNT within this operating temperature. Therefore, this observation revealed the presence of HBP on the surface of MWCNT.

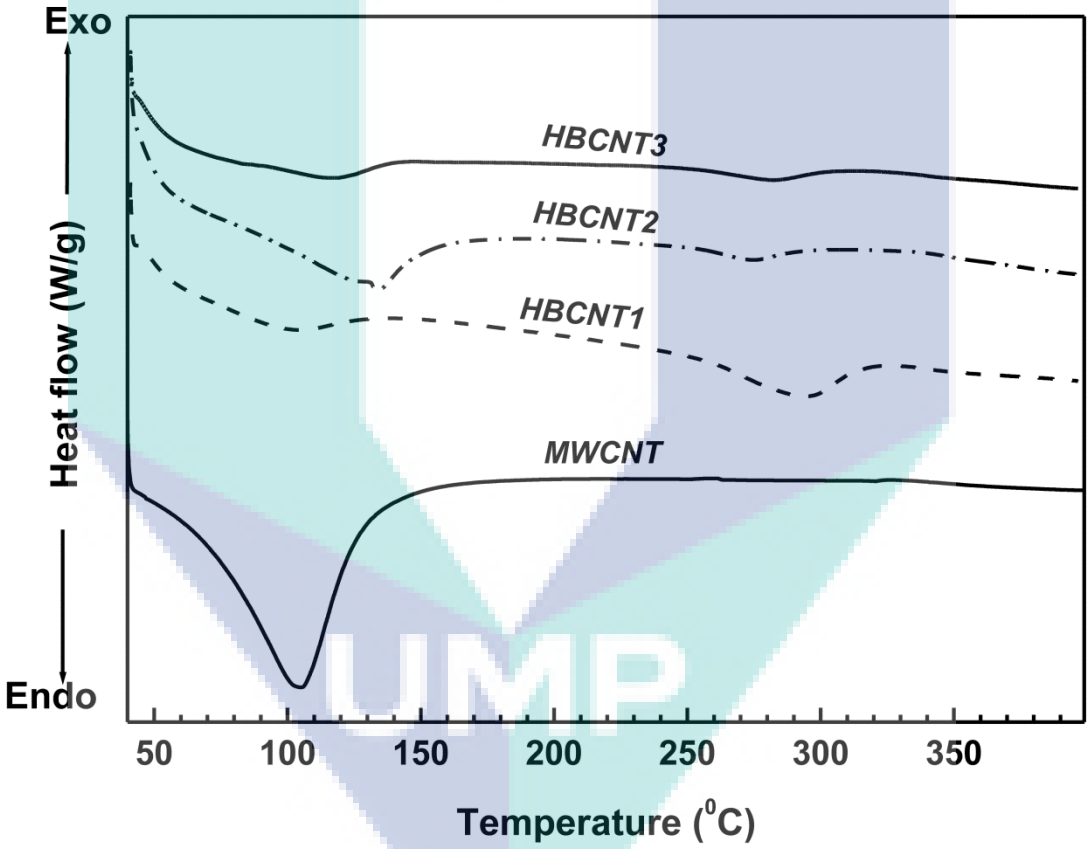

Figure 4.21: DSC thermograms of MWCNT, HBPCNT1, HBPCNT2 and HBPCNT3

(iii) Thermogravimetric Analysis of HBCNT as a function of HBP Concentration

Figure 4.22 represents the thermogravimetric behavior of pristine MWCNT, HBCNT1, HBCNT2 and HBCNT3. Initially pristine MWCNT was slowly lost around 11% weight from 30°C to 386°C temperature. However, the weight was sharply falling after 386°C to 695°C. At the end of heating it contained 24.5% residue. Likewise, HBCNTs were weight lost around 7% from 30°C to 240°C. The HBCNT1 thermogram represents 85% residue at the ranges of 240-280°C. The weight was slowly lost around 10 % from 280 to 700°C and finally, it contained 75% residue. Likewise, HBCNT2 was contained 90% residue at the range of 240-275°C. The weight steadily lost after 275^{0}C and contained 83% residue. Whereas HBCNT3 sharply weight lost 39% from 280 to 695^{0}C and at the end of heating, it contained 54% residue.

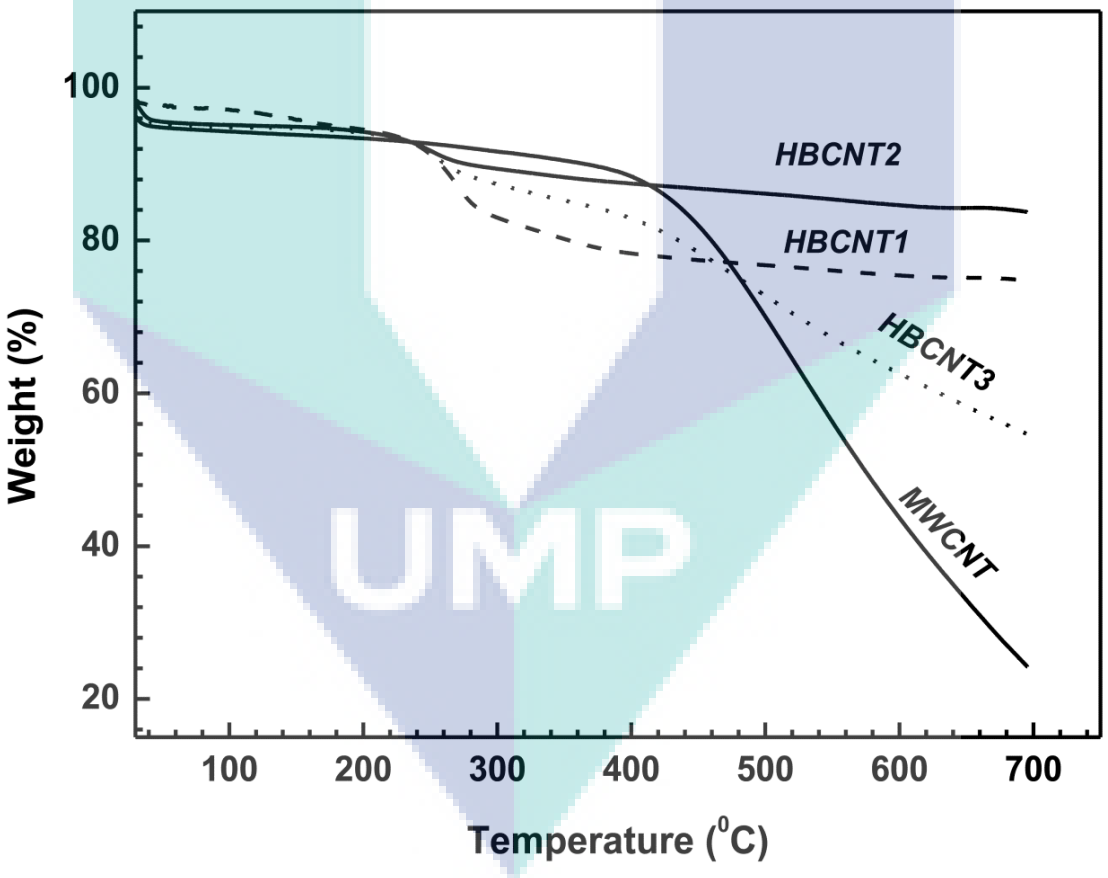

Figure 4.22: TGA thermograms of MWCNT and HBCNT

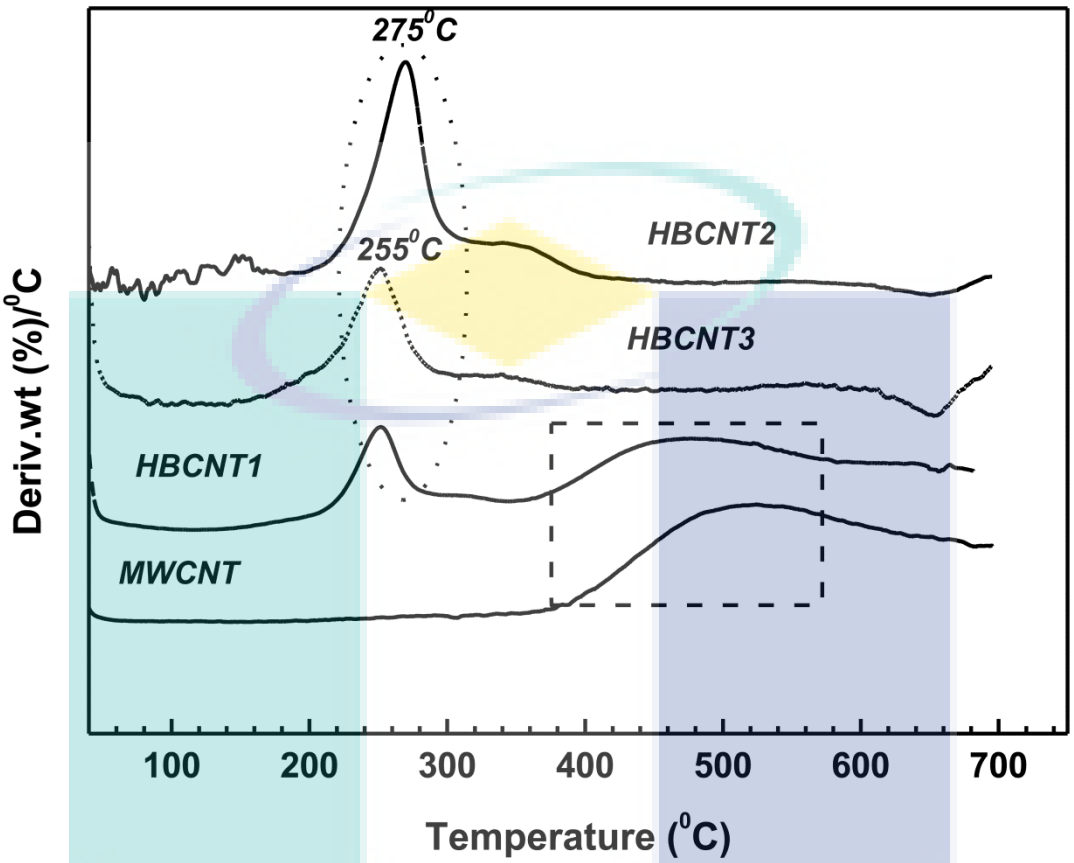

Figure 4.23: DTG thermograms of MWCNT and HBCNT

Therefore, TGA and DTG thermograms extensively clarify that HBP adhered on the surface of pristine MWCNT. In addition, the concentrations of HBP influence to remove the flaw of MWCNT. The thermal stability, residue content and decomposition stages notice that 10 wt% HBP is the optimum percentage to coat MWCNT.

(iv) Curing Behavior of HBCNT-UPR nanosuspensions

Figure 4.24 illustrates the curing exotherms of HBCNT-UPR1, HBCNT-UPR2 and HBCNT-UPR3 nanosuspensions. They revealed curing nature of HBCNT incorporated UPR matrix. Typically UPR is cured with styrene in the presence of peroxide through free radical copolymerization (Rouison et al., 2004). The nanosuspensions exhibited a distinguishable curing exotherm at a particular temperature. The corresponding curing temperatures of HBCNT-UPR1, HBCNT-UPR2 and HBCNT-UPR3 present in Table 4.5. In addition, HBCNT-UPR2 suspension cured

at 92^{0}C as the lowest temperature whereas MWCNT incorporated UPR suspension cured at 109^{0}C. Moreover, MWCNT-UPR nanosuspension exhibited 17.05 kJ/mol as the highest activation energy. The activation energy of HBCNTs is tabulated in Table 4.5.

Table 4.5: Curing temperatures and activation energies of HBCNT-UPR nanosuspensions

Samples	Curing Temperature (°C)	E_a (kJ/mol)
HBCNT-UPR1	99	16.60
HBCNT-UPR2	92	16.30
HBCNT-UPR3	97	16.52

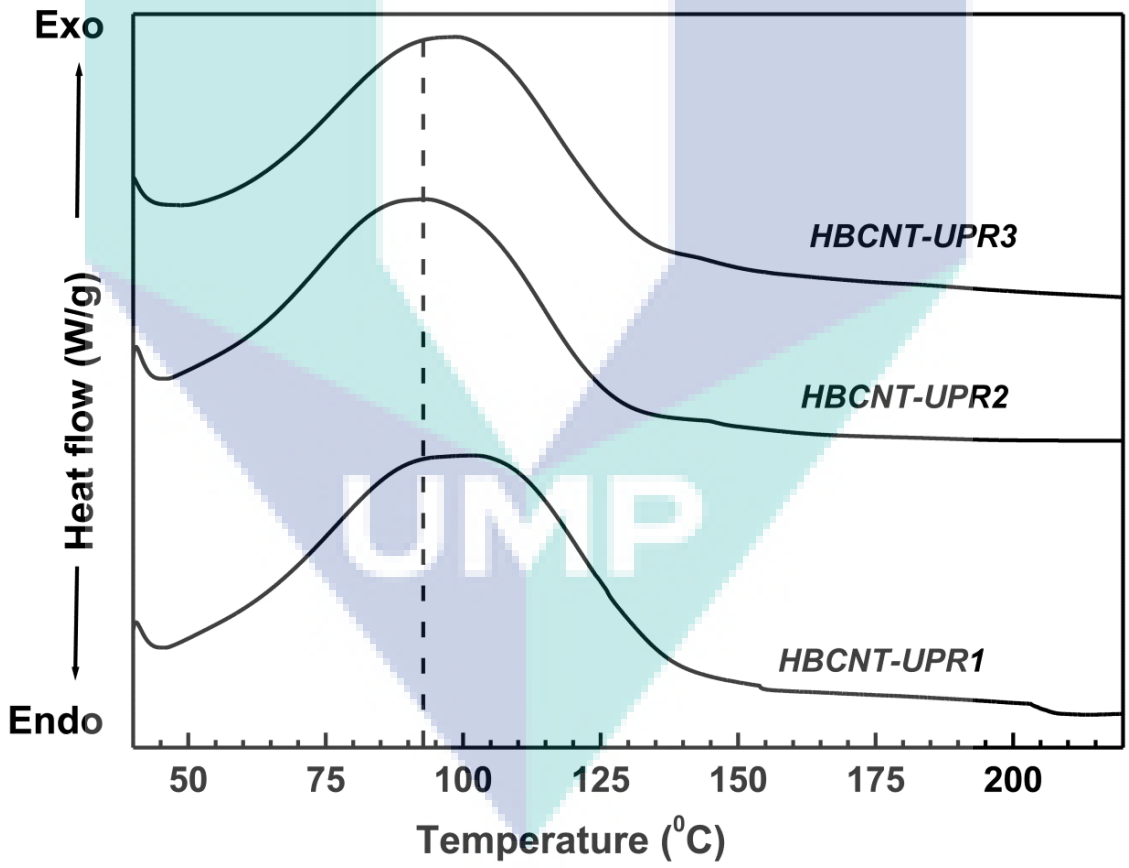

Figure 4.24: Curing thermograms of HBCNT-UPR1, HBCNT-UPR2 and HBCNT-UPR3

Therefore, curing temperature of HBCNT-UPR nanosuspension is a function of HBP concentration. The activation energy depends on the curing temperature as well. HBCNT-UPR2 nanosuspension revealed the lowest activation energy at 92°C; therefore 10 wt% HBP coated MWCNT performed as the best anti scavenger during curing of HBCNT-UPR2 nanosuspension (Martınez and Galano, 2010; Dodiuk et al., 2005). Additionally, the degree of dissociation in functional group of HBP molecule dependent on the HBP concentration which is a driving force to adsorb on the surface of CNT(Dorsa Parviz et al., 2012). The scheme of anti scavenger MWCNT presents in Figure 4.25.

In summary, structural and thermal analysis concur that HBP coated MWCNT exhibits better properties as compared to pristine MWCNT. However, these properties depend on the concentration of HBP. Among three concentrations of HBP 10 wt% has considered as the optimum amount of HBP to coat MWCNT. Later 10 wt% HBP coated MWCNT would be incorporated as OPHBCNT in UPR. Finally, OPHBCNT-UPR nanocomposite would be prepared for subsequent analysis.

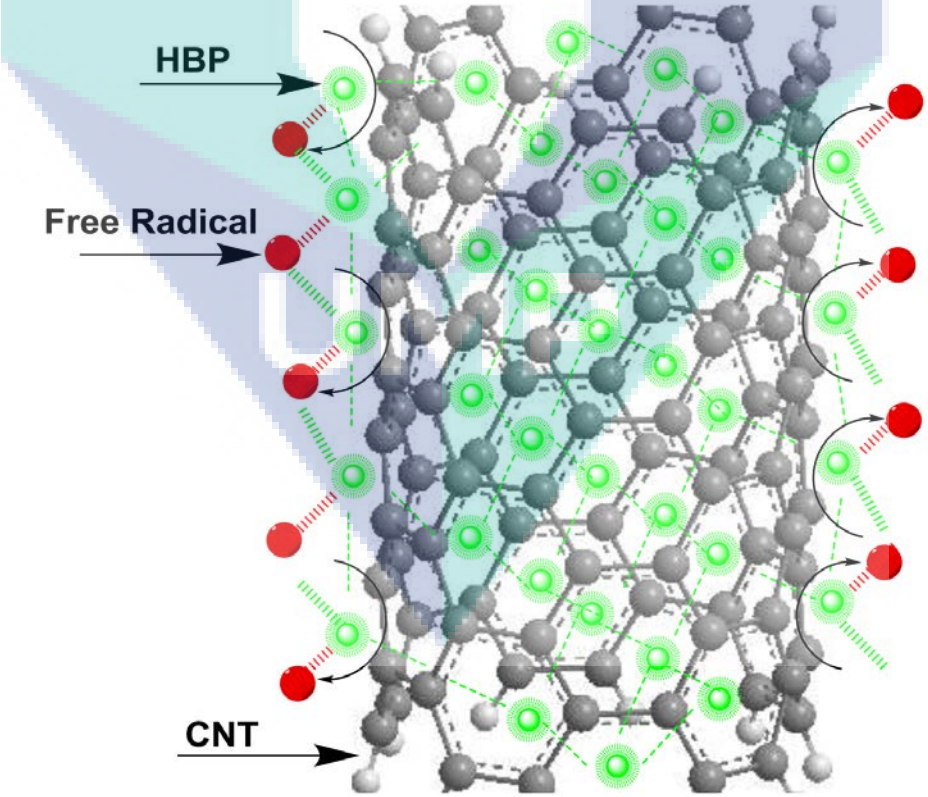

Figure 4.25: Schematic HBP coated MWCNT Anti scavenger

4.4.2 Comparative Characterization of UPR, CNT-UPR and HBCNT-UPR Nanocomposite

(i) Chemical interaction of HBP /MWCNT and between HBP coated MWCNT and UPR

The FTIR spectra of MWCNT, OPHBCNT, OPCNT-UPR and OPHBCNT-UPR nanocomposites are demonstrated in Figure 4.26. In addition, Table 4.6 represents the characteristic peaks and vibrational mode of these materials.

Table 4. 6: The characteristic FTIR peaks of MWCNT, OPHBCNT, OPCNT-UPR and OPHBCNT-UPR nanocomposites.

Samples	Wave number (cm^{-1})	Vibrational mode(s)
MWCNT	3436	Free O-H stretching and bending
	1633	
OPHBCNT	3434	O-H stretching
	1722	C=O stretching
	1638	C-C stretching
	1458-1280	C-H stretching
OPCNT-UPR	3695-3467	H-bonded O-H stretching
	1724	C=O stretching of carboxylic group
	1584-1453	-C=C- stretching in benzene
	1265-1066	-C-O stretching in carboxylic group
OPHBCNT-UPR	3664	O-H stretching
	1756	C=O stretching
	1292	C-O stretching
	941	O-H bending

The main features of MWCNT spectrum exhibit free O–H stretching at 3436 cm^{-1} and bending at 1633 cm^{-1}, which is assigned to O–H groups of adsorbed moisture (Sebastian Oswald et al., 2007). Evidently, the majority of the O–H vibrations originate

from moisture in the sample rather than from the functional groups attached to the surface of the MWCNTs. The sharp peak at around 1633 cm^{-1} is due to the C–C stretching of aromatic ring. In OPHBCNT spectrum, the peak at 3434 cm^{-1} is due to the formation of hydrogen bond between HBP and MWCNT. The peak at 1722 cm^{-1} is related to C=O stretching in ester. Furthermore, the C–C stretching is shifted to 1638 cm^{-1}, expressing the π-π interaction of HBP and MWCNT. Besides, multiple peaks at around 1458 to 1280 cm^{-1} are due to C–H stretching, rocking of alkane etc., which reveal the presence of HBP on MWCNT surface.

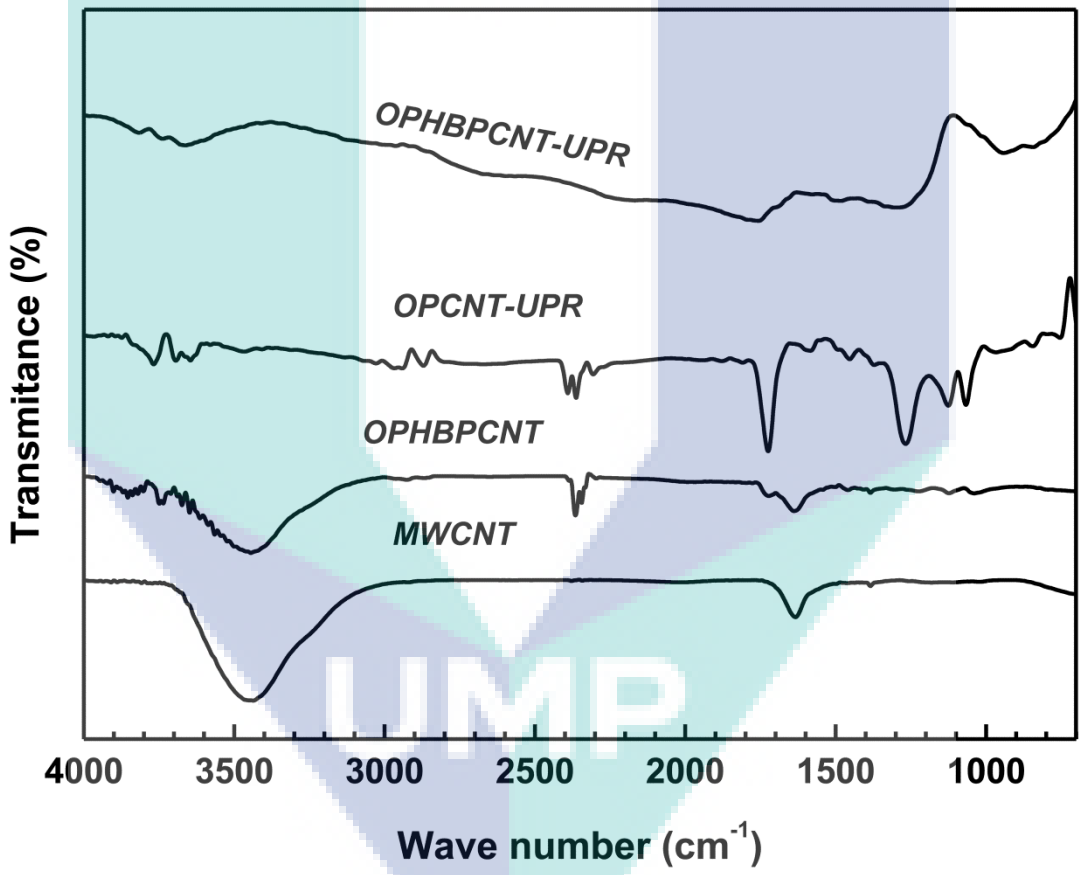

Figure 4.26: FTIR spectra of MWCNT, HBCNT, OPCNT-UPR, OPHBCNT-UPR

Besides, the OPCNT- UPR nanocomposite spectrum expresses the interaction between the surface O-H group of MWCNT and >C=O / C-O groups of UPR. The peaks appear at 3467-3695 cm^{-1} revels O-H stretching as a result of formation of H-bond (Alam et al., 2012; Desai and Haque, 2005). In addition, >C=O and C-O

functional groups peak shifted to1724 cm^{-1} and 1066-1265 cm^{-1} respectively, which mean the formation of hydrogen bond interaction between MWCNT and UPR.

On the other hand, OPHBCNT-UPR spectrum shows the absorption peak at 3664cm^{-1} which reveals that hydrogen bond exist in this nanocomposite. The corresponding stretching peaks of C=O and C-O are appeared at 1756cm^{-1} and 1292cm^{-1} which notice that C=O and C-O in esters performed interaction with UPR in the nanocomposite. Likewise, the O-H bending peak in HBCNT-UPR appears at 941cm^{-1} reveals the O-H of carboxylic groups in UPR interact with HBPCNT. The schematic interaction among HBP, MWCNT and UPR is illustrated in Figure 4.27.

Finally, the FTIR analysis confirmed the existence of HBP on the surface of MWCNT, furthermore, the HBP coated MWCNT participated in strong interaction with UPR matrix.

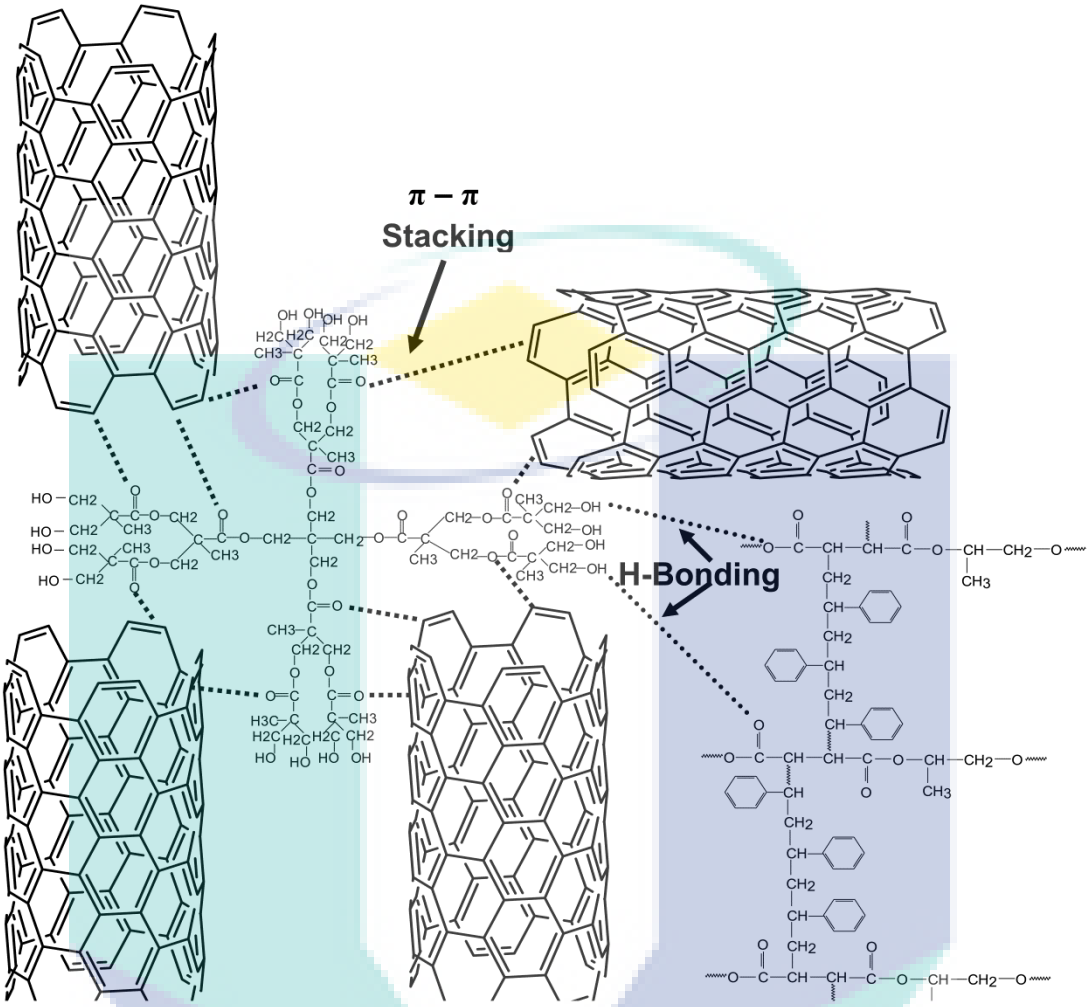

Figure 4.27: Schematic interaction of HBP, MWCNT and UPR

(ii) Plain surface morphology of OPCNT-UPR and OPHBCNT-UPR nanocomposites

Figure 4.28 represents the plain surface morphology of MWCNT-UPR and HBCNT-UPR nanocomposites. It is obvious that HBCNTs are noticeably embedded and homogeneously dispersed into UPR matrix, whereas pristine MWCNTs in MWCNT-UPR are loosely and randomly stacked. Therefore, it is recommended that wettability of UPR is relatively higher to HBPCNT as compare to pristine MWCNT.

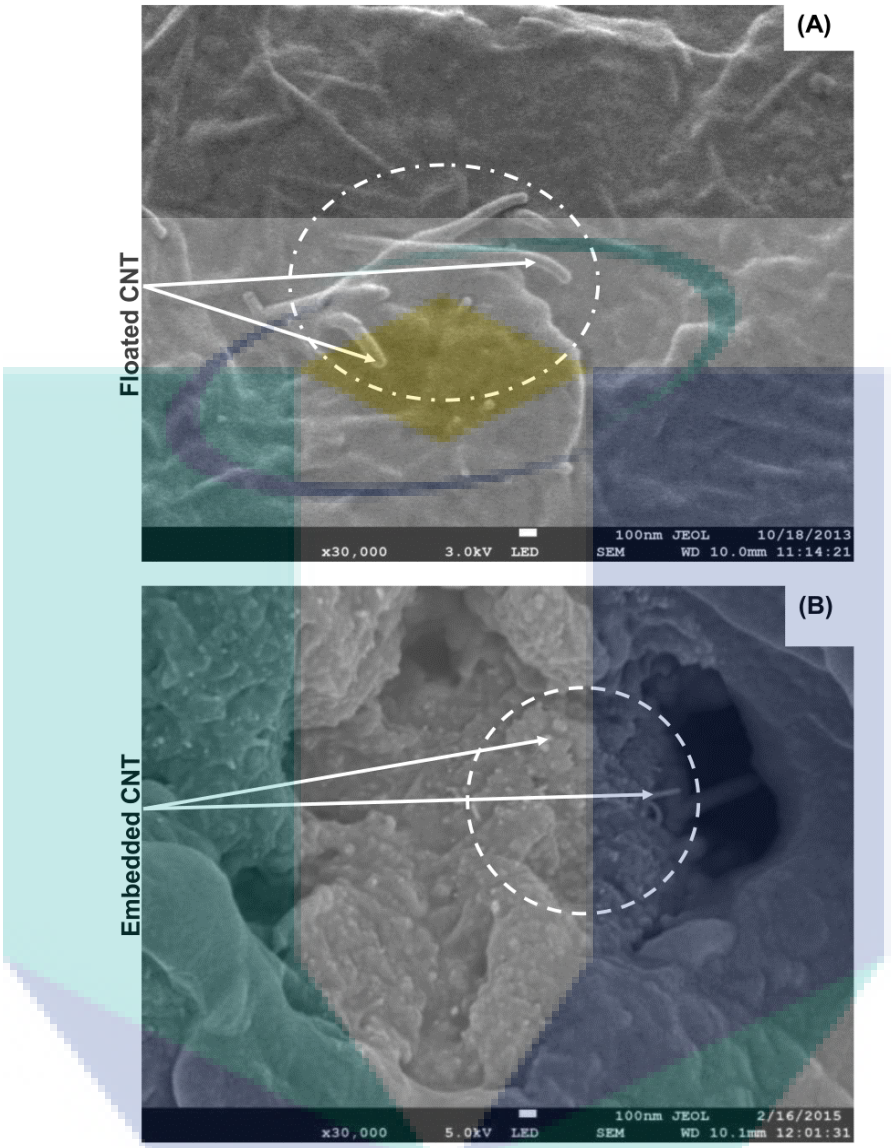

Figure 4.28: Plain surface morphology of (A) OPCNT-UPR and (B) OPHBCNT-UPR nanocomposites

(iii) Mechanical properties of neat UPR, OPCNT-UPR and OPHBCNT-UPR nanocomposites

The *TS* and *TM* of neat UPR, OPCNT-UPR and OPHBCNT-UPR nanocomposites are presented in Figure 4.29. The corresponding *TS* values of these samples are around 28.72±1.20, 40±1.31 and 48.5±1.63 MPa and *TM* are 1247±122, 1698±190 and 2156.5±101 MPa. Thus, the *TS* and *TM* of OPHBCNT-UPR nanocomposite increased by an amount of 21.5% and 27% as compared to OPCNT-

UPR nanocomposite respectively. Additionally, the *TS* and *TM* of OPHBCNT−UPR nanocomposite increased by 68% and 73.73% correspondingly as compared to the neat resin.

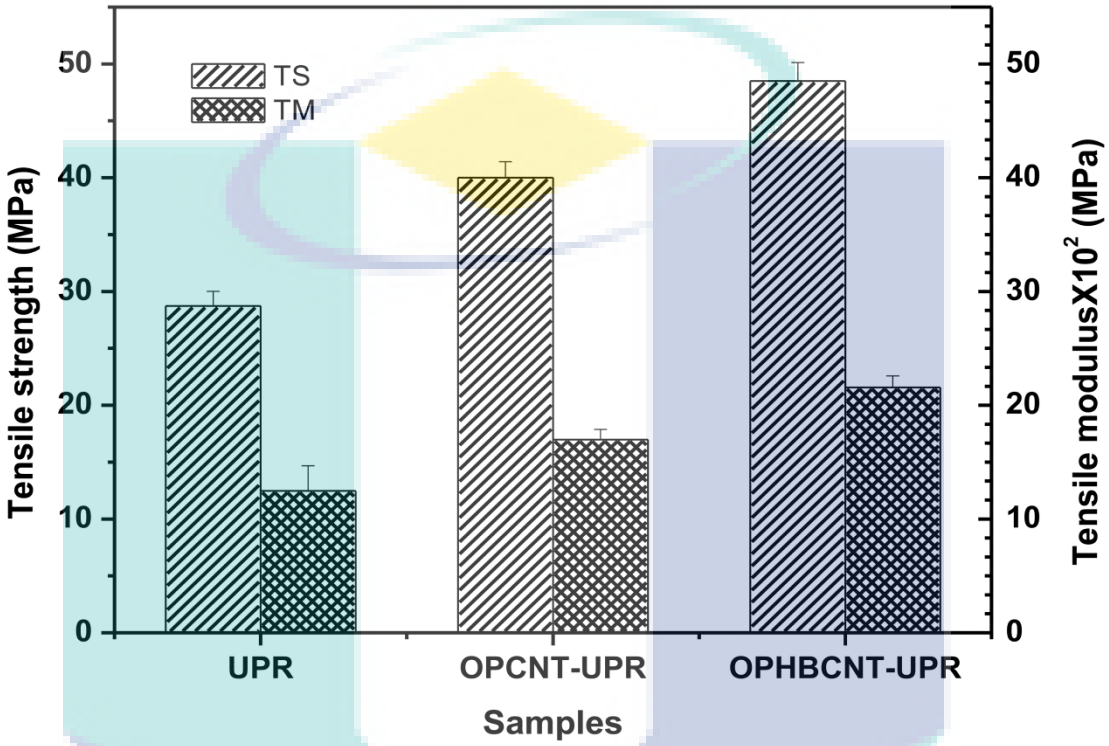

Figure 4.29: TS and TM of UPR, OPCNT-UPR and OPHBCNT-UPR nanocomposites

The plots of *IS* and *EB* for different samples are shown in Figure 4.30. The values of *IS* and *EB%* for UPR are 3.58±0.37 kJ/m^2 and 4.6±0.25% and those for OPCNT-UPR are 4.70±0.29 kJ/m^2 and 4.36±0.14%, as well as for OPHBCNT-UPR are 3.33±37 kJ/m^2 and 4±0.23% respectively. Therefore, the *IS* and *EB%* of OPHBCNT-UPR were decreased by an amount of 29% and 8.25% as compare to OPCNT-UPR respectively. Likewise, *IS* and *EB* of OPHBCNT-UPR nanocomposite decreased by an amount of 7 % and 13.04% as compared to neat UPR.

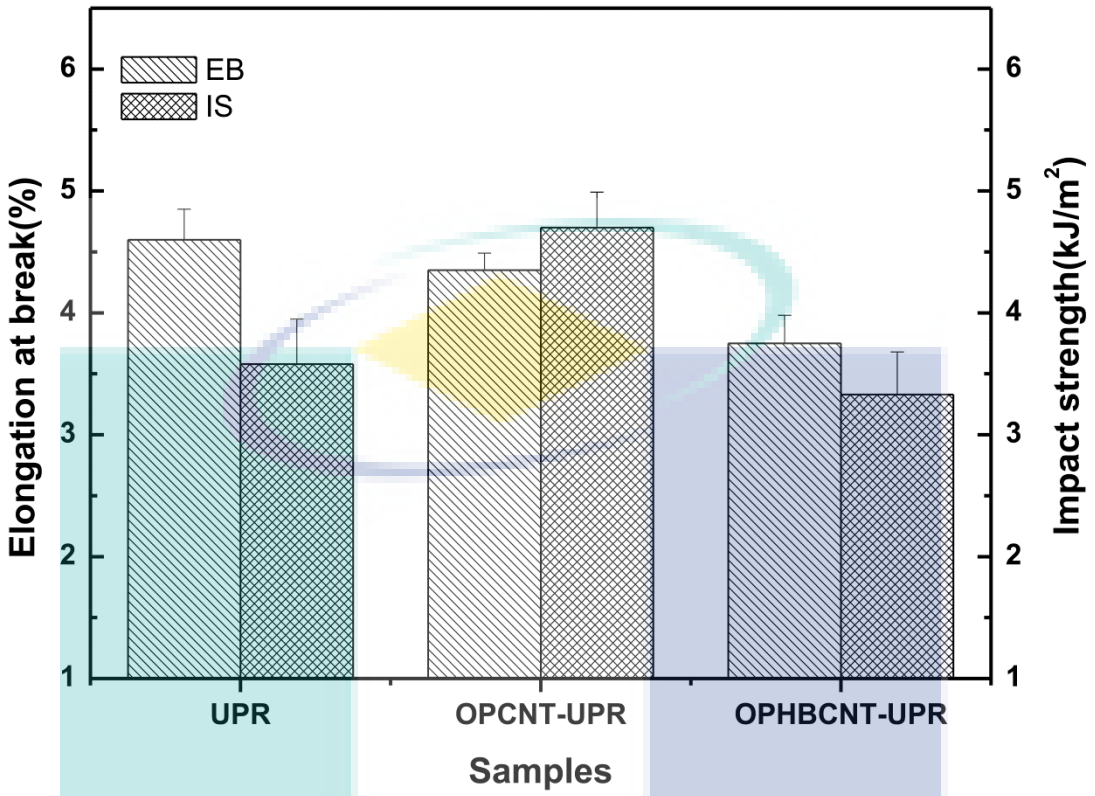

Figure 4.30: IS and EB of UPR, OPCNT-UPR and OPHBCNT-UPR nanocomposites

These properties reveal that HBCNT increases the stiffness of the neat resin. In addition, these results clearly demonstrate a good reinforcement effect of HBP coated MWCNT on the mechanical properties of the nanocomposite.

(iv) Fracture morphology of OPHBCNT-UPR nanocomposite

The fracture morphology of OPCNT-UPR (A) and OPHBCNT−UPR (B) are demonstrated in Figure 4.31. Surface crack, entangled MWCNT pull out, broken MWCNT, bridge of MWCNT have marked by arrows and dotted circles. There are no visible fractures found in OPHBCNT-UPR nanocomposite micrograph, huge fracture tips are visible on that surface. In addition, HBCNT not only unbroken but also shielded the crack propagation through bridging. These results also support a better adhesion between HBCNTs and UPR molecules. Thus, HBP coating on MWCNT surface revealed a good avenue for sound dispersion and well interaction with matrix.

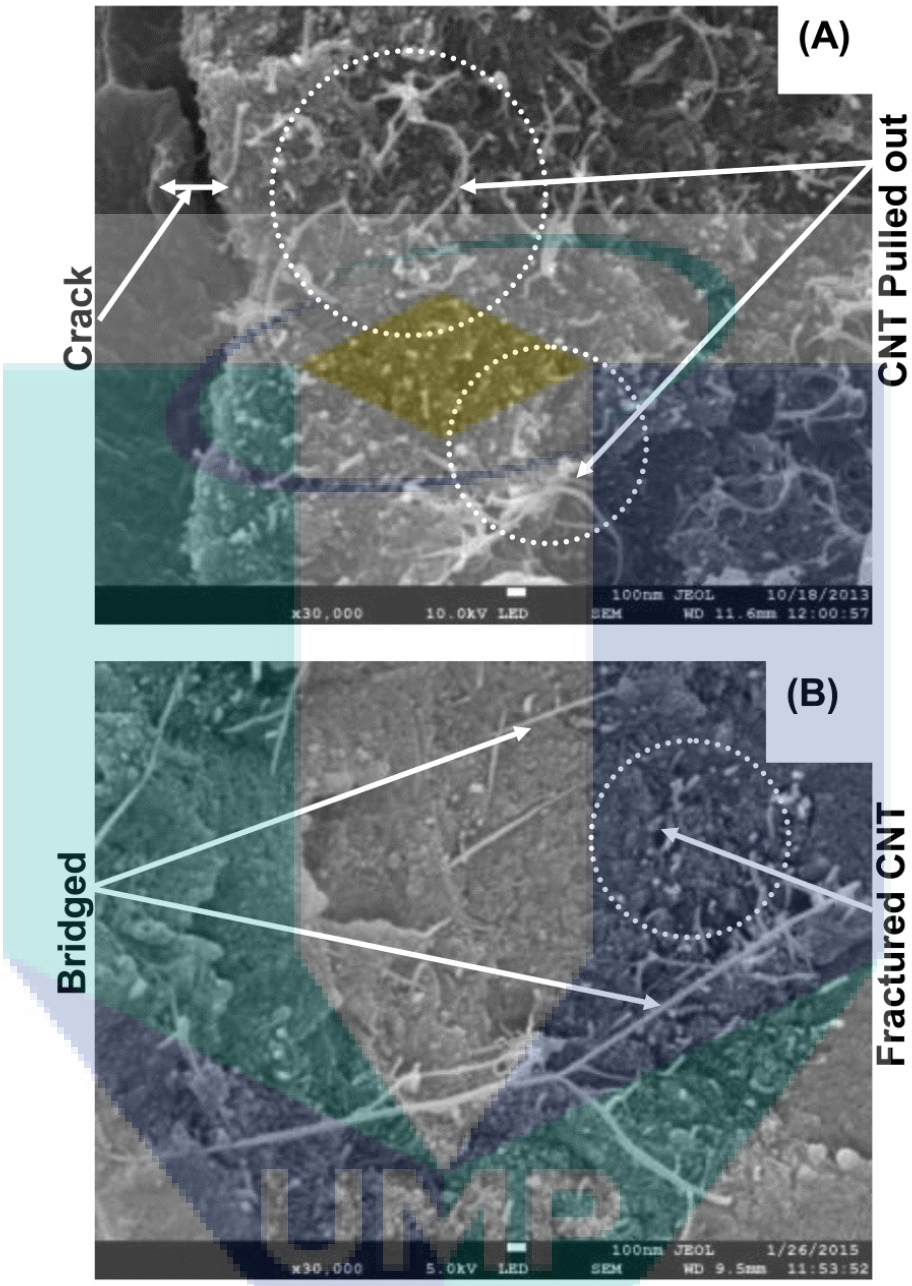

Figure 4.31: Fracture surface of OPCNT-UPR (A) and OPHBCNT-UPR (B) nanocomposites

Conversely, noticeable fracture is found on the surface of OPCNT-UPR. Several nanotubes were pulled out during stretching of that nanocomposite. Therefore, HBCNT can lead to modify the segmental morphology of nanocomposite and influence the mechanical properties as reported elsewhere (Kim et al., 2006; Desai and Haque, 2005).

(v) Comparative XRD Analysis of neat resin, OPCNT-UPR and OPHBCNT-UPR Nanocomposites

Figure 4.32 represents the XRD profiles of neat UPR, OPCNT-UPR and OPHBCNT-UPR nanocomposites and Table 4.7 illustrates the lattice parameter and crystalinity of these samples. The peak position of OPHBCNT incorporated UPR nanocomposite is shifted to a lower scattering angle at 17.63°, which reveals a lattice constant of 4.93 Å. On the other hand, the corresponding scattering angles of neat UPR and OPCNT-UPR are appeared at 23.43° and 18.91° which corresponds to partial crystalline and amorphous natures. The average lattice spacing of UPR and OPCNT-UPR was estimated around 3.7 Å and 4.61Å respectively. Therefore increase in lattice parameter of OPHBCNT-UPR nanocomposite as compare to OPCNT-UPR may be ascribed to the better intercalation between HBCNT nano tubes and matrix, providing a lattice distortion in UPR crystals. Moreover from these observations, it can be conferred that the HBCNTs are distributed well in UPR matrix, leading to an increase in the interfacial adhesion among HBCNT filler and matrix, which is consistent with the previously reported result for carbon black reinforced epoxy/resin (Abdel-Aal et al. 2008). Furthermore, a decrease in peak width and increase in peak intensity of OPHBCNT-UPR nanocomposite is also observed. The estimated degrees of crystallinity (χ_c), for OPHBCNT-UPR nanocomposite is 27%. In practical, decrease in peak width notice that the crystal size of the nanocomposite increases and more population of UPR molecules were taken part in crystallization due to HBP functionalization of MWCNT.

Table 4.7: Comparative FWHM, lattice spacing and crystal size, percentage of crystallinity of OPHBCNT-UPR nanocomposite

Samples	2θ	FWHM	dÅ	DÅ	λ	χ (%)
UPR	23.43	9.44	3.7	8.4		14
OPCNT-UPR	18.91	5.20	4.61	15.26	1.514	24
OPHBCNT-UPR	17.63	4.75	4.93	16.68		27

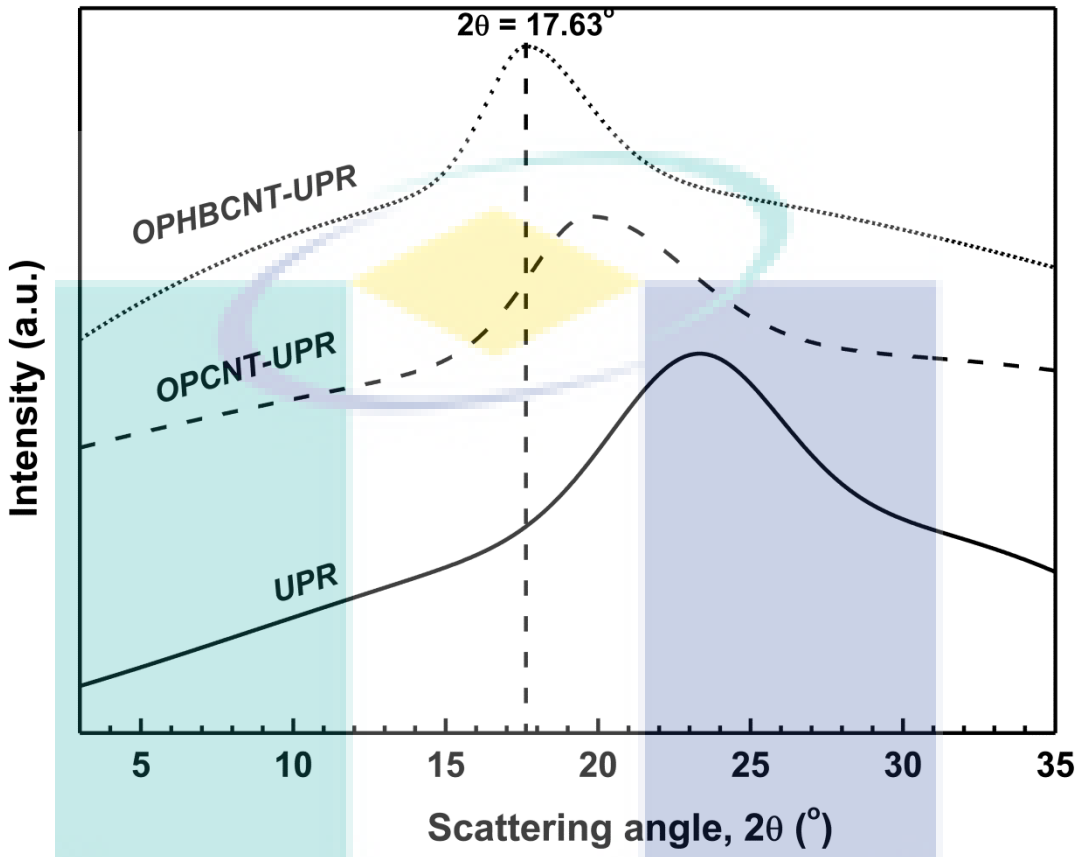

Figure 4.32: XRD profiles of UPR, OPCNT-UPR and OPHBCNT-UPR

(vi) Thermal transition of OPHBCNT-UPR Nanocomposites

Figure 4.33 depicts the DSC thermograms of neat UPR, OPCNT−UPR and OPHBCNT−UPR nanocomposite. The endothermic peak at the lower temperature region for all samples, ascribe to the glass transition temperature (T_g); recommend thermal motion of polymer chain molecules. The exothermic transition in OPHBCNT-UPR thermogram represents crystallization exotherm (T_c). In addition, the endothermic transition at the higher temperatures is related to the melting temperature (T_m) of UPR and nanocomposites as well. Table 4.8 represents the characteristic temperature of those transitions. Instead of one endothermic peak as shown by UPR matrix, both nanocomposites exhibit a split melting endotherm into two peaks (T_{m1} and T_{m2}).

The presence of double melting endotherms in nanocomposites, indicate the formation of bond between MWCNT and UPR. The sharp peak at T_{m2} is a precursor to identifying the binding energy between nanotubes and UPR molecules. The peak appearance of DSC thermogram and FTIR spectra, suggesting the formation of the bond between the HBP coated MWCNT and UPR molecule.

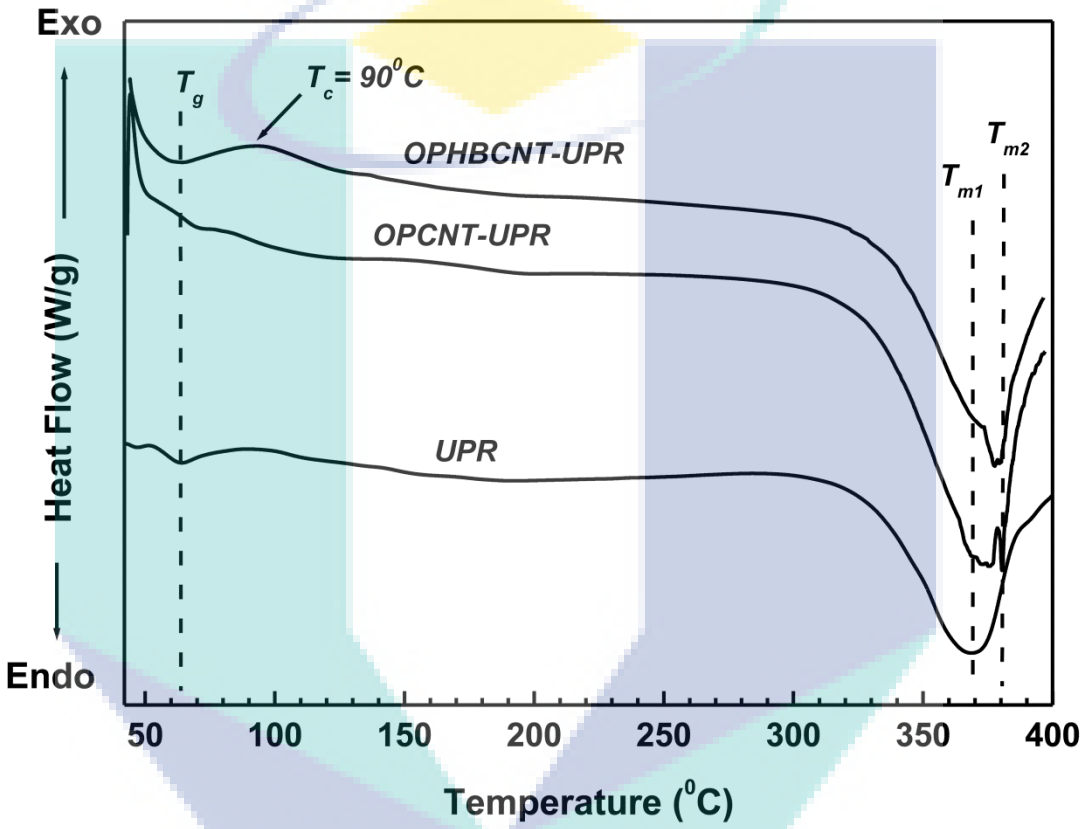

Figure 4.33: DSC thermograms of UPR, OPCNT-UPR and OPHBCNT-UPR nanocomposites

Table 4. 8: Characteristic transition temperature OPHBCNT-UPR nanocomposite in DSC and TGA thermograms

Samples	T_g (°C)	T_c (°C)	T_{m1}(°C)	T_{m2}(°C)	T_d
UPR	62	-	370	-	378
OPCNT-UPR	68	-	375	380	395
OPHBCNT-UPR	62	88	376	381	399

Evidently, in spite of plasticization effect as well as the flexibility of HBCNT, the nanocrystalline regions of OPHBCNT-UPR nanocomposite become relatively well ordered, as a result the T_c exotherm is appeared as well as enhanced the sharpness of recrystallization temperature (Allaoui and Bounia 2009; Seymour and Cooper 1973). The nucleating effect of the well dispersed HBCNTs has considered in the crystallinity of nanocomposite. Such a crystallization and enhancement of crystallinity in UPR by introducing carbon black has been pronounced in a recently published article (Alam et al., 2014).

(vii) Thermogravimetric Analysis of OPHBCNT-UPR nanocomposite

The thermogravimetric curves of UPR and OPCNT-UPR and OPHBCNT-UPR nanocomposites are presented in Figure 4.34. The materials were disintegrated in some stages. Thermal decomposition of UPR took place at around 313°C and came to an end at around 446°C. In contrast, OPCNT-UPR and OPHBCNT-UPR nanocomposites' degradation began at relatively higher temperature than UPR matrix (Cao and Lee, 2003; Martı´nez and Galano, 2010).The degradation of cross-linked resin has been ascribed by the dissociation of C−C chain bonds and release of styrene at the site of dissociation (Abdalla et al., 2007; Manfredi et al., 2006).

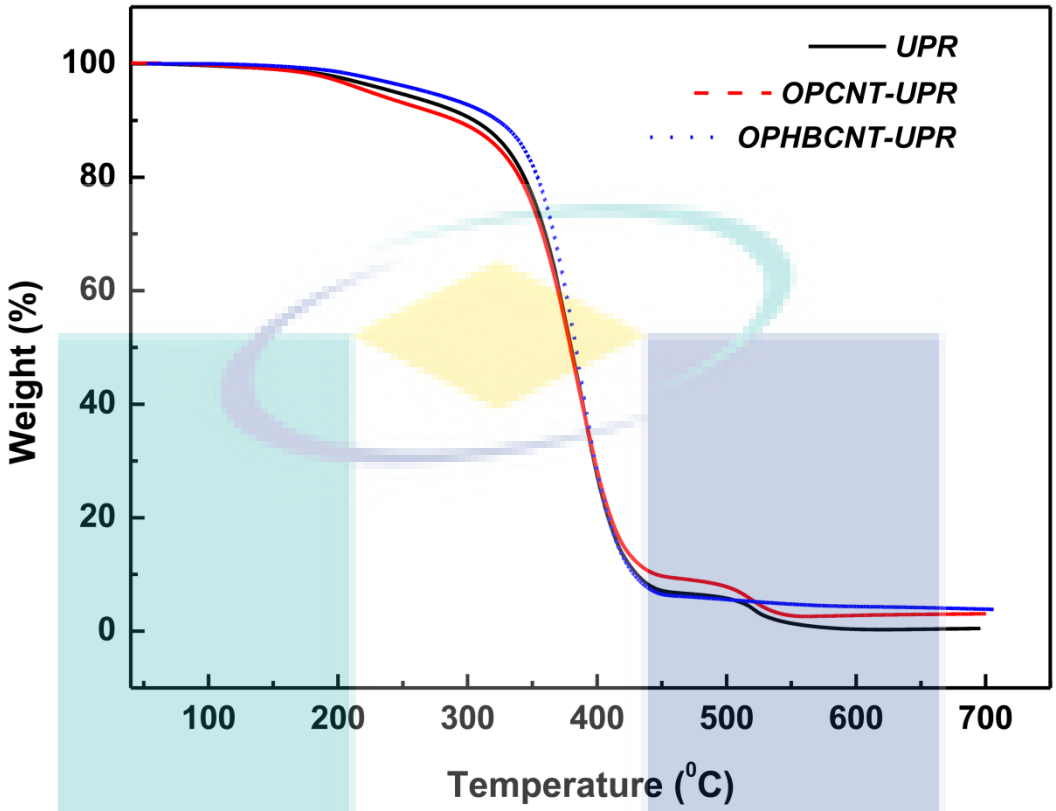

Figure 4.34: TGA thermograms of UPR, OPCNT-UPR and OPHBCNT-UPR nanocomposites

While, degradation temperature (T_d) can be obtained from TGA traces, the T_d at 50% weight loss of a sample as a sign of structural deterioration. Therefore, T_d values assessed for UPR, OPCNT-UPR and OPHBCNT-UPR from TGA curves are introduced in Table 4.8. The residue content at 600°C shows a significant difference between the OPCNT-UPR and HBCNT-UPR nanocomposites perhaps due to HBP coated MWCNT loading in resin (Kubota, 1975).

The DTG thermograms in Figure 4.35 illustrate the decomposition stages of UPR and OPCNT-UPR and OPHBCNT-UPR nanocomposites. The decomposition stages are mentioned by dotted rectangle and circle.

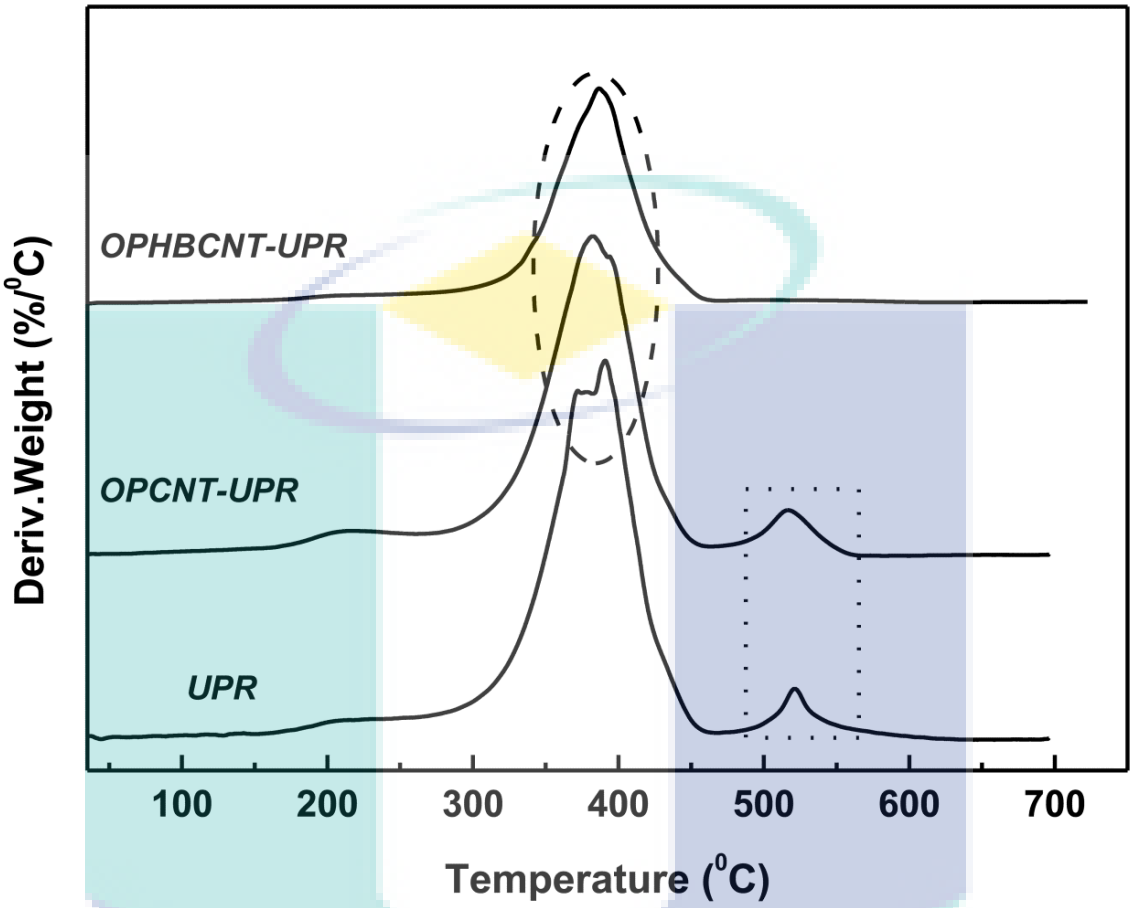

Figure 4.35: DTG thermograms of UPR, OPCNT-UPR and OPHBCNT-UPR nanocomposites

The shoulder like first stage peak of UPR and OPCNT-UPR are appeared at around 200-245°C which referred as the degradation temperature of unreacted styrene, polyester resin (Manfredi et al., 2006). The second stage split decomposition of them is demonstrated at around 300-400°C. In this temperature range, degradation of OPCNT−UPR nanocomposite was quite different from UPR where OPCNT−UPR nanocomposite was disintegrated at higher temperature than that of UPR. The third decomposition stage of them is at around 500-550°C which perhaps due to C-C chain session. On the other hand OPHBCNT-UPR nanocomposite was decomposed only one stage at around 400°C.

This decomposition is most likely due to the good interaction between HBCNT and UPR, as revealed by FTIR and mechanical properties of that nanocomposite. It is

considered that in the case of OPHBCNT-UPR nanocomposite, either formation of bonding or strong interface between HBCNT and UPR, which acts as single phase component. As a result, OPHBCNT-UPR nanocomposite decomposed only single stage.

4.5. CHARACTERIZATION OF SHELLAC COATED MWCNT AND SHELLAC COATED MWCNT REINFORCED NANOCOMPOSITES

4.5.1 Optimization of Shellac Concentration

(i) Structural analysis of shellac coated MWCNT

Figure 4.36 represents the X-ray diffraction profiles of MWCNT, SLCNT1, SLCNT2 and SLCNT3. MWCNT profile shows a well defined peak at around 2θ = 25.71° with FWHM of 2.92° which corresponds to the plane of hexagonal graphite-like structure of MWCNT (Nouralishahi et al., 2014). Similarly the scattering peaks of SLCNT1, SLCNT2 and SLCNT3 are appeared at around 25.82°, 25.72°, 25.79° respectively. In addition the corresponding FWHM of these nanotubes are 2.07°, 2.72°, 2.70°. From these observation, the crystallite size (*D*) of pristine MWCNT, shellac coated MWCNTs have been estimated by Scherer's equation (Liu et al., 2014).

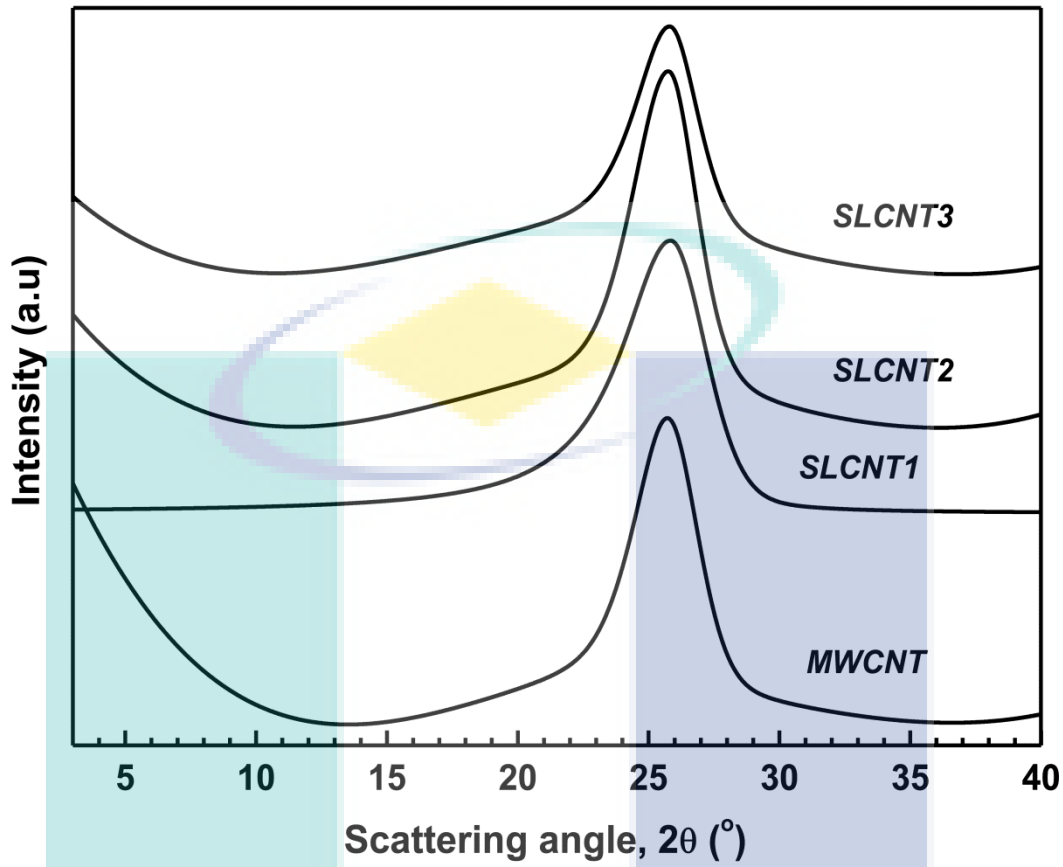

Figure 4.36: XRD profiles of MWCNT and Shellac coated MWCNT (SLCNT)

The crystal size of pristine MWCNT, SLCNT1, SLCNT2 and SLCNT3 were estimated about 2.30 nm, 2.07nm, 2.72nm, and 2.7nm correspondingly. These results suggest that surface of MWCNTs were coated by shellac, thereby increasing the crystal size. The peak intensity of SLCNT2 revealed as the highest at 25.74° as compared to that of MWCNT, SLCNT1 and SLCNT3. Therefore MWCNTs were well aligned in SLCNT2. Finally this observation recommends that 10 wt% shellac can be considered a satisfactory amount for non-covalent functionalization of MWCNT.

(ii) DSC analysis of shellac coated MWCNT

Figure 4.37 represents the DSC thermograms of MWCNT and shellac coated MWCNT. The MWCNT exhibits only endothermic peak at around 103°C as glass transition (T_g). Likewise, shellac coated MWCNTs show glass transition endotherm at different temperature. The corresponding glass transition temperature of SLCNT1,

SLCNT2 and SLCNT3 are appeared at about 109°C, 112°C and 93°C. It is significant that there were no melting endotherms appeared on the thermograms of shellac coated CNT which notice shellac was uniformly coated on the surface of MWCNT. However at high concentration of shellac the T_g value of SLCNT3 decreased remarkably, it means 15 wt% was an excess amount predominant on the glass transition. Therefore, high concentration of shellac performed as plasticizer. Due to plasticizing effect of shellac which reduce the intermolecular forces as well as rigidity of SLCNT structure and increase the mobility of polymer chain as a result decrease glass transition temperature of SLCNT3 to 93°C (Pavlidou and. Papaspyrides, 2008). Only SLCNT2 nanotubes exhibit glass transition at the highest temperature. It seems that molecular motion of shellac was confined as well as nucleation effect was influenced at that shellac concentration. (Pavlidou and. Papaspyrides, 2008; Matthias Seiler, 2006). Therefore 10 wt% shellac was the adequate amount for potential coating and non-covalent functionalization of pristine MWCNT.

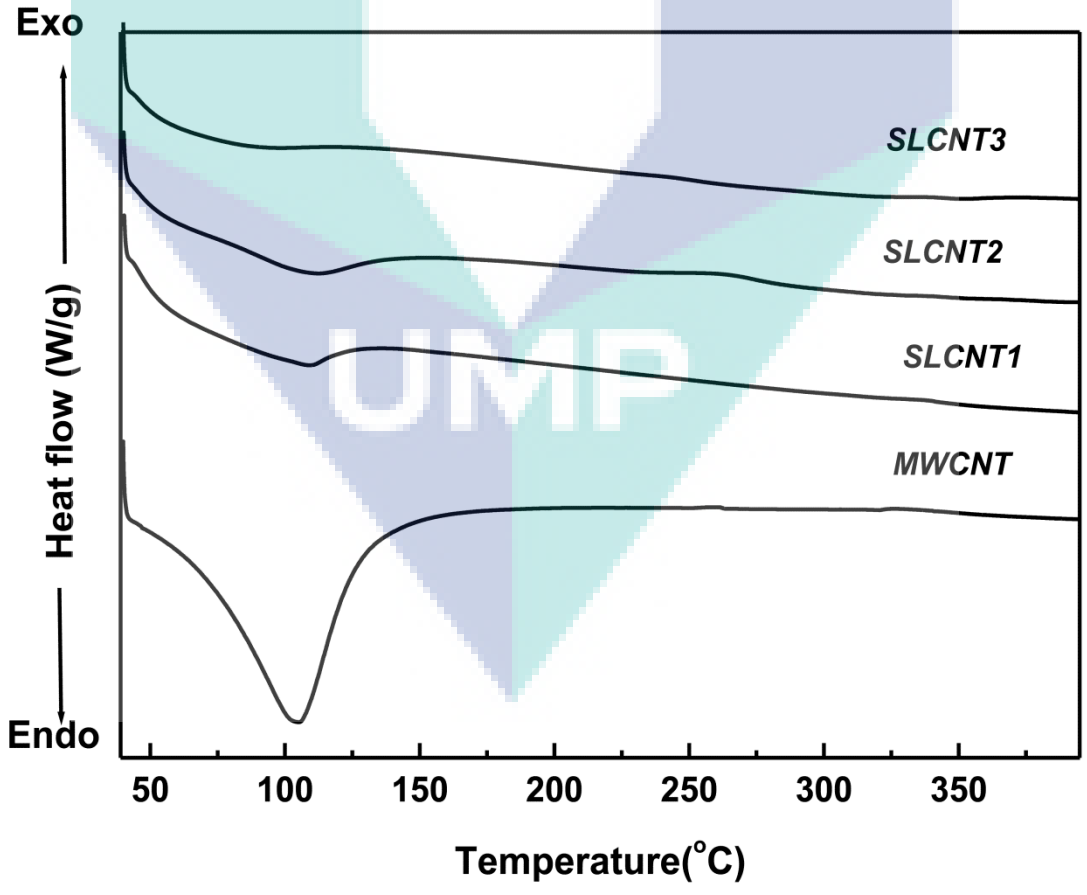

Figure 4.37: DSC Thermograms of MWCNT and Shellac coated MWCNT

(iii) Thermogravimetric analysis of SLCNT

Figure 4.38 represents the decomposition behavior of pristine MWCNT, SLCNT1, SLCNT2 and SLCNT3. MWCNT was steadily lost 11% weight at the beginning of heating temperature from 30°C to 386°C which was sharply falling after 386°C to 695°C. At the end of heating it was partially decayed and finally contained 24.5% residue. However shellac coated MWCNTs was steadily losing weight within the temperature range. Moreover the degradation rate of SLCNT was depended on the shellac concentrations. Finally the residue content at 700°C was decreased as the shellac content on the surface of MWCNT was increased which are represented in Table 4.9. These observations notice that thermal stability of SLCNT is greater at low concentration of shellac solution.

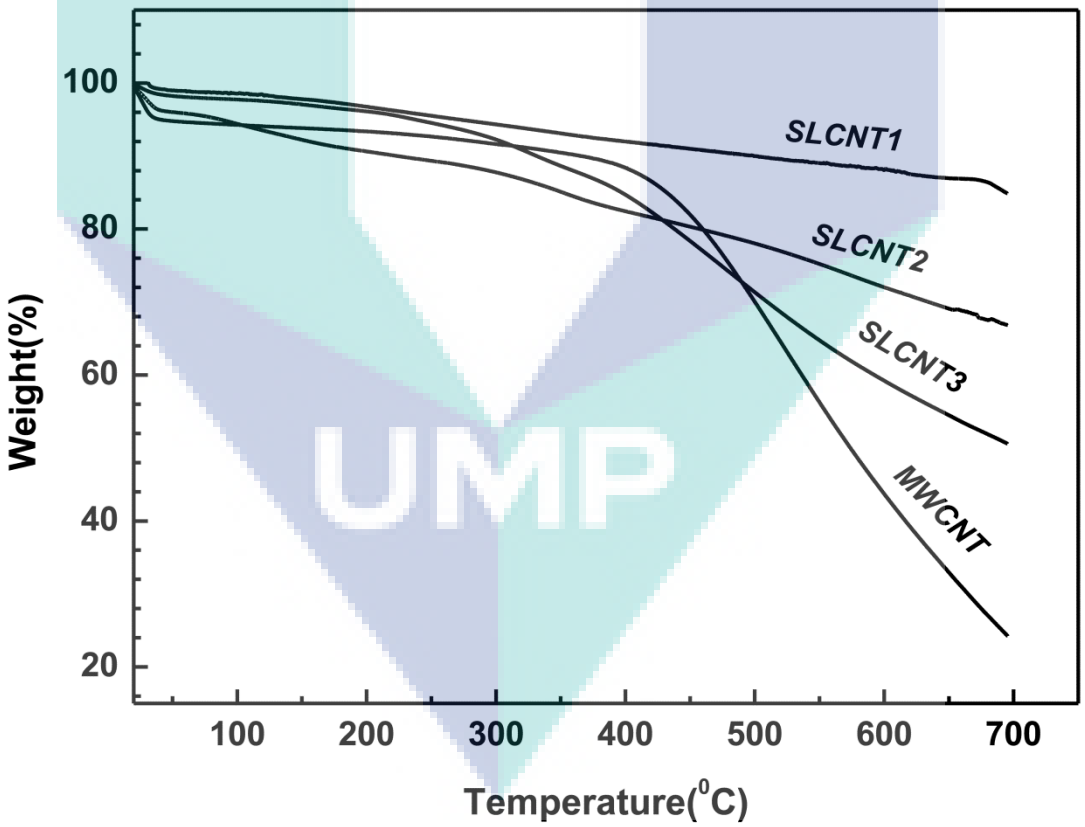

Figure 4.38: TGA thermograms of MWCNT and Shellac coated MWCNT (SLCNT)

Table 4. 9: T_g, T_c and residue content of SLCNT at different concentration of shellac

Samples	T_g (°C)	Residue at 700°C (wt %)
MWCNT	103	24.5
SLCNT1	109	84.67
SLCNT2	112	66.97
SLCNT3	93	50.71

Figure 4.39 represents the degradation pattern of pristine MWCNT, SLCNT1, SLCNT2 and SLCNT3. MWCNT was decomposed only one stage at around 400 to 600, whereas shellac coated nanotubes were decomposed at different stages. The decomposition of SLCNT1 is perhaps due to a small amount of shellac does not able to coat most of the MWCNT. On the contrary, at a high concentration of shellac in SLCNT3, shellac seems to be coagulated then could not effectively coat the MWCNT. Therefore, decomposition behavior of SLCNT3 was as like as MWCNT. However, SLCNT2 exhibited a limited number of decomposition stages as compared to the SLCNT1, SLCNT3 and MWCNT.

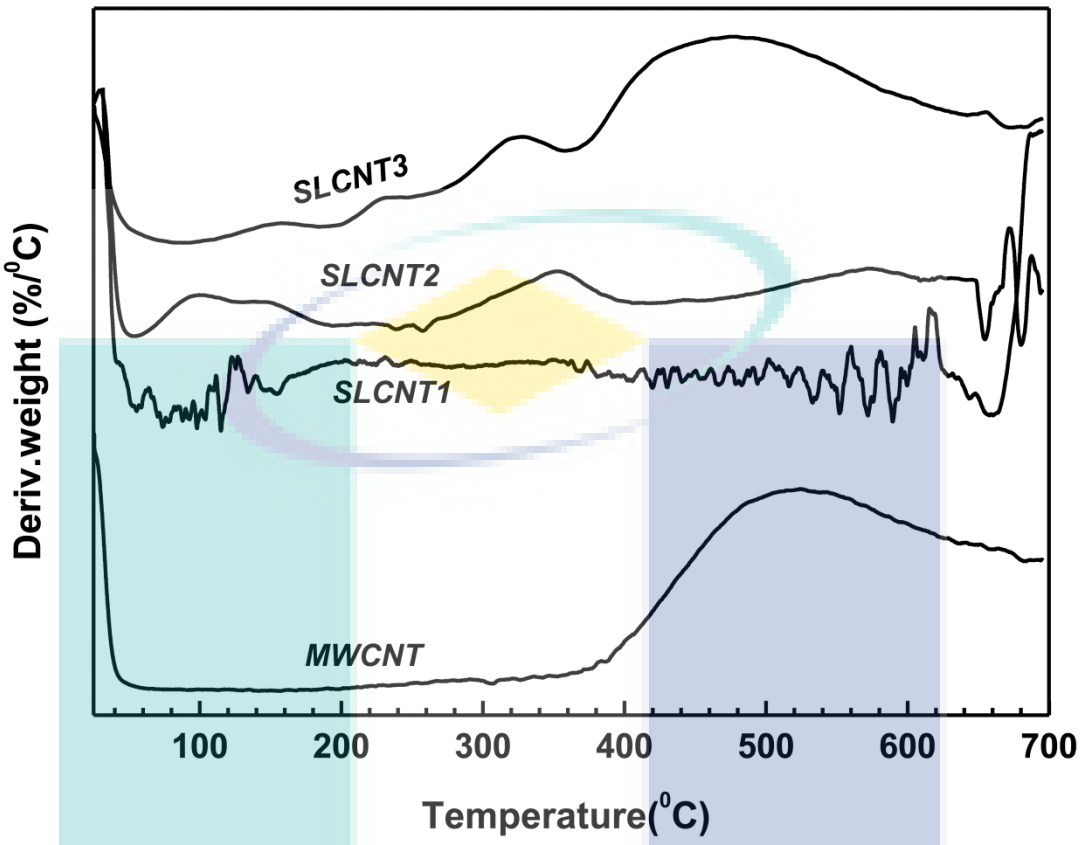

Figure 4.39: DTG Thermograms of MWCNT and Shellac coated MWCNT (SLCNT)

Finally, TGA and DTG thermograms extensively clarify that shellac was coated on the surface of MWCNT. In addition, the concentration of shellac influenced to remove the flaw of MWCNT. The thermal stability, residue content and decomposition stages of SLCNT2 noticed that 10wt% shellac was the best percentage to coat MWCNT.

(iv) Curing behavior of SLCNT-UPR nanosuspensions

Figure 4.40 demonstrate dynamic DSC thermograms of UPR, SLCNT-UPR1, SLCNT-UPR2 and SLCNT-UPR3 nanosuspensions. The thermograms reveal the curing nature of neat UPR and SLCNT nanotubes incorporated UPR nanosuspensions. The UPR was cured through free radical copolymerization with styrene (Rouison et al., 2004). All specimens were exhibited a distinguishable curing exotherm at a particular temperature. Comparative curing temperature of UPR, OPCNT-UPT, SLCNT-UPR1, SLCNT-UPR2 and SLCNT-UPR3 nanocomposites are presented in Table 4.10.

Table 4. 10: Comparative curing temperatures and activation energies of UPR, CNT-UPR and SLCNT-UPR nanosuspensions

Samples	Curing Temperature (°C)	E_a (kJ/mol)
UPR	93	16.34
OPCNT-UPR	109	17.05
SLCNT-UPR1	103	16.78
SLCNT-UPR2	99	16.60
SLCNT-UPR3	105	16.87

In addition, SLCNT-UPR2 suspension was cured at 99°C which was 10°C lower than the curing temperature of OPCNT-UPR nanosuspension as well. Moreover the curing temperature of SLCNT-UPR2 is the lowest temperature among the SLCNT-UPR nanosuspensions. The activation energy was calculated according to ASTM E-698-99 from equation [4.4] (Dodiuk et al., 2005). The observed curing temperatures and estimated activations energies are tabulated in Table 4.10.

Therefore, activation energy is function of curing temperature. Similarly curing temperature of SLCNT-UPR nanocomposites are function of shellac concentration. Moreover, shellac concentration is a driving force to non covalent functionalization of MWCNT as an anti-scavenger (Dorsa Parviz et al., 2012). SLCNT-UPR2 revealed the lowest activation energy at 99°C temperature where CNT coated with 10wt% shellac which performed as the best anti scavenger during curing process of SLCNT-UPR2 nanosuspension (Dodiuk et al., 2005; Martınez and Galano, 2010).

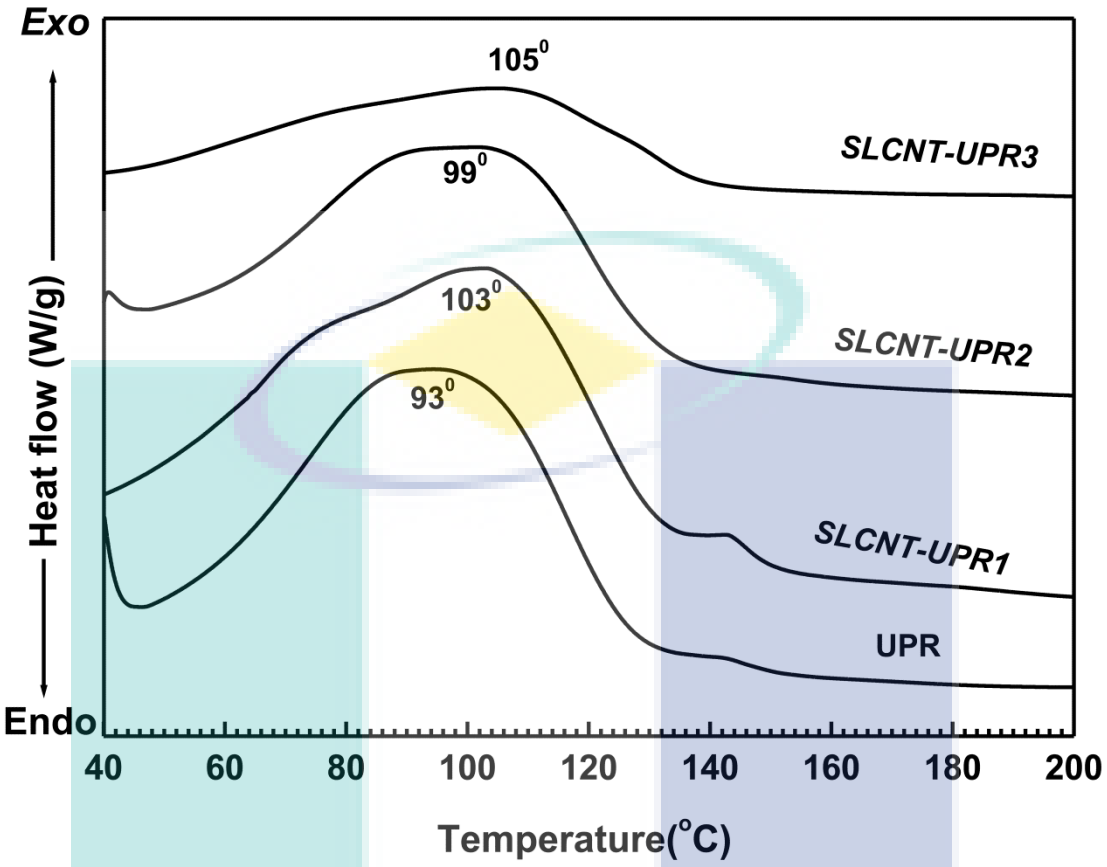

Figure 4.40: Curing exotherms of UPR and SLCNT-UPR nanosuspensions

In summary structural and thermal analysis is concurred that shellac coated MWCNT exhibits better properties as compared to pristine MWCNT. However, these properties were dependent on the concentration of shellac. Among these concentrations of shellac, 10 wt% with respect to MWCNT quantity is considered as the optimum amount. Later that amount of shellac has used to coat MWCNT which incorporated as OPSLCNT in UPR matrix. Finally OPSLCNT-UPR nanocomposite has prepared for subsequent characterizations.

(v) Interaction of Shellac and MWCNT

Figure 4.41 demonstrates the FTIR spectra of MWCNT, shellac and OPSLCNT. In addition, Table 4.11 shows the characteristic peaks and vibrational mode of these materials. Additionally Figure 4.42 represents the schematic interaction between shellac molecules and MWCNT.

The MWCNT spectrum exhibits free O–H stretching at 3436 cm^{-1} and bending at 1633 cm^{-1}, which is assigned to O–H groups of adsorbed moisture or covalently bonded functional groups (Osswald et al., 2007). Basically O–H vibrations originate from moisture in the sample rather than from the functional groups attached to the surface of the MWCNTs. The sharp peak at around 1633 cm^{-1} is due to the C–C stretching of aromatic ring.

The spectrum of shellac represents the peak at around 3332, 2920, 2852 1705, 1019 cm^{-1}. These peaks represented the presence of -C=C- unsaturation, O-H in Carboxylic group, -C-H in alkane, >C=O in ester linkage and =C-H in the shellac molecule respectively.

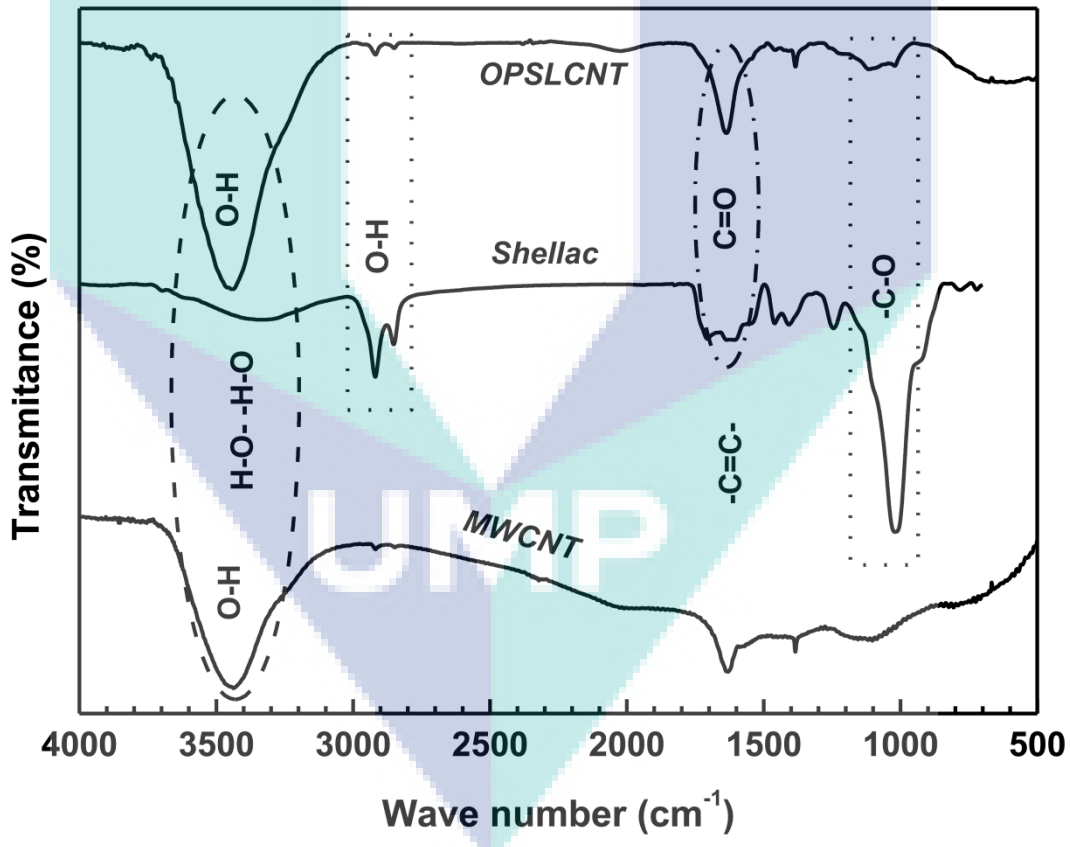

Figure 4.41: FTIR spectra of MWCNT, Shellac and OPSLCNT

In OPSLCNT spectrum, relatively narrow and strong peak at 3443cm^{-1} is appeared due to formation of hydrogen bond between shellac and MWCNT. The peak at 2919 cm^{-1} becomes weak due to O-H in carboxylic groups of shellac interact with

MWCNT surface through hydrogen bonding. In addition the distinguishable peak at 1636 cm^{-1} is noticed the presence of ester linked >C=O group on the surface of MWCNT. The peak at around 1383cm^{-1} represents the C–H bending of alkane, which reveals the presence of shellac layer on MWCNT surface (Soradech et al., 2013).

Table 4.11: Characteristic FTIR peaks of MWCNT, shellac and shellac coated MWCNT (OPSLCNT)

Samples	Wave number (cm-1)	Vibrational modes
MWCNT	3436	
	1633	Free O-H stretching and bending
Shellac	3332	-C=C-H stretching
	2920	O-H stretch in Carboxylic acid
	2852	C-H stretching in alkane
	1705	C=O stretching esters
	1459	C-H bending in alkane
	1019	-C-O stretching alcohol, esters
OPSLCNT	3443	O-H stretching, H-bonding in alcohol
	2919	O-H stretch in Carboxylic acid
	1636	>C=O stretching
	1383	C-H bending in alkane

Finally, it is significant that the sharp peak which was appeared at 1019 cm^{-1} for –C-O functional group in shellac spectrum has been disappeared from OPSLCNT spectrum. It corresponds to π-π interaction or ether linkage between shellac and MWCNT.

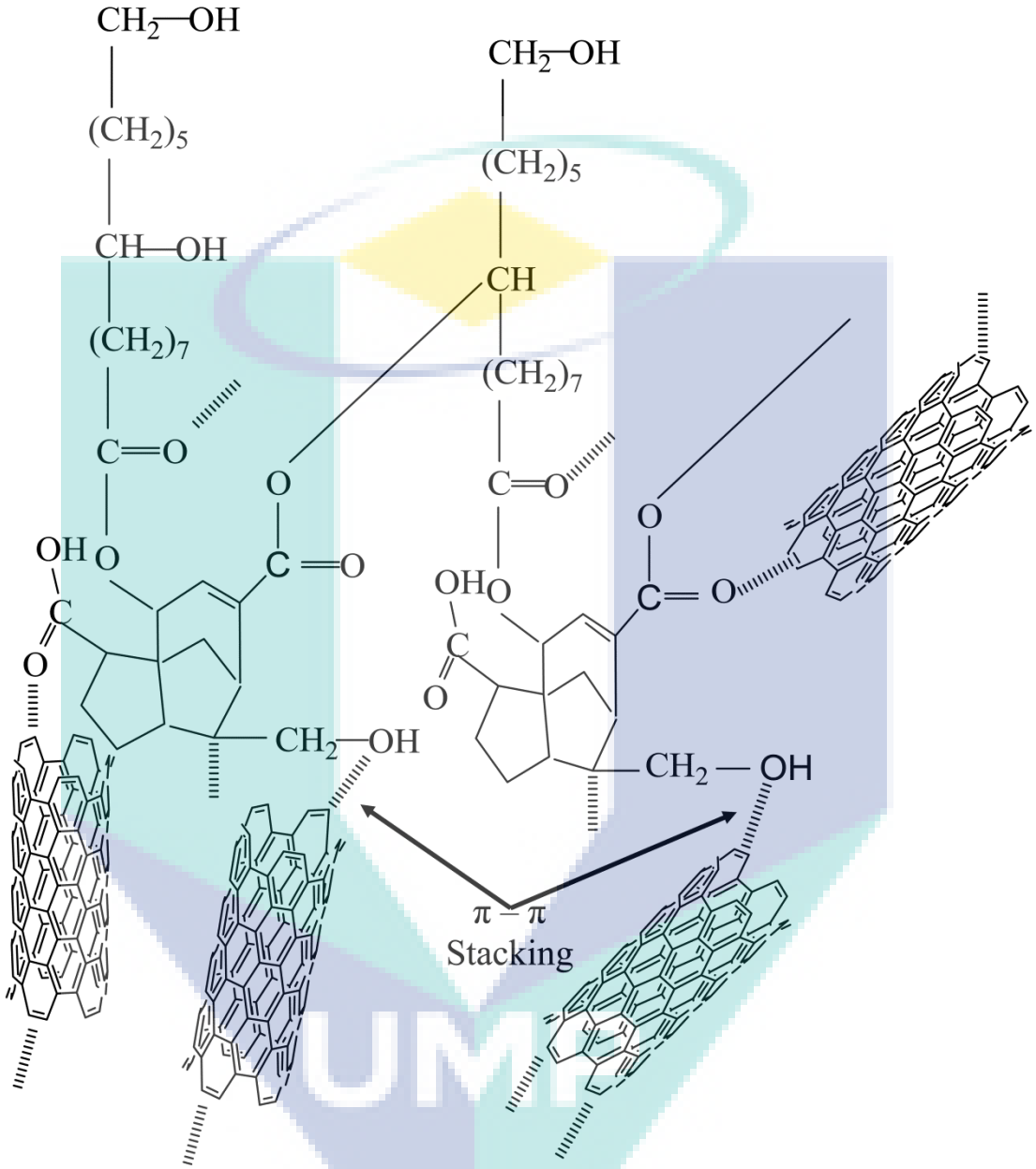

Figure 4.42: Schematic interactions between Shellac and MWCNT in SLCNT

4.5.2 Comparative Characterization of UPR, CNT-UPR and SLCNT-UPR Nanocomposites

(i) Interaction SLCNT and UPR in SLCNT-UPR nanocomposite

Figure 4.43 demonstrates the FTIR spectra of neat UPR, OPCNT-UPR and OPSLCNT-UPR nanocomposites. Table 4.12 introduces the characteristic peak values and vibrational modes of existing functional groups in these materials. The schematic interaction between SLCNT and UPR is represented in Figure 4.44 as well. The peak in UPR spectrum at around 3027cm^{-1} is due the =C-H stretching. The strong as well as sharp peak at 1722 cm^{-1} is related to >C=O of carboxylic group.

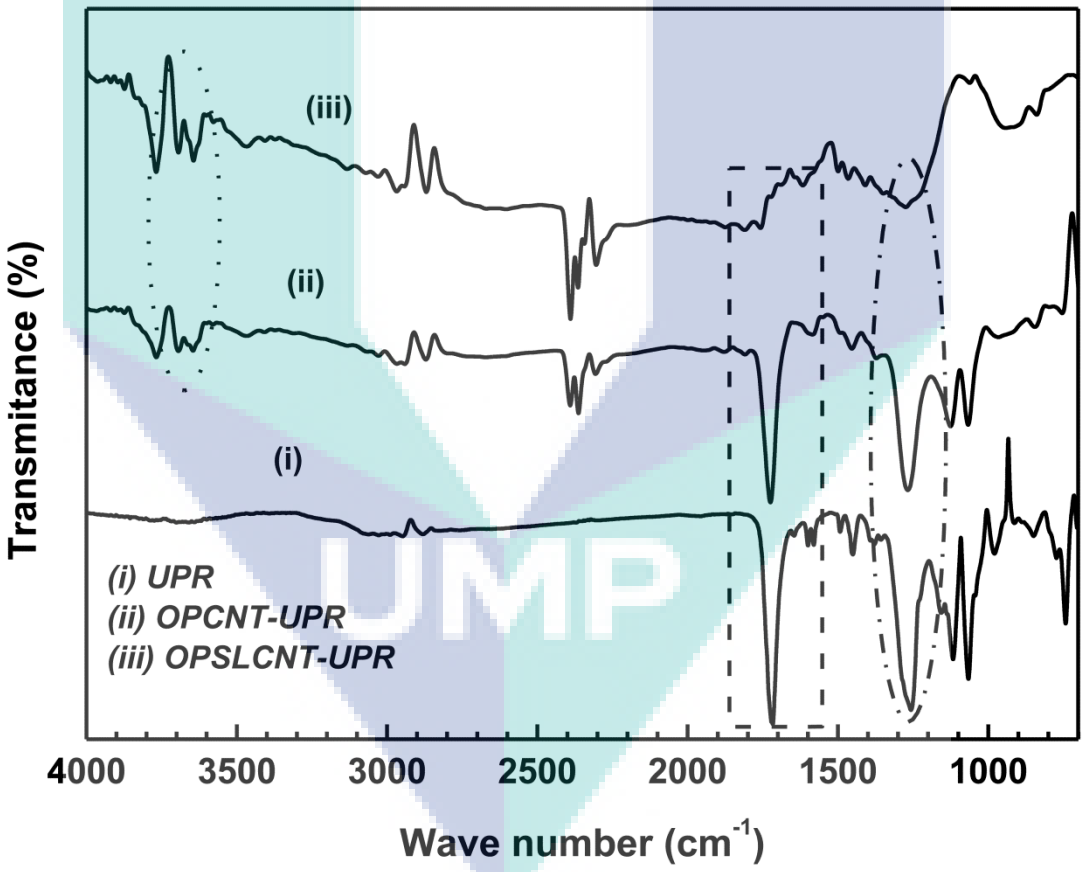

Figure 4.43: FTIR spectra of (i) neat resin, (ii) OPCNT-UPR and (iii) OPSLCNT-UPR Nanocomposites

The peaks at around 1599-1494 cm^{-1} correspond to the -C=C- in benzene ring of styrene. However, some authors believe, the peaks which appears at around 1590 cm^{-1}

is related to carboxyl and carbonyl group. The peaks appear at 1257-1067 cm^{-1} is due to C-O stretching of unsaturated polyester resin (Nurul Munirah Abdullah and Ishak Ahmad, 2013).

Table 4.12: FTIR characteristic peaks of UPR, OPCNT-UPR and OPSLCNT-UPR

Samples	Wave number (cm^{-1})	Vibrational mode(s)
UPR	3027	C-H stretching of =C-H
	1722	C=O stretching of carboxylic group
	1599-1449	-C=C- stretching in benzene
	1257-1118	-C-O stretching in carboxylic group
OPCNT-UPR	3695-3467	H-bonded O-H stretching
	1724	C=O stretching of carboxylic group
	1584-1453	-C=C- stretching in benzene
	1265-1066	-C-O stretching in carboxylic group
OPSLCNT-UPR	3645	O-H stretching, H-bonded
	2968w-2870	C-H stretching in alkane
	1616	C-C stretching in aromatic ring
	1499-1408	C-C stretching in aromatic ring
	1274	C-O stretching in ether link
	941	O-H bending carboxylic acid

Besides, the spectrum of OPCNT- UPR nanocomposite states the interaction between the surface O-H group of MWCNT and >C=O / C-O groups of UPR. The peaks appear at 3695-3467 cm^{-1} revels O-H stretching as a result of formation of H-bond (Alam et al., 2012). In addition, >C=O and C-O functional groups peaks at around 1724 cm^{-1} and 1066-1265 cm^{-1} respectively, which imply formation of hydrogen bond interaction between MWCNT and UPR.

Furthermore, the spectrum of OPSLCNT-UPR nanocomposite shows the absorption peak at 3645cm^{-1} which reveals that strong hydrogen bond exists in this nanocomposite. The carbonyl and C-O peak becomes weak and broad in this spectrum. These changes in the spectrum of OPSLCNT-UPR are significantly noticed that shellac

coated MWCNT effectively interact with UPR matrix through hydrogen bond and ether link.

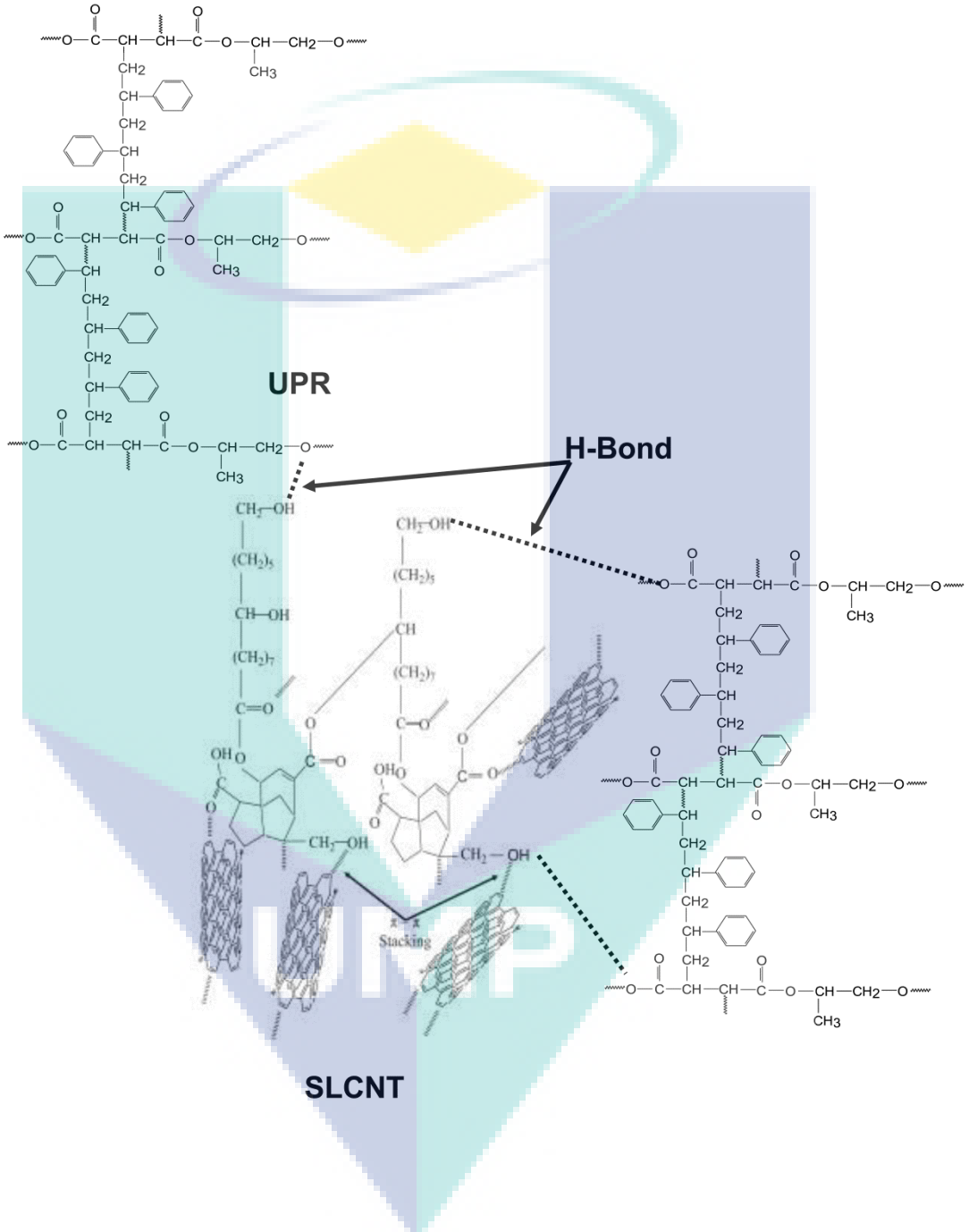

Figure 4.44: Schematic interaction between SLCNT and UPR

(ii) Plain surface morphology of OPCNT-UPR and OPSLCNT-UPR nanocomposites

The plain surface morphologies of OPCNT-UPR (A) and OPSLCNT-UPR (B) nanocomposites are demonstrated in Figure 4.45. These micrographs reveal the compatibility of pristine nanotubes and shellac coated nanotubes with UPR matrix. SLCNTs were clearly rooted in the matrix of OPSLCNT-UPR nanocomposite, several ends of SLCNT as like white tips mentioned by dotted circle are visible in plain surface. Furthermore, it seems that SLCNTs were stayed as less entangled in matrix. They were sound dispersed and potentially embedded in UPR.

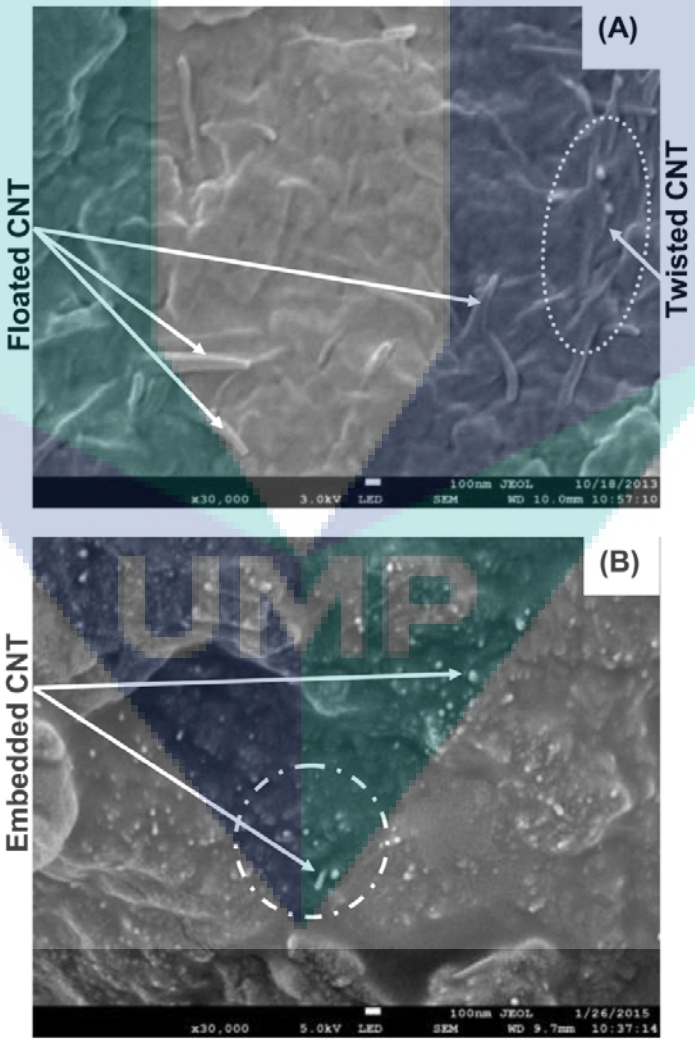

Figure 4.45: FESEM Plain surface of OPCNT-UPR (A) and OPSLCNT-UPR (B) nanocomposites

On the other hand, pristine CNTs were floated on the surface of OPCNT-UPR nanocomposite. In addition a long fiber like object is visible in surface. Moreover there were some twisted MWCNTs are visible in the plain surface of OPCNT-UPR. Therefore it is suggested that SLCNT was more compatible with UPR as compare to pristine MWCNT.

(iii) Mechanical properties of SLCNT-UPR nanocomposite

The *TS* and *TM* of neat UPR, OPCNT-UPR and OPSLCNT-UPR are stated in Figure 4.46. The corresponding *TS* values of these nanocomposites are 28.72±1.20, 40±1.32 and 47±1.5 MPa and *TM* values are around 1247±122, 1698±190 and 1952±178 MPa respectively. Therefore the *TS* of OPSLCNT-UPR nanocomposite was increased by 62.95% and 16.4% as compare to neat UPR and OPCNT-UPR nanocomposite respectively. Similarly the *TM* of OPSLCNT-UPR nanocomposite were increased 56.53% and 14.95% as compare to neat UPR and OPCNT-UPR nanocomposite correspondingly.

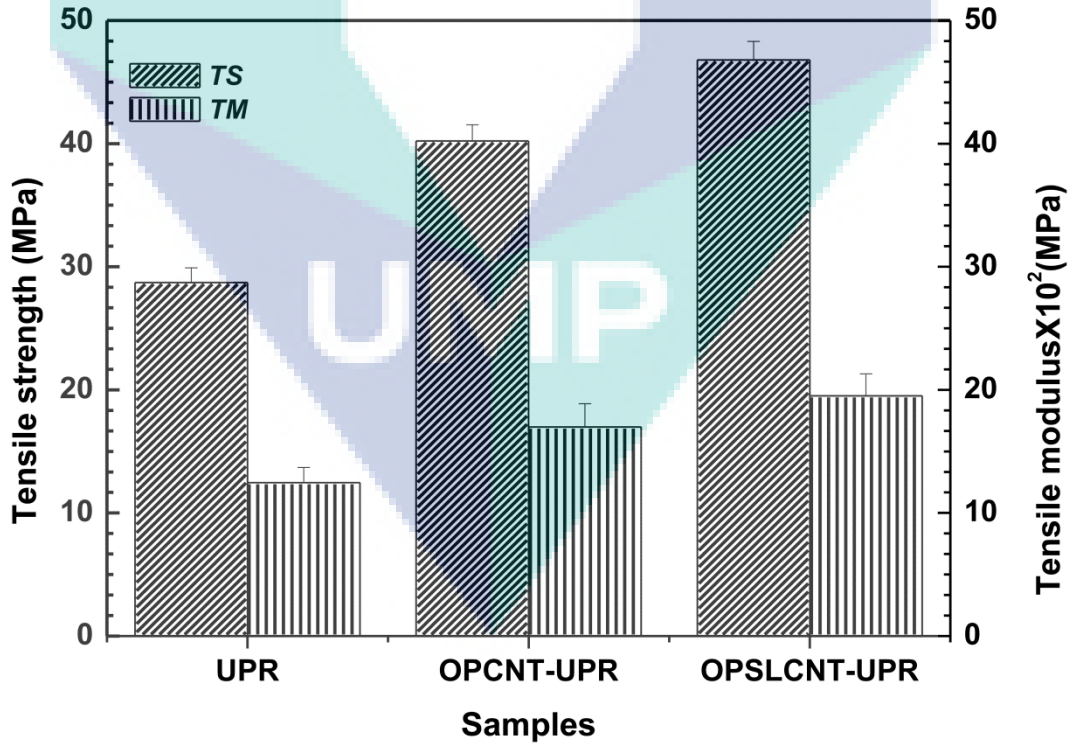

Figure 4.46: Tensile strength and Tensile Modulus of UPR, OPCNT-UPR and OPSLCNT-UPR Nanocomposites

Figure 4.47 demonstrates the reinforcement effect of shellac coated MWCNT on the *IS* and *EB* in OPSLCNT-UPR nanocomposite. The corresponding *IS* and *EB%* values of OPSLCNT-UPR nanocomposite are 5.53±0.28 kJ/m^2 and 5±0.22%. The EB of OPSLCNT-UPR nanocomposite was increased 8.7% and 15% as compare to neat UPR and OPCNT-UPR nanocomposite respectively. Therefore *IS* was increased by 54.5% and 18% as compare to neat resin and OPCNT-UPR nanocomposite correspondingly.

Thus, observations notice that toughness of OPSLCNT-UPR nanocomposite was increased. It concurs that incorporation of shellac coated MWCNT in UPR matrix improved the interaction between the interfacial region of SLCNT and UPR which enhance this property (Rozman et al., 2001). In addition these results clearly demonstrate a good reinforcement effect of shellac on the mechanical properties of nanocomposite.

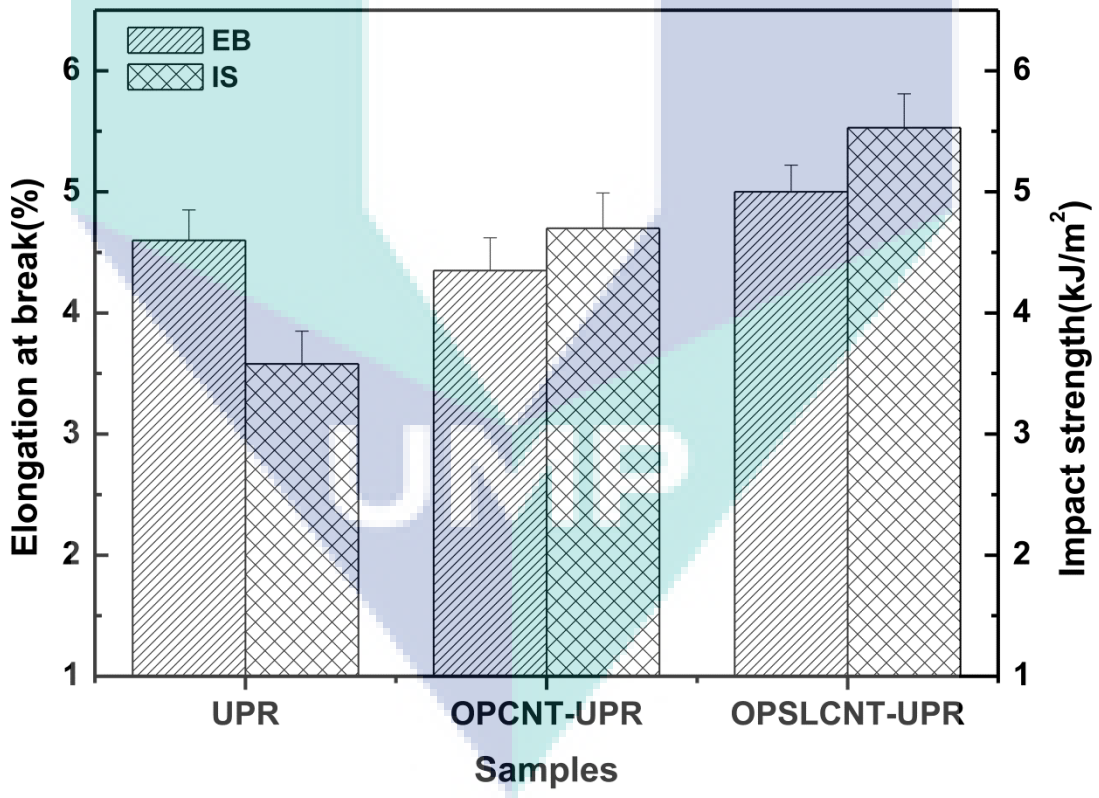

Figure 4.47: Elongation at break and Impact strength of UPR, OPCNT-UPR and OPSLCNT-UPR nanocomposite

(iv) Fracture morphology of SLCNT-UPR nanocomposites

The fracture morphologies of OPCNT-UPR (a) and OPSLCNT−UPR (b) nanocomposite are exhibited in Figure 4.48. There are numerous fracture CNT ends are clearly visible in the surface of OPSLCNT-UPR nanocomposite. Additionally SLCNT nanotubes not only unbroken but also shielded the crack propagation through crack bridging. Whereas distinguished fracture is found in the surface of OPCNT-UPR nanocomposite. Several CNTs are entangled and pulled out during breaking of that nanocomposite.

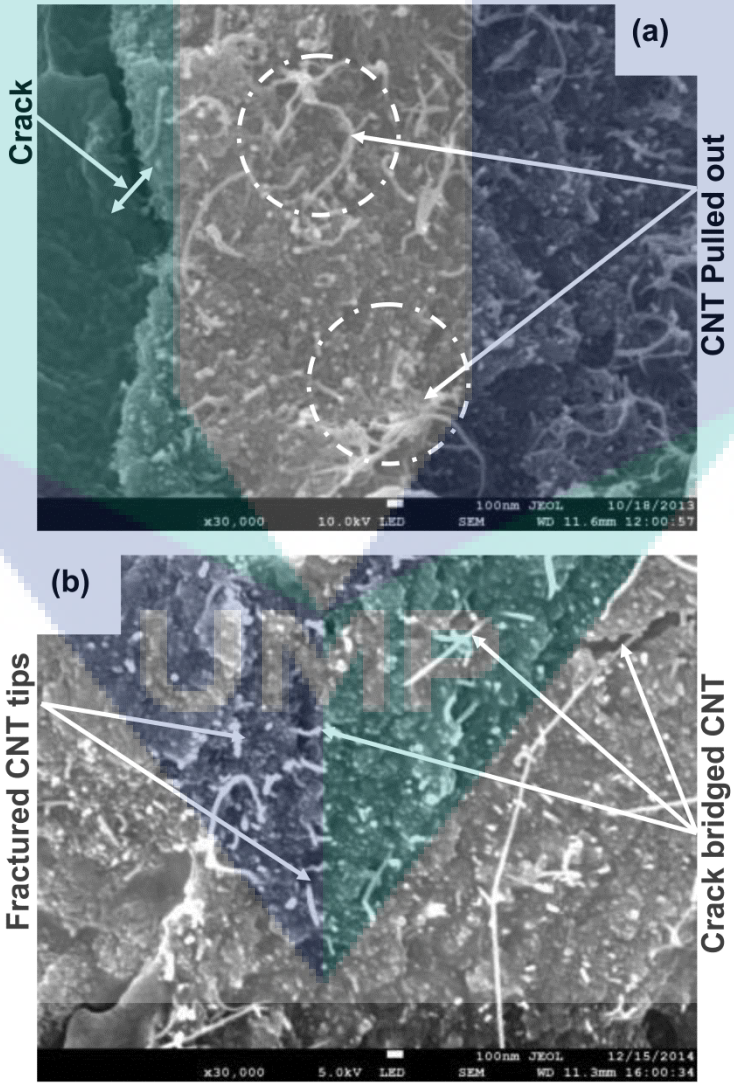

Figure 4.48: Fracture surfaces of OPCNT-UPR (a) and OPSLCNT-UPR (b) Nanocomposites

These fracture patterns agree to increase the mechanical properties of OPSLCNT-UPR nanocomposite. Moreover, these observations support a better interaction between SLCNTs and UPR molecules as well. Thus, shellac coating on the surface of MWCNT reveals a good possibility of sound dispersion in matrix and well interaction with UPR. In the light fracture behavior, OPSLCNT can lead to modify the morphology of nanocomposite and influence the mechanical properties as reported elsewhere (Desai and Haque 2005; Kim et al. 2006).

(v) X-ray diffraction of SLCNT-UPR nanocomposite

The X-ray diffraction peaks of neat UPR, OPCNT-UPR and OPSLCNT-UPR nanocomposites are demonstrated in Figure 4.49. The scattering peak of OPSLCNT - UPR nanocomposite was appeared at18.20°. However, the corresponding scattering angles of neat UPR and OPCNT-UPR are at 23.43° and 18.91°.The shape of these peaks is neither so diffused nor so sharp, therefore they exhibit partially crystalline in nature. The lattice constant of OPSLCNT - UPR nanocomposite is 4.78 Å whereas OPCNT-UPR represents as 4.61Å, which is smaller than OPSLCNT-UPR nanocomposite. It may be attributed to the better intercalation of SLCNT nanotubes with matrix, similar intercalation behavior of layered clay materials in UPR nanocomposite had stated elsewhere (Byung-Wan Jo et al., 2008). From these observations, it confer that the SLCNTs well disperse in UPR matrix, leading to an increase the interfacial adhesion between SLCNT nano tubes and UPR (Abdel-Aal et al. 2008).

The estimated degrees of crystallinity (χ_c) of OPSLCNT-UPR nanocomposite is around 26.5%. Comparative lattice parameter and crystallinity index of matrix and nanocomposites are illustrated in Table 4.13.

Table 4.13: Comparative FWHM, lattice spacing and crystal size, percentage of crystallinity of OPSLCNT-UPR nanocomposite

Samples	2θ	FWHM	dÅ	DÅ	λ	χ (%)
UPR	23.43	9.44	3.7	8.4		14
OPCNT-UPR	18.91	5.20	4.61	15.26	1.514	24
OPSLCNT-UPR	18.2	5.8	4.78	13.67		26.5

Practically scattering peak intensity of OPSLCNT-UPR nanocomposite notices that SLCNT was performed as efficient nucleating agent as compare to pristine MWCNT thus peak intensity is greater than OPCNT-UPR nanocomposite. Therefore more population of UPR molecules took part recrystallization in OPSLCNT-UPR nanocomposite.

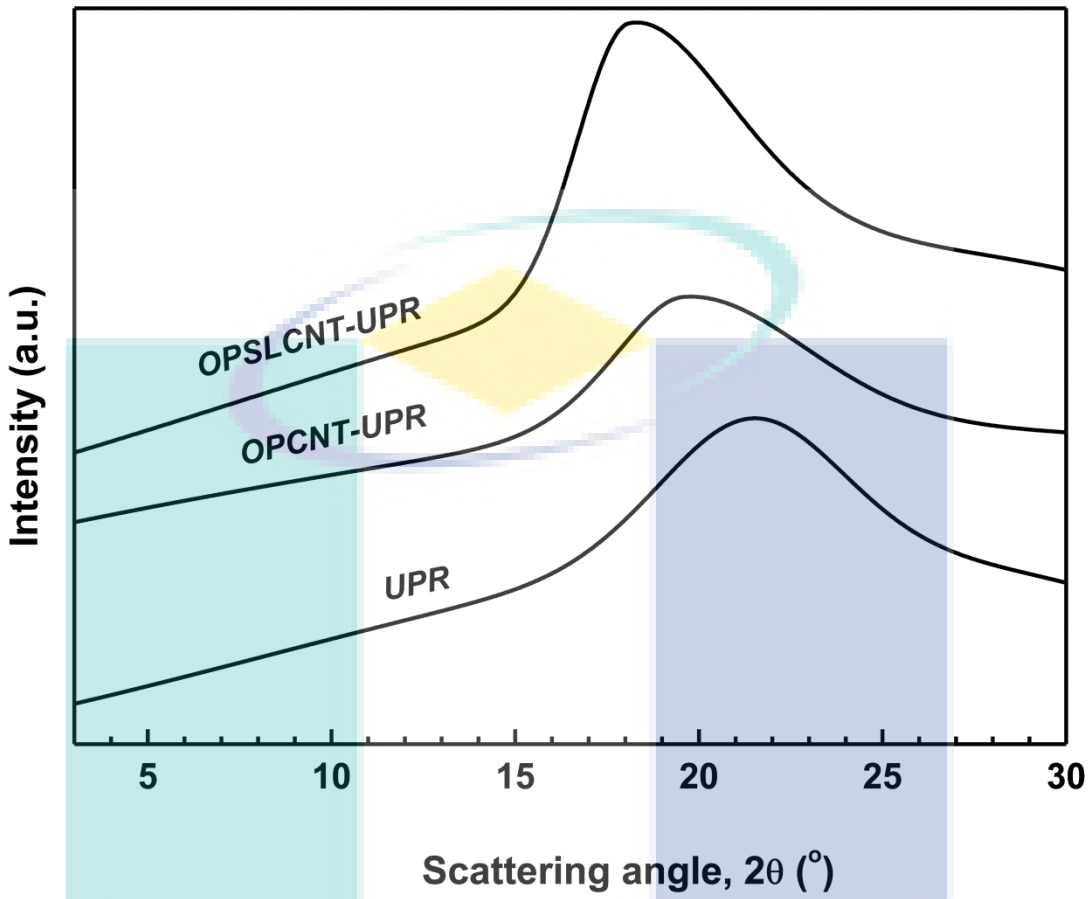

Figure 4.49: X-ray Diffraction of neat UPR, OPCNT-UPR and OPSLCNT-UPR nanocomposites

(vi) Differential scanning calorimetry of SLCNT-UPR nanocomposite

The thermal transitions in DSC thermograms of UPR, OPCNT-UPR and OPSLCNT-UPR are stated in Figure 4.50. The glass transition endotherm of all samples are exhibited in the range of 62-68°C which appeared due to molecular motion at low temperature. The OPSLCNT-UPR nanocomposite exhibited a shoulder like crystallization exothermic transition (T_c) at around 145°C. In addition the endothermic transition at the higher temperatures correspond the melting temperature (T_m) of UPR and nanocomposites. Table 4.14 represents the characteristic temperature of those thermograms.

Table 4.14: Characteristic transition temperatures of UPR, OPCNT-UPR and OPSLCNT-UPR nanocomposites in DSC and TGA thermograms

Samples	T_g (°C)	T_c (°C)	T_{m1}(°C)	T_{m2}(°C)	T_d (°C)
UPR	62	-	370	-	378
OPCNT-UPR	68	-	375	380	395
OPSLCNT-UPR	68	145	376	381	400

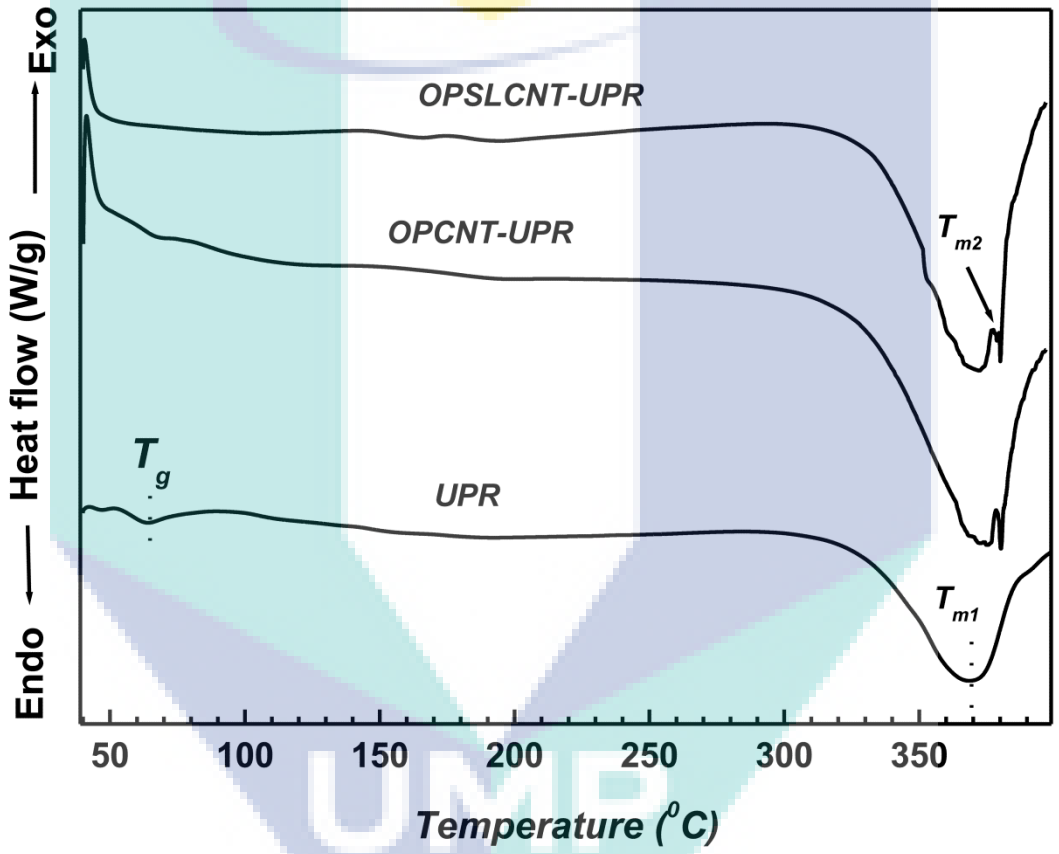

Figure 4.50: DSC thermograms of neat resin, OPCNT-UPR and OPSLCNT-UPR nanocomposites

The nanocomposites exhibit a remarkable split melting endotherm into two distinguishable peaks (T_{m1} and T_{m2}) instead of single endothermic melting peak of neat UPR matrix.

(vii) Thermogravimetric analysis of SLCNT-UPR nanocomposite

Figure 4.51 demonstrates the degradation behavior of UPR, OPCNT-UPR and OPSLCNT-UPR nanocomposites. The degradation of cross-linked resin has been ascribed by the dissociation of C−C chain bonds and release of styrene at the site of dissociation (Abdalla, et al., 2007; Manfredi et al., 2006). Therefore, that decomposition of UPR and OPCNT-UPR were took place at around 313°C and came to an end at around 446°C, whereas OPSLCNT-UPR was started degradation at 350°C temperature as higher compare to OPCNT-UPR nanocomposite (Cao and Lee, 2003; Martı´nez and Galano, 2010). The degradation temperature (T_d) can be obtained from TGA thermograms at 50% weight loss of a sample as an indication of structural deterioration.

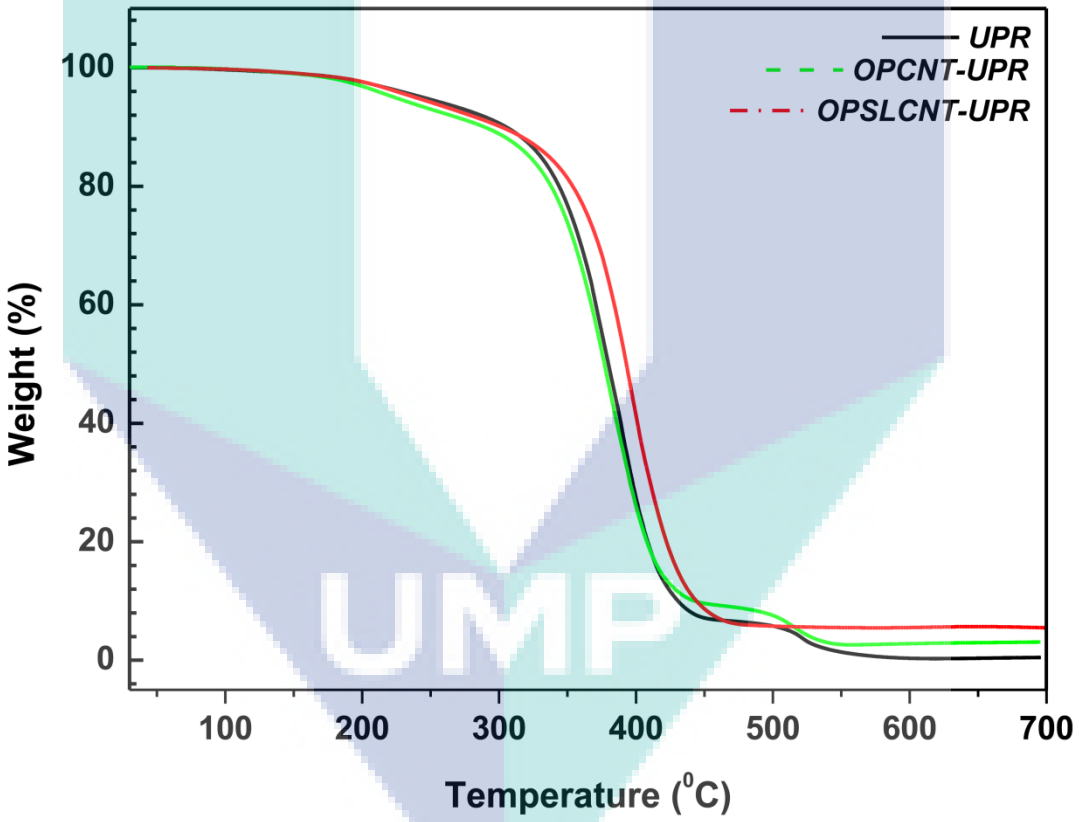

Figure 4.51: TGA Thermograms of UPR, OPCNT-UPR and OPSLCNT-UPR nanocomposites

Therefore, T_d values assessed for UPR, OPCNT-UPR and OPSLCNT-UPR from TGA curves are stated in Table 4.14. The residue content at 600°C shows a significant difference between the OPCNT-UPR and OPSLCNT-UPR nanocomposites, perhaps due to shellac coated MWCNT incorporated in resin (Kubota, 1975).

The DTG thermograms in Figure 4.52 state the decomposition stages of UPR and OPCNT-UPR and OPSLCNT-UPR nanocomposites. OPSLCNT-UPR was decomposed only a single stage at around 400°C. Whereas there are two distinguishable peaks clearly visible in the thermograms of UPR and OPCNT-UPR. The shoulder like peak of UPR and OPCNT-UPR at around 200-245°C are suggested as the degradation temperature of unreacted styrene, polyester resin (Manfredi et al., 2006). Second stage strong split decomposition is demonstrated at around 300-400°C. In this stage OPCNT−UPR nanocomposite was decomposed at higher temperature than UPR. The third decomposition stage is at around 500-550°C perhaps due to C-C chain session.

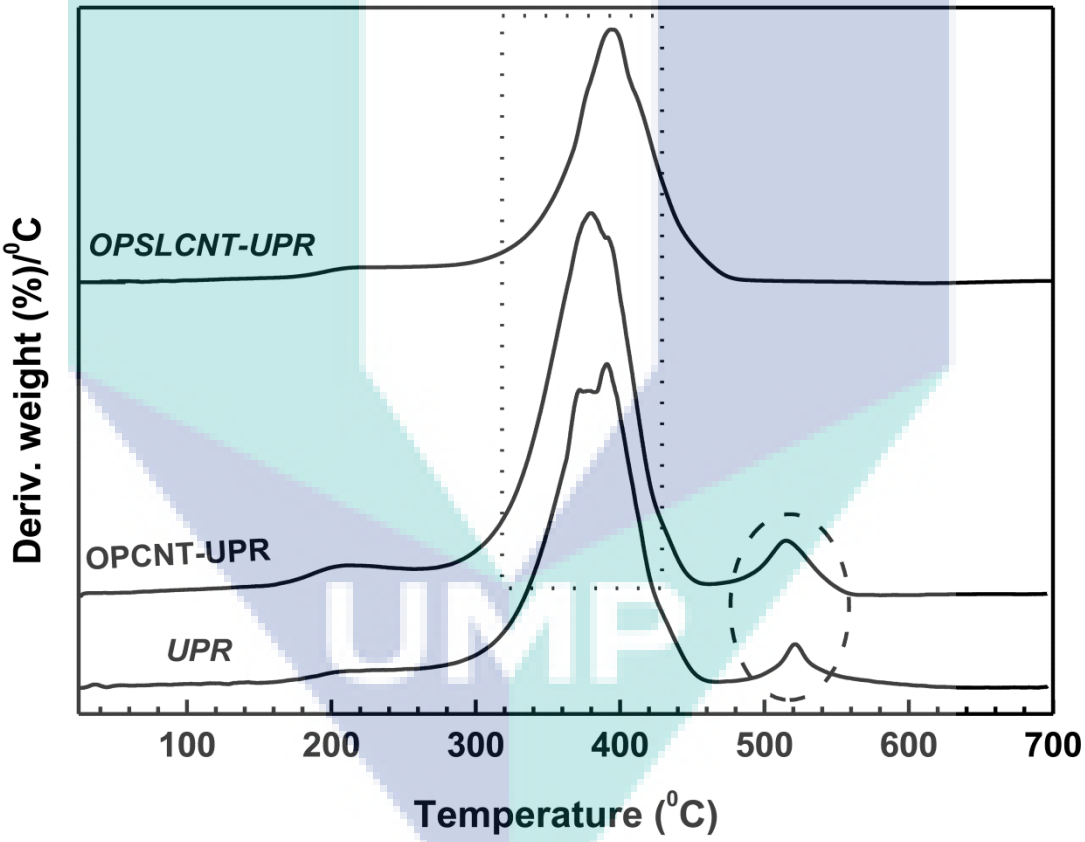

Figure 4.52: DTG Thermograms of UPR, OPCNT-UPR and OPSLCNT-UPR Nanocomposites

It is most likely due to the well interaction between SLCNT and UPR which advocated by FTIR and mechanical properties. It appear that not only formation of bonding and strong interface between SLCNT and UPR but also shellac might be

removed the flaws of MWCNT during coating process. Therefore OPSLCNT-UPR nanocomposite was decomposed only single stage throughout the heating rang thermo gravimetric analysis.

CHAPTER 5

CONCLUSIONS AND RECOMMENDATIONS

5.1 CONCLUSIONS

MWCNT was pre-dispersed in THF solvent and 1.5 hr was optimized as pre-dispersion sonication time. In addition, pre-dispersed MWCNT was mixed with UPR matrix and post dispersion sonication time was optimized as 2 hr. Moreover, THF-MWCNT-UPR nanosuspension exhibited higher viscosity at low shear rate as compared to MWCNT-UPR nanosuspension which confers that pre-dispersed MWCNT showed well dispersion in UPR matrix. Surface morphology revealed good dispersion of MWCNT in THF-MWCNT-UPR nanocomposite as well. Furthermore, the mechanical property of pre-dispersed MWCNT reinforced nanocomposite is greater as compared to that of directly dispersed MWCNT-UPR nanocomposite.

The Modified Halpin–Tsai model revealed 0.3 wt% MWCNT as optimum quantity and showed a good linearly fitted data with this model. Besides, the TS and EB of 0.3CNT-UPR nanocomposite is 40 MPa and 4.3% corresponding to the highest and lowest values among nanocomposites. However, the curing temperature of UPR was increased from 93°C to 109°C after incorporation of 0.3 wt% pristine MWCNT.

The pristine MWCNT was modified with 5, 10 and 15 wt% of HBP. The optimum concentration of HBP was measured by XRD, DSC and TGA studies. The crystal size and glass transition temperature of 10 wt% HBP coated MWNT (HBCNT2) was increased to 29% and 32°C, respectively. In addition, the curing temperature of HBCNT2 incorporated nanosuspension was reduced from 109°C to 92°C as well as the activation energy was reduced. Furthermore, the TS and TM values of OPHBCNT-UPR nanocomposite were increased by an amount of 21.5% and 27%, respectively as compared to those of OPCNT-UPR nanocomposite. Surface morphology of OPHBCNT-UPR nanocomposite illustrates well dispersion and strong crack shielding

behavior of HBCNT. Moreover, HBCNTs were found to be tightly bounded with matrix. OPHBCNT-UPR nanocomposite became stiffer as compare to MWCNT reinforced UPR nanocomposite.

In case of shellac, concentration was optimized through structural and thermal analysis of shellac coated SLCNT nanotubes and curing temperature of SLCNT-UPR nanosuspension. The crystal size of 10 wt% shellac coated MWCNT (SLCNT2) increased 18%, which is the highest increment as compared to pristine MWCNT and other SLCNT. In addition, the glass transition temperature of SLCNT2 increased by 9°C as compared to pristine MWCNT and curing temperature of nanosuspension reduced to 99°C. Surface morphology reveals that shellac coated MWCNTs extensively dispersed and compatible with UPR as compared to OPCNT-UPR nanocomposite. The nucleating efficiency of shellac coated MWCNT is higher than pristine MWCNT. Moreover, mechanical properties revealed that shellac coated MWCNT reinforced nanocomposites became tough.

5.2 RECOMMENDATIONS

The study findings led to the following recommendations:

(i) After pre-dispersing in suitable solvent, MWCNT can be well dispersed in UPR matrix to fabricate nanocomposites for potential applications.

(ii) The effect of solvent evaporation temperature on CNT-UPR nanocomposites will open a door for future research which seems quite promising from the aspect of many potential applications.

(iii) In this work 0.3 wt% MWCNT has evaluated as optimum amount in UPR matrix. Incorporation of higher amount of MWCNT might hold promise for future research work which can be loaded by varying other process variables such as demoisturization time, stirring time or applying surface modification chemistry.

(iv) Purified shellac or shellac derivatives seem attractive/potential candidate to modify CNT nanotubes which will hopefully facilitate their dispersion in polymer matrix.

(v) Hybrid CNT's incorporation with other thermoset matrices (such as epoxy, alkyd resin) to fabricate hybrid nanocomposites can be another approach for future research.

REFERENCES

Abdalla, M., Dean, D., Robinson, P. and Nyairo, E. 2008.Cure behavior of epoxy/MWCNT nanocomposites: the effect of nanotube surface modification. *Polymer*. **49:** 3310–3317.

Abdel-Aal N., El-Tantawy F., Al-Hajry A. and Bououdina M. 2008. Epoxy resin/plasticized carbon black composites. Part II. Correlation among network structure and mechanical properties. *Polymer Composites*. **29(7):** 804-808.

Alam, A.K.M.M., Beg, M.D.H., Mina, M.F., Khan, M.R. and Prasad, D.R.M. 2012. Structures and Performances of Simultaneous Ultrasound and Alkali Treated Oil Palm Empty Fruit Bunch Fiber Reinforced Poly(Lactic Acid) Composites. *Composites Part A.* **43:** 1921-1929.

Alam, A.K.M.M., Shubhra, Q.T.H., Islam, M.R. and Barai, S. 2011. Preparation and characterization of natural silk fiber reinforced polypropylene and synthetic e-glass fiber reinforced polypropylene composites: a comparative study. *Journal of composite Materials*. **45(22):** 2301-2308.

Alam, M.K., Islam, M.T., Mina, M.F. and Gafur, M.A. 2014. Structural,mechanical, thermal and electrical properties of carbon black reinforced polyester resin composites. *J Applied Polymer Science.* doi:10.1002/app.40421

Albdiry, M.T. and Yousif, B.F. 2013. Morphological structures and tribological performance of unsaturated polyester based untreated/silane-treated halloysite nanotubes. *Materials and Design.* **48:** 68–76.

Alexandre, M. and Dubois, P. 2000. Polymer-layered silicate nanocomposites; preparation, properties and uses of a new class of materials. *Material Science Engineering.* **28(1/2):** 1–63

Alhazov, D., and Zussman, E. 2012.Study of the energy absorption capabilities of laminated glass using carbon nanotubes. *Composites Science and Technology.* **72:** 681–687.

Bahr, J.L., Mickelson, E.T., Bronikowski, M.J., Smalley, R.E. and Tour, J.M. 2001. Dissolution of small diameter single-wall carbon nanotubes in organic solvents? *Chemical Communication.* **2:** 193–194.

Bai J.B. 2003. Evidence of the reinforcement role of chemical vapour deposition multi-walled carbon nanotubes in a polymer matrix. *Carbon.* **41:**1325–8.

Bai, J.B. and Allaoui, A. 2003. Effect of the length and the aggregate size of MWNTs on the improvement efficiency of the mechanical and electrical properties of nanocomposites – experimental investigation. *Composites Part A.* **34:** 689–694.

Bal S. 2010. Dispersion and reinforcing mechanism of carbon nanotubes in epoxy nanocomposites. *Bulletin of Materials Science*. **33:** 27–31.

Banerjee, T.S., Bhaumik, G., Yu, C.L., Swaminathan, B., Giri, A.K., Srivastava, S. and Bhattacharjee, S.B. 1984. Evaluation of the Genotoxicity of Lac Dye. *Food Chemical Toxicology*. **22:** 677-679.

Barber, A.H., Cohen, S.R. and Wagner, H.D. 2003. Measurement of Carbon Nanotube-Polymer Interfacial Strength. *Applied Physics Letter.* **82:** 4140-4142.

Barnes, C.E. 1938. Chemical Nature of Shellac. Industrial Engineering Chemistry. **30:** 449-451

Barrau, S., Demont, P., Perez, E., Peigney, A., Laurent, C. and Lacabanne, C. 2003. Effect of Palmitic Acid on the Electrical Conductivity of Carbon Nanotubes-epoxy Resin Composites. *Macromolecules.* **36:** 9678-9680.

Baskaran, D., Dunlap, J.R., Mays, J.W.and Bratcher, M.S. 2005. Grafting efficiency of hydroxy-terminated poly(methyl methacrylate) with multiwalled carbon nanotubes. *Macromolecule Rapid Communication.* **26:** 481–6.

Burguen R.O., Quagliata M.J., Mohanty A.K., Mehta G., Drzal L.T. and Misra M. 2005. Hybrid biofiber-based composites for structural cellular plates, *Composites: Part A.* **36:** 581-593.

Cadek, M., Coleman, J.N., Ryan, K.P., Nicolosi, V., Bister, G., Fonseca, A., et al. 2004. Reinforcement of polymers with carbon nanotubes: the role of nanotube surface area. *Nanoletters.* **4:** 353–6.

Cadenato, A., Salla, J.M., Ramis, X., Morancho, J.M., Marroyo, L.M. and Martin, J.L. 1997. Determination of gel and vitrification times of thermoset curing process by means of TMA, DMTA and DSC techniques. *J Thermal Analysis*. **49:** 269–279.

Caminade, A.M. and Majoral, J.P. 2010. Dendrimers and nanotubes: a fruitful association. *Chemical Society Review*. **39:** 2034–2047.

Campidelli, S., Sooambar, C., Diz, E.L., Ehli, C, Guldi, D.M. and Prato, M. 2006 Dendrimer-functionalized single-wall carbon nanotubes: synthesis,

characterization, and photoinduced electron transfer. *J American Chemical Society.* **128:** 12544–52.

Cao L. X. and Lee, J. 2003.Control of shrinkage and residual styrene of unsaturated polyester resins cured at low temperatures: I. Effect of curing agents. *Polymer* **44:** 1893–902.

Cao, J., Wang, Q., Rolandi, M., Dai, H. 2004. Aharonov–Bohm interference and beating in single-walled carbon-nanotube interferometers. *Phys Rev Lett*. **93(21):** 216803.

Cao, L., Yang, W., Yang, J., Wang, C. and Fu, S. 2004. Hyperbranched poly(amidoamine)-modified multi-walled carbon nanotubes via grafting-from method. *Chemistry Letter*. **33:** 490–491.

Cooper, C.A., Ravich, D., Lips, D., Mayer, J., and Wagner, H.D. 2002. Distribution and alignment of carbon nanotubes and nanofibrils in a polymer matrix. *Composite Science and Technology*. **62:** 1105–1112.

Cornell, E.W., Fadeyev, V., Haber, C., Jin, J., Nordmeyer, R. and Golden, M. 2007. Using Optical Metrology to Reconstruct Sound Recordings. *Nucl. Instrum. Methods Phys. Res. Sect. A-Accel. Spectrom. Dect. Assoc. Equip.* **579:** 901-904.

Cox, H.L. 1952. The elasticity and strength of paper and other fibrous materials. Br *J Appl Phys* **3:** 72–9.

Daohong Zhang, Jing Wang, Tingcheng Li, Aiqing Zhang, Jia, D. 2011. Synthesis and Characterization of a Novel Low-Viscosity Unsaturated Hyperbranched Polyester Resin. *Chemical Engineering Technology*. **34(1):** 119–126.

Dassios, K. G., Alafogianni, P., Antiohos, S. K., Leptokaridis, C., Barkoula, N.M. and Matikas, T. E. 2015. Optimization of Sonication Parameters for Homogeneous Surfactant-Assisted Dispersion of Multiwalled Carbon Nanotubes in Aqueous Solutions. *J. Physical Chemistry. C* **119:** 7506−7516.

Datsyuk, V., Kalyva, M., Papagelis, K., Parthenios, J., Tasis, D., Siokou, A., Kallitsis, I. and Galiotis, C. 2008. Chemical oxidation of multiwalled carbon nanotubes. *Carbon.* **46:** 833−840.

David Rohindra, Keiichi Kuboyama and Ougizawa, T. 2012. Dominant factors affecting the pressure dependence of melting temperatures in homologous series of aliphatic polyesters. *European Polymer Journal*. **48:** 1768–1776.

Davis, J. J., Coleman, K. S., Azamian, B. R., Bagshaw, C. B. and Green, M. L. H. 2003. Chemical and Biochemical Sensing with Modified Single Walled Carbon Nanotubes. *Chemistry AEuropeanJournal*. **9:** 3732.

Davis, M. E., Katz, A., Ahmad, W. R. 1996. Rational Catalyst Design via Imprinted Nanostructured Materials.*Chemistry of Materials.* **8:** 1820-1839.

Desai, A.V. and Haque, M.A. 2005. Mechanics of the interface for carbon nanotube–polymer composites. *Thin-Walled Structures.* **43:** 1787–1803.

Di Maio, E., Iannace, S., Sorrentini, L. and Nicolais, L. 2004. Isothermal crystallization in PCL/clay nanocomposites investigated with thermal and rheometric methods. *Polymer*. **45:** 8893–88100.

Engel, P. S., Billups, W. E., Abmayr, D. W., Tsvaygboym, K., Wang, R. 2008.The Reaction of Carbon Nanotubes with Organic Peroxides. *J. Physical Chemistry. C* **112:** 695-700.

Esumi, K., Ishigami, M., Nakajima, A., et al., 1996. Chemical treatment of carbon nanotubes. *Carbon.* **34:** 279–81.

Falvo, M.R., Clary, G.J., Taylor II R.M., Chi, V., Brooks, F.P. and Washburn, S., et al. 1997. Bending and buckling of carbon nanotubes under large strain. *Nature* **389:**582–4.

Farag, Y. and Leopold, C.S. 2009. Physicochemical Properties of Various Shellac Types. *Dissolution Technology*. **16:** 33-39.

Fell, J.T., Rowe, R.C., Newton, J.M. 1979. Mechanical Strength of Film Coated Tablets. *J. PharmacyAnd Pharmacology*. **31:** 69-72

Fenoglio, I., Tomatis, M., Lison, D., Muller, J., Fonseca, A. and Nagy, J.B., et al. 2006. Reactivity of carbon nanotubes: free radical generation or scavenging activity? *Free Radical Biology and Medicine.* **40:** 1227–33.

Fernando, K.A.S., Lin, Y., Zhou, B., Grah, M., Joseph, R., Allard, L.F., et al. 2005. Poly(ethylene-co-vinyl alcohol) functionalized single-walled carbon nanotubes and related nanocomposites. *J Nanoscience Nanotechnology*. **5:** 1050–5.

Fink, J.K. 2005. Reactive polymers : fundamentals and applications, by William Andrew, Inc.

Fornes T.D. and Paul D.R. 2003. Modeling properties of nylon 6-clay nanocomposites using composite theories. *Polymer*. **44:** 4993–5013.

Fr´echet, J.M.J. and Tomalia, D.A. 2001. Dendrimers and Other Dendritic Polymers. John Wiley & Sons Ltd., West Sussex, UK,.

Galano, A. 2008. Carbon Nanotubes as Free-Radical Scavengers. *J. Physical Chemistry C.* **112:** 8922.

Galano, A. 2009. Influence of Diameter, Length, and Chirality of Single-Walled Carbon Nanotubes on Their Free Radical Scavenging Capability. *J. Physical Chemistry. C.* **113:** 18487.

Galano, A. **2010**. Carbon nanotubes: promising agents against free radicals. *Nanoscale* **2:** 373

Gan, Z., Abe, H. and Doi, Y. 2002. Temperature-induced polymorphic crystals of poly(butylene adipate). *Macromolecular Chemistry Physics.* **203:** 2369–2374.

Gao, C. and Yan, D. 2004. Hyperbranched polymers: from synthesis to applications. *Progress in Polymer Science.* ***29*****:** 183-275.

Genhua, Z., Wu, J., Wang, W. and Pan, C. 2004. Characterizations of expanded graphite/polymer composites prepared by in situ polymerization. *Carbon.* **42(14):** 2839-2847.

Gojny, F.H. and Malte H.G. Wichmann, Bodo Fiedler, Wolfgang Bauhofer, Karl Schulte, 2005.Influence of nano-modification on the mechanical and electrical properties of conventional fibre-reinforced composites. *Composites: Part A.* **36:** 1525–1535.

Gojny, F.H., Malte, H.G. Wichmann, Bodo Fiedler and Schulte, K. 2005. Influence of different carbon nanotubes on the mechanical properties of epoxy matrix composites – A comparative study. *Composites Science and Technology* **65:** 2300–2313.

Goodman, I. and Rhys, J. A. 1965. Polyesters; Saturated Polymers; Iliffe Books; London; 1

Goodman, I. Encyclopedia of Polymer Science and Engineering; 2nd ed.; 12; Wiley; New York; 1988.

Goswami, D.N. 1979. Dielectric Behavior of Natural Resin Shellac. *J. Applied Polymer Science.* **23:** 529-537

Goswami, D.N., Prasad, N., Baboo, B., Kumar, K.K. and Ansari, M.F. 2009. Degradation of Lac with Storage and a Simple Method to Check the Same. *Pigment Resin Technology.* **38:** 211-217

Guo, Z., Lei, K., Li, Y., Wai, H., Prikhodko, S. and Thomas Hahn, H. 2008.Fabrication and characterization of iron oxide nanoparticles reinforced vinyl-ester resin nanocomposites. *Composites Science and Technology.* **68**: 1513–1520.

Guojian, W., Zehua, Q., Lin, L., Quan, S. and Jianlong, G. 2008. Study of SMA graft modified MWNT/PVC composite materials. *Materials Science and Engineering A.* **472:** 136–139.

Hagenmaier, R.D. and Baker, R.A., 1993. Reduction in gas exchange of citrus fruit by wax coatings. *Journal of Agricultural and Food Chemistry* .**41 (2):** 283–287.

Halpin, J.C. and Tsai, S.W. 1969. Effects of environmental factors on composite materials. AFML-TR-67-423.

Halpin, J.C., Affdl and Kardos, J.L. 1976. The Halpin-Tsai Equations: A Review, *Polymer Engineering and Science*, **16(5):** 344-52.

Hou Cui-ling, Li Tie-hu, Zhao Ting-kai, Liu He-guang, Liu Le-hao, Zhang Wen-juan, 2013. Electromagnetic wave absorbing properties of multi-wall carbon nanotube/Fe_3O_4 hybrid materials. *New Carbon Materials* **28(3):**184–90.

Hsu-Chiang Kuan, Chen-Chi M. Ma, Wei-Ping Chang , Siu-Ming Yuen ,Hsin-Ho Wu and Tzong-Ming Lee, 2005.Synthesis, thermal, mechanical and rheological properties of multiwall carbon nanotube/waterborne polyurethane nanocomposite. *Composites Science and Technology* **65**: 1703–1710.

Hu, H., Zhao, B., Hamon, M.A., et al., 2003. Sidewall functionalization of single-walled carbon nanotubes by addition of dichlorocarbene. *J American Chemical Society*. **125:** 14893–14900.

Iijima S. 1991.Helical microtubules of graphitic carbon. *Nature.* **354:**56–58

Iijima, S. 1993, Single-shell carbon nanotubes of 1-nm diameter. *Nature*. **363:** 603 - 605.Islam, M. F., Rojas, E., Bergey, D. M., Johnson, A. T. and Yodh, A. G. 2003. High weight fraction surfactant solubilization of single-wall carbon nanotubes in water. *Nano Letter*. **3:** 269−273.

Iijima, S., Brabec, C., Mati, A., Bernholc, J. 1996. Structural flexibility of carbon nanotubes. *J Chemical Physics*. **104(5):**2089–92.

Kang, Y. J., and Taton, T. A. 2003. Micelle-encapsulated carbon nanotubes: A route to nanotube composites. *Journal of the American Chemical Society.* **125(19):** 5650-5651.

Karshak, V. V. and Vinogradova, S. V. 1965. Polyesters; Pergamon; New York;

Kathi, J. and Rhee, K. 2008. Surface modification of multi-walled carbon nanotubes using 3-aminopropyltriethoxysilane. *J Material Science*. **43(1):** 33–7.

Kayatin, M.J.and Davis, V.A. 2009. Visco-elasticity and Shear Stability of Single-Walled Carbon Nanotube/ Unsaturated Polyester Resin Dispersions. *Macromolecules* **42:** 6624–6632.

Kim, J.A., Seong, D.G., Kang, T.J. and Youn, J.R. 2006. Effects of surface modification on rheological and mechanical properties of CNT/epoxy composites. *Carbon.* **44(10):**1898–1905

Kim, K. T. and Jo, W. H. 2010. Noncovalent Functionalization of Multiwalled Carbon Nanotubes Using Graft Copolymer with Naphthalene and Its Application as a Reinforcing Filler for Poly(styrene-co-acrylonitrile). *J. Polymer Science, Part A: Polymer Chemistry*. **48:** 4184−4191.

Kim, K.S., Bae, D.J., Kim, J.R., et al. 2002. Modification of electronic structures of a carbon nanotube by hydrogen functionalization. *Advance Materials*. **14:** 1818–1821.

Kuan, H.C., Ma, C.C.M., Chang, W.P., Yuen, S.M.,Wu, H.H., Lee, T.M. 2005. Synthesis, thermal, mechanical and rheological properties of multiwall carbon nanotube/waterborne polyurethane nanocomposite. *Composites Science and Technology*. 65:1703–1710.

Kubota, H. 1975. Curing of highly reactive polyester resin under pressure: kinetic studies by differential scanning calorimetry. *J Applied Polymer Science*. **19:** 2279–2297.

Lau , K.T., Lu , M., Lam , C.K., Cheung, H.Y., Sheng, F.L. and Li, H.L. 2005. Thermal and mechanical properties of single-walled carbon nanotube bundle-reinforced epoxy nanocomposites: the role of solvent for nanotube dispersion, *Composites Science and Technology*. **65:** 719–725.

Lau, K., Lu, M., Lam, C., Cheung, H., Sheng, F.L. and Li, H.L. 2005. Thermal and mechanical properties of single-walled carbon nanotube bundle reinforced epoxy nanocomposites: the role of solvent for nanotube dispersion. *Composites Science and Technology*. **65(5):** 719–725.

Lee, D.S. and Han, C.D. 1987. A chemorheological model for the cure of unsaturated polyester resin. *Polymer Engineering and Science*. **27:** 955–63.

Li, C., Chou, T.W. 2003. Elastic moduli of multi-walled carbon nanotubes and the effect of van der Waals forces. *Composites Science and Technology*. **63:**1517–1524.

Liao, Y.H., Marietta-Tondin, O., Liang, Z., Zhang, C. and Wang, B. 2004. Investigation of the dispersion process Of SWNTs/SC-15 epoxy resin nanocomposites. *Material Science and Engineering A.* **385:** 175–181.

Lin, X., Liu, X., Jia, J., Shen, X. and Kim, J.K. 2014. Electrical and mechanical properties of carbon nanofiber/graphene oxide hybrid papers. *Composite Science and Technology*. **100:** 166–173

Liu X.M., Huang Z.D., Oh S.W., Zhang B. and Ma P.C. 2012. Carbon nanotube (CNT)-based composites as electrode material for rechargeable Li ion batteries: a review. *Compos Sci Technol* **72**: 121–44.

Lou, X. D., Daussin, R., Cuenot, S., Duwez, A. S., Pagnoulle, C., Detrembleur, C., Bailly, C., Jerome, R. 2004. Synthesis of pyrene containing polymers and noncovalent sidewall functionalization of multiwalled carbon nanotubes. *Chemistryof Materials.* **16:** 4005−4011.

Lu, K.L., Lago, M., Chen, Y.K., Green, M.L.H., Harris, P.J.F. and Tsang, S.C. 1996. Mechanical damage of carbon nanotubes by ultrasound. *Carbon.* **34:** 814–6.

Mallick, P.K. 2008. Fiber reinforced composite materials manufacturing and design. 3rd ed. Taylor & Francis, Inc.;

Mallick, P.K., 1993. Fiber-reinforced Composites: Materials, Manufacturing and Design. CRC Press.

Martı´nez, A. and Galano, A. 2010. Free Radical Scavenging Activity of Ultrashort Single-Walled Carbon Nanotubes with Different Structures through Electron Transfer Reactions. *J. Physics and Chemistry. C* **114:** 8184–8191

Martin, J.L. 2007. Kinetic analysis of two peaks in the curing of an unsaturated polyester resin catalyzed with MEKP and cobalt octoate. *Polymer Engineering Science*. **47(1):** 62–70.

Martınez A. and Galano A. 2010. Free radical scavenging activity of ultrashort singlewalled carbon nanotubes with different structures through electron transfer reactions. *J Physical Chemistry C.* **114:** 8184–91.

Mast, W.C., Smith, L.T. and Fisher, C.H. 1945. Emulsion Polymerization of Acrylic Esters. *Industrial Engineering Chemistry.* **37:** 365-369

Mina, M.F., Beg, M.D.H, Islam, M.R., Nizam, A., Alam, A.K.M.M. and Yunus, R.M. 2014. Structures and Properties of Injection Molded Biodegradable Poly(Lactic Acid) Nanocomposites Prepared with Untreated and Treated Multi-Walled Carbon Nanotubes. *Polmer Engineering and Science*. **54(2):** 317-326.

Minfang, M. and Winey, K. I. 2007.Improved Load Transfer in Nanotube/Polymer Composites with Increased Polymer Molecular Weight, *J. Physical Chemistry C.* **111**: 17923-17927

Mintmire, J.W., White, C.T. 1995. Electronic and structural-properties of carbon nanotubes. *Carbon.* **33(7):** 893–902.

Montazeri, A., Javadpour, J., Khavandi, A., Tcharkhtchi, A., Mohajeri, A. 2010. Mechanical properties of multi-walled carbon nanotube/epoxy composites. *Materials and Design.* **31:**4202–4208.

Monti, M., Terenzi, A., Natali, M., Gaztelumendi, I., Markaide, N., Kenny, J.M., et al. 2010.Development of unsaturated polyester matrix–carbon nanofibers nanocomposites with improved electrical properties. *J Applied Polymer Science.* **117:**1658–1666.

Morgan, P. W. 1965. Condensation Polymers; By Interfacial and Solution Methods; Inerscience Publishers; New York .

Nanda Gopal Sahoo, Sravendra Rana, Jae Whan Cho, Lin Li and Siew Hwa Chan, 2010. Polymer nanocomposites based on functionalized carbon nanotubes. *Progress in Polymer Science.* **35**: 837–867.

Nativ-Roth, E., Levi-Kalisman, Y., Regev, O., and Yerushalmi-Rozen, R. 2002. On the route to compatibilization of carbon nanotubes. *Journal of Polymer Engineering*. **22(5):** 353-368.

Nevin, A., Comelli, D., Valentini, G. and Cubeddu, R. 2009. Total Synchronous Fluorescence Spectroscopy Combined with Multivariate Analysis: Method for the Classification of Selected Resins, Oils, and Protein- Based Media Used in Paintings. *Analytical Chemistry.* **81:** 1784-1791.

Oberlin, A. And Endo, M. 1976. Filamentous growth of carbon through benzene decomposition. *J Crystal Growth.* **32:**335–49.

Ogasawara T, Ishida Y, Ishikawa T, Yokota R. 2004. Characterization of multi-walled carbon nanotube/phenylethynyl terminated polyimide composites. *Composite Part A.* **35:** 67–74.

Ogasawara T., Ishida Y., Ishikawa T. and Yokota, R. 2004.Characterization of multi-walled carbon nanotube/phenylethynyl terminated polyimide composites. *Compos Part A.* **35:** 67–74

Pagani, G., Green, M. J., Poulin, P., Pasquali, M. 2012. Competing mechanisms and scaling laws for carbon nanotube scission by ultrasonication. *Proc. Natl. Acad. Sci.U.S.A.* **109:** 11599−11604.

Pan, B., Cui, D., Xu, P. Ozkan, C., Feng, G., Ozkan, M., Huang, T., Chu, B. Li, Q., He, R. and Hu, G. 2009. Synthesis and characterization of polyamidoamine dendrimer-coated multi-walled carbon nanotubes and their application in gene delivery systems, *Nanotechnology.* **20:** 125101.

Pantarotto, D., Partidos, C. D., Graff, R., Hoebeke, J., Briand, J. P., Prato, M., Bianco, A. 2003, Synthesis, Structural Characterization, and Immunological Properties of Carbon Nanotubes Functionalized with Peptides. *J. American Chemical Society.* **125:** 6160-6164.

Park, C., Ounaies, Z., Watson, K.A., Crooks, R.E., Smith, J., Lowther, S.E., et al. 2002. Dispersion of single wall carbon nanotubes by in situ polymerization under sonication. *Chemical Physics Letter*. **364:** 303–308.

Pavlidou, S. and Papaspyrides, C.D. 2008. A review on polymer–layered silicate nanocomposites. *Progress in Polymer Science.* **33:** 1119–1198

Perez, L.D., Giraldo, L.F. , Brostow, W. and Lopez, B. 2007. Poly(methyl acrylate) plus Mesoporous Silica Nanohybrids:Mechanical and Thermophysical Properties. *e-Polymers.* **29**: 1-11.

Price, B. K., Lomeda, J. R. and Tour, J.M. 2009. Aggressively Oxidized Ultra-Short Single-Walled Carbon Nanotubes Having Oxidized Sidewalls. J. *Chemistry of Materials.*. **21(17):** 3917-3923.

Prolongo, S.G., et al., 2008. Effects of dispersion techniques of carbon nanofibers on the thermo- physical properties of epoxy nanocomposites. *Composites Science and Technology*. **68(13):** 2722–2730.

Qian, D., Dickey, E.C., Andrews, R. and Rantell, T. 2000. Load transfer and deformation mechanisms in carbon nanotube-polystyrene composites. *Applied Physics Letter*. **76:** 2868–2870.

Quanxiang Li , Church , J.S., Kafi , A., Naebe, M. and Fox, B. L. 2014. An improved understanding of the dispersion of multi-walled carbon nanotubes in non-aqueous solvents. *J Nanoparticle Research.* **16:** 2513. DOI 10.1007/s11051-014-2513-0.

Qui, Z.B., Ikehara, T. and Nishi, T. 2003. Melting behavior of poly(butylenes succinate) in miscible blends with poly(ethylene oxide). *Polymer*. **44:** 3095–3099.

Ruoff, R.S. and Lorents, D.C. 1995. Mechanical and thermal-properties of carbon nanotubes. *Carbon.* **33(7):** 925–30.

Safadi, B., Andrews, R. and Grulke, E.A. 2002. Multiwalled carbon nanotube polymer composites: synthesis and characterization of thin films. *J Applied Polymer Science*. **84:** 2660–2669.

Sahoo, N. G., Rana, S., Cho, J. W. L. S. H., and Chan, Li. 2010. Polymer nanocomposites based on functionalized carbon nanotubes. *Progress in Polymer Science*. **35(7):** 837-867.

Sanchez, C., Julian, B., Belleville, P. and Popall, M. 2005. Applications of hybrid organic–inorganic nanocomposites, *Journal of Materials Chemistry.* **15:** 3559–3592.

Sandanayaka, A.S.D., Takaguchi, Y., Uchida, T., Sako, Y., Morimoto, Y., Araki, Y. and Ito, O. 2006. Light-induced electron transfer on the single wall carbon nanotube surrounded in anthracene dendron in aqueous solution. *Chemistry Letter*. **35:** 1188–1189.

Scholl, M., Kadlecova, Z., Klok, H. A. 2009. Dendritic and hyperbranched polyamides. *Progress in Polymer Science.* **34(1):** 24-61.

Schultz, R. M. L., Moore, V. C., Leonard, A. D., Price, B. K., Kosynkin, D. V., Lu, M., Partha, R., Conyers, J. L. and Tour, J. M. 2009. Antioxidant Single-Walled Carbon Nanotubes.*J. American Chemical Society.* **131:** 3934.

Seyhan, A.T., Gojny, F.H., Tanoglu, M. and Schulte, K. 2007. Critical Aspects Related to Processing of Carbon Nano-tube/unsaturated Thermoset Polyester Nanocomposites. *European Polymer Journal.* **43 (2):** 374–379.

Shelimov, K.B., Esenaliev, R.O., Rinzler, A.G., Huffman, C.B.and Smalley, R.E. 1998. Purification of single-wall carbon nanotubes by ultrasonically assisted filtration. *Chemical Physics Letter*. **282:** 429–434.

Sheng, N., Boyce, M.C., Parks, D.M., Rutledge, G.C., Abes, J.I. and Cohen, R.E. 2004. Multiscale micromechanical modeling of polymer/clay nanocomposites and the effective clay particle. *Polymer*. **45:** 487–506.

Singh, A.N., Upadhye, A.B., Mhaskar, V.V., Dev, S., Pol, A.V., Naik, V.G. 1974(b). Chemistry of Lac Resin 7. Pure Lac Resin 3: Structure. *Tetrahedron* **30:** 3689-3693.

Spitalsky, Z., Tasis, D., Papagelis, K.and Galiotis, C. 2010. Carbon nanotube-polymer composites: Chemistry, processing, mechanical and electrical properties. *Progress in Polymer Science*. **35(3):** 357-401.

Star, A., and Stoddart, J. F. 2002. Dispersion and Solubilization of Single-Walled Carbon Nanotubes with a Hyperbranched Polymer. *Macromolecules*, **35(19):** 7516-7520.

Stephen, R. and Thomas, S. 2010. Chapter :Nanocomposites: State of the Art, New Challenges and Opportunities, Book name: RUBBER Nanocomposites Preparation, Properties, And Applications, Sabu Thomas, John Wiley & Sons (Asia) Pte Ltd, 2 Clementi Loop, 02-01, Singapore 129809,.

Steuerman, D. W., Star, A., Narizzano, R., Choi, H., Ries, R. S., and Nicolini, C. 2002. Interactions between conjugated polymers and single-walled carbon nanotubes. *Journal of Physical Chemistry B* .**106(12):** 3124-3130.

Strano, M. S., Moore, V. C., Miller, M. K., Allen, M. J., Haroz, E. H., Kittrell, C., Hauge, R. H., Smalley, R. E. 2003. The role of surfactant adsorption during ultrasonication in the dispersion of single-walled carbon nanotubes. *J. Nanoscience and Nanotechnology*. **3:** 81−86.

Tagmatarchis, N., Prato, M.J.2004. Functionalization of carbon nanotubes via 1,3-dipolar cycloadditions. J *Material Chemistry*. **14:** 437–9.

Tai, N.H., Yeh, M.K. and Liu, J.H. 2004. Enhancement of the mechanical properties of carbon nanotube/phenolic composites using a carbon nanotube network as the reinforcement. *Carbon.* **42:** 2774–2777.

Tasis, D., Tagmatarchis, N., Bianco, A.and Prato, M. 2006. Chemistry of carbon nanotubes. *Chemical Reviews.* **106:** 1105- 1136.

Thostenson, E. T., Tsu-Wei Chou, 2004. Nanotube buckling in aligned multi-wall carbon nanotube composites. *Carbon* **42:** 3003–3042

Trezza, T.A. and Krochta, J.M. 2001. Specular Reflection, Gloss, Roughness and Suface Heterogeneity of Biopolymer Coatings. *J. Applied Polymer Science* **79:** 2221-2229.

Tschirch, A. and Farner, A. 1899. Studien über den Stocklack.. *Arch. Pharm.* **237:** 35-48

Unger, E., Graham,V, Kreupl, F., Liebau, M. and Hoenlein, W.2002. Electrochemical functionalization of multiwalled carbon nanotubes for solvation and purification. *Current Applied Physics.* **2:** 107–111.

Upadhye, A.B., Wadia, M.S., Mhaskar, V.V., Dev, S. 1970.Chemistry of Lac Resin 4. Pure Lac Resin 1: Isolation and Quantitative Determination of Constituent Acids. *Tetrahedron.* **26:** 4177-4187

Valencia-Chamorro, S.A., Pérez-Gago, M.B., del Río, M. and Palou, L., 2009. Effect of antifungal hydroxypropyl methylcellulose (HPMC)-lipid edible composite coatings on postharvest decay development and quality attributes of coldstored 'Valencia' oranges. *Postharvest Biology and Technology.* **54 (2):** 72–79.

Valentini, L., Armentano, I., Ricco, L., Alongi, J., Pennelli, G., Mariani, A., Russo, S. and Kenny, J. M. 2006. Selective interaction of single-walled carbon nanotubes with conducting dendrimer.*Diamond Related Materials.* **15:** 95-99.

Wadia, M.S., Khurana, R.G., Mhaskar, V.V.and Dev, S. 1969. Chemistry of Lac Resin 1. Lac Acids (Part 1): Butolic, Jalaric and Laksholic Acids. *Tetrahedron.* **25:** 3841-3854.

Wang, T.Z. and Tseng, C.G. 2007. Polymeric carbon nanocomposites from multiwalled carbon nanotubes functionalized with segmented polyurethane. *J Applied Polymer Science*. **105:**1642–1650.

Watts, P. C. P., Fearon, P. K., Hsu, W. K., Billingham, N. C., Kroto, H. W. and Walton, D. R. M. 2003. Carbon nanotubes as polymer antioxidants. *J. Materials Chemistry.* **13:** 491-495.

Wildoer, J.W.G., Venema, L.C., Rinzler, A.G., Smalley, R.E. and Dekker, C. 1998. Electronic structure of atomically resolved carbon nanotubes. *Nature.* **391:** 59–62.

Wu, C.S. 2007. Characterizing composite of multiwalled carbon nanotubes and POE-g-AA prepared via melting method. *J Applied Polymer Science*. **104:**1328–37.

Wu, H.L., Yang, Y.T., Ma, C.C.M. and Kuan, H.C. 2005. Molecular mobility of freeradical- functionalized carbon-nanotube/siloxane/poly(urea urethane) nanocomposites. *J Polymer Science Part A Polymer Chemistry*. **43:** 6084–6094.

Wu, Z., Zhou, C., Qi, R. and Zhang, H. 2002. Synthesis and characterization of nylon 1012/clay nanocomposite. *J Applied Polymer Science*. **83:**2403–2410.

Xia, H. S., Wang, Q. and Qiu, G. H. 2003. Polymer-encapsulated carbon nanotubes prepared through ultrasonically initiated in situ emulsion polymerization. *Chemistry of Materials*. **15(20):** 3879-3886.

Xie, H., Liu, B., Yuan, Z., Shen, J. and Cheng, R. 2004. Cure kinetics of carbon nanotube/tetrafunctional epoxy nanocomposites by isothermal differential scanning calorimetry. *J Polymer Science Polymer Physics*. **42:** 3701–3712.

Xu, Y., Gao, C., Kong, H., Yan, D., Jin, Y. Z. and Watts, P. C. P. 2004. Growing Multi hydroxyl Hyperbranched Polymers on the Surfaces of Carbon Nanotubes by in Situ Ring-Opening Polymerization. *Macromolecules.* **37:** 8846-8853.

Yang, B.X., Shi, J.H., Pramoda, K.P. and Goh, S.H. 2007. Enhancement of stiffness, strength, ductility and toughness of poly(ethylene oxide) using phenoxy-grafted multiwalled carbon nanotubes. *Nanotechnology*. **18:**125606–7.

Yang, Y.S. and Lee L. J. 1988. Microstructure formation in the cure of unsaturated polyester resins. *Polymer*. **29:**1793–1800.

Yu, J., Grossiord, N., Koning, C.E., Loos, J. 2007. Controlling the dispersion of multi-wall carbon nanotubes in aqueous surfactant solution. *Carbon*. **45(3):** 618–623.

Yu, M.F., Lourie, O., Dyer, M.J., Moloni, K., Kelly, T.F., Ruoff, R.S. 2000. Strength and breaking mechanism of multiwalled carbon nanotubes under tensile load. *Science*. **287:** 637–640.

Zeng J., Saltysiak B., Johnson W.S., Schiraldi D.A. and Kumar S. 2004. Processing and properties of poly(methyl methacrylate)/carbon nanofiber composites. *Compos Part B*. **35:**173–8.

Zhang J., Wang X., Ma J., Liu S. and Yi, X. 2013. Preparation of cobalt hydroxide nanosheets on carbon nanotubes/carbon paper conductive substrate for supercapacitor application. *Electrochimical Acta*. **104**: 110–116.

Zhu, J., Kim, J.D., Peng, H., Margrave, J.L., Khabashesku, V.N. and Barrera, E.V. 2003. Improving the dispersion and integration od single-walled carbon nanotubes in epoxy composites through functionalization. *Nano Letter*. **3:**1107–13.

APPENDIX A

LIST OF PUBLICATIONS

Journal papers

1. A. K. M. Moshiul Alam, M. D. H. Beg, R.M. Yunus, M. F. Mina, K. H. Maria, T. Mieno, 2016. Evolution of Functionalized Multi-Walled Carbon Nanotubes by Dendritic Polymer Coating and their Anti-Scavenging Behavior during Curing Process, ***Materials Letters*.167:**58–60.

2. A.K. M. Moshiul Alam, M.D.H. Beg, A. R.M. Yunus, 2016. Micro Structure and Fractography of Multiwalled Carbon Nanotube Reinforced Unsaturated Polyester Nanocomposites. ***Polymer Composites***, DOI: 10.1002/pc.23911.

3. M.D.H. Beg, **A. K. M. Moshiul Alam**, R.M. Yunus, M.F. Mina, 2015. Improvement of Interaction between Pre-Dispersed Multi Walled Carbon Nanotubes and Unsaturated Polyester Resin. ***Journal of Nanoparticle Research***, 17(1), 1-13.DOI 10.1007/s11051-014-2846-8.

4. **A.K.M. Moshiul Alam,** M.D.H. Beg, Rosli Mohd. Yunus, 2015. Influence of Carbon Nano Tubes on the Thermo-Mechanical Properties of Unsaturated Polyester Nanocomposite, ***Material Science and Engineering***, 78(1),012023, doi:10.1088/1757-899X/78/1/012023

5. Rosli Mohd Yunus, **A.K.M. Moshiul Alam**, Mohammad Dalour Beg, 2015. Effect of Multi Walled Carbon Nanotubes on Pyrolysis Behavior of Unsaturated Polyester Resin, ***Materials and Metallurgical Engineering***. 2(3),

Conferences

1. Rosli Mohd Yunus, **A.K.M. Moshiul Alam,** Mohammad Dalour Beg, Effect of Multi Walled Carbon Nanotubes on Pyrolysis Behavior of Unsaturated Polyester Resin,

ICNMN 2015: 17th International Conference on Nanostructured Materials and Nanotechnology,, Miami, USA, March 9-10, 2015.

2. **A.K.M. Moshiul Alam,** M.D.H. Beg, Rosli Mohd. Yunus Influence of Carbon Nano Tubes on the Thermo-Mechanical Properties of Unsaturated Polyester Nanocomposite, 9th CUTSE 2014, Curtin University Sarawak, Malaysia, December 3 – 4, 2014

3. **A.K.M. Moshiul Alam,** M.D.H. Beg, Rosli Mohd. Yunus, Effect of solvent dispersion on the mechanical and thermal properties of multi walled carbon nanotubes-reinforced unsaturated polyester nanocomposite, Composites Australia and CRC-ACS, April7-9, 2014, Newcastle, Australia.

Materials Letters 167 (2016) 58–60

Contents lists available at ScienceDirect

Materials Letters

journal homepage: www.elsevier.com/locate/matlet

Evolution of functionalized multi-walled carbon nanotubes by dendritic polymer coating and their anti-scavenging behavior during curing process

A.K.M. Moshiul Alam [a,*], M.D.H. Beg [a,*], R.M. Yunus [a], M.F. Mina [b], K.H. Maria [c], T. Mieno [c]

[a] Chemical and Natural Resources Engineering, Universiti Malaysia Pahang, Gambang 26300, Kuantan, Malaysia
[b] Department of Physics, Bangladesh University of Engineering and Technology, Dhaka 1000, Bangladesh
[c] Graduate School of Science and Technology, Shizuoka University, Shizuoka 422, Japan

ARTICLE INFO

Article history:
Received 2 September 2015
Received in revised form
4 November 2015
Accepted 27 December 2015
Available online 30 December 2015

Keywords:
Carbon nanotube
Nanocomposite
Raman
Thermal analysis

ABSTRACT

Improvement of curing performance of unsaturated polyester (UPR) by multi-walled carbon nanotubes (MWCNT) is essential for industrial application of MWCNT reinforced UPR nanocomposites. For this purpose, hyper branched polyester coated MWCNT (HBPCNT) has been prepared by solvent evaporation technique, and HBPCNT loaded UPR nanosuspension has been cured and investigated with differential scanning calorimetric method. Structures and morphologies of pristine MWCNTs and HPBCNTs have also been investigated. Significant differences in the natures of these two types of CNTs are observed. HBPCNT remarkably reduces the curing temperature by 11 °C during crosslinking in HBPCNT-UPR nano-suspension, thereby acting as a potential anti-scavenger for curing process.

1. Introduction

Nowadays, carbon nanotubes (CNTs) is much attracted by researchers because of its robust mechanical and electrical properties, which make them to be used as an ideal reinforcing agent in polymer nanocomposites. Despite their outstanding properties, CNTs hold some drawbacks, which abstain from their potential use in composite fabrication. The main drawbacks are their poor dispersion and compatibility with polymer matrices. It is noteworthy that when polymeric nanocomposites are prepared from casting approach, the curing process delays due to free radical scavenging nature of carbon nano filler [1]. Other notable drawbacks of CNTs are that they are aggregated into bundles and ropes through van der Waals force, stabilized by numerous π–π interactions and entangled with each other due to their high aspect ratio [2]. If each CNT cannot be separated from the bundles, their remarkable properties cannot be fully exploited. To materialize them as potential reinforcing fillers for composites, extensive effort is required to break the bundles to obtain individual CNT.

Destructive and nondestructive techniques are employed to split the CNT bunches. Of these, nondestructive technique, such as non-covalent functionalization, attracts much attention to modify the nanotube side wall without any defect [3]. This type of modification can be carried out with those polymers that contain functional end groups. For instance, multi-hydroxyls hyper-branched polyesters (HBP) are highly branched macromolecules with three-dimensional dendritic architecture, containing huge functional hydroxyl end groups [4]. Because of their high solubility, and abundance of functional groups, HBP have potential applications in wide range of fields from drug delivery to material coatings. Besides, the large number of reactive end-groups of a hyper-branched polymer are capable for rapid cross-linking and are thus potential to design thermosetting network [5]. Considering these advantages, the present work is designed to coat multi-walled CNT (MWCNT) by HBP. This work reports a novel coating approach of MWCNTs through solvent evaporation that act as anti-scavengers during curing process.

2. Materials and methods

MWCNTs having diameters 10–24 nm, lengths 10–30 μm, and numbers of walls 6–15 were collected from Timesnano, China. 2-2-bis (methylol) propionic acid as hyper branched polyester (HBP), generation 2, and methyl ethyl keton peroxide (MEKP) were purchased from Sigma-Aldrich. Orthophthalic unsaturated polyester resin (UPR) was used as received from Luxchem Polymer Industries Sdn. Bhd., Malaysia.

HBP coated MWCNTs (HBPCNT) was prepared by 2:1 (w/w)

* Corresponding authors.
E-mail addresses: alam.alam@yahoo.com (A.K.M.M. Alam), dibeg@yahoo.com (M.D.H. Beg).

http://dx.doi.org/10.1016/j.matlet.2015.12.139
0167-577X/

Micro Structure and Fractography of Multiwalled Carbon Nanotube Reinforced Unsaturated Polyester Nanocomposites

A.K.M. Moshiul Alam, M.D.H. Beg, R.M. Yunus
Faculty of Chemical and Natural Resources Engineering, Universiti Malaysia Pahang, Malaysia

In this study unsaturated polyester resin (UPR) was reinforced with different concentration of pre-dispersed multiwalled carbon nanotube (MWCNT). The rheology, structural analysis, fracture behavior, morphology, and thermal analysis of nanocomposites were carried out as a function of MWCNT content. Shear thinning behavior exhibited distinguishable dispersion quality of 0.3 wt% MWCNT in UPR matrix. Structural analysis reveals that MWCNT enhanced the nucleation of nanocomposites. The crystallinity of nanocomposites was increased by 71% after incorporation of 0.3 wt% MWCNT. Bending strength (BS) and bending modulus (BM) of nanocomposites were increased as well as 0.3 wt% MWCNT exhibited crack shielding in nanocomposites. The glass transition (T_g) and melting transition (T_m) of nanocomposites was increased by 6°C and 10°C respectively as compare to neat UPR. Additionally thermal stability of 0.3 wt% MWCNT incorporated nanocomposites was significantly improved as compare to UPR and nanocomposites which contained 0.1 and 0.5 wt% MWCNT. POLYM. COMPOS., 00:000–000, 2016. © 2016 Society of Plastics Engineers

INTRODUCTION

Unsaturated polyesters (UPR) are widely used for industrial and consumer applications. They are available and cost effective; in addition they are cured in a variety of ways without altering the physical properties of the finished product. They are utilized as non-reinforcing or reinforcing composite materials. UPR are usually used for boats, cars, and shower stalls, building panels, and corrosion-resistant tanks, pipes and so on. Consequently, the UPR compete favorably in traditional markets. However, they have some limitations for engineering application due to their weak thermo-mechanical properties, especially, the brittleness of this resin is not acceptable for any sort of indoor and outdoor applications [1–3]. Therefore to overcome these drawbacks different type fillers are incorporated in this matrix to fabricate reinforced composites [4, 5].

Fillers are usually incorporated in polymer matrix to alter polymer properties and frequently improve their performance [6]. Different types of fillers are available to reinforce UPR, for instance, natural fiber, synthetic fiber, organic and inorganic particles etc. were used elsewhere [7–11]. The reinforcing efficiency of those fillers is defeated by nanofillers. Incorporation of nano-sized fillers, in polymers is generally referred to as nanocomposites. Nanocomposites have attracted great interest due to their wide possible range of applications and commercial opportunities [12].Nano filler not only improve the mechanical properties but also restrained the deterioration of outdoor application properties and increased the thermal stability. Therefore many researchers have been highlighted on inclusion of different nanoparticles in several thermoset resins [13, 14].

Carbon nanotubes (CNTs) have drawn much attention due to a combination of distinctive properties, for instance high strength, stiffness, flexibility, in addition to high electrical and thermal conductivity. These properties attract researchers to fabricate CNT reinforced nanomaterials for different applications [15]. To date in the area of nanotechnology, researches are emphasizing on incorporation of CNTs in polymer matrix to fabricate smart nanocomposites for advance applications. Single, double and multiwalled carbon nanotubes (MWCNT) are independently used for reinforcing polymer matrix. Additionally, enhancement of nanocomposites properties is a function of CNT content, CNT dispersion and interaction between CNT and matrix [16, 17]. Adequate amount of MWCNT is an outstanding reinforcing agent for resolving the brittleness of thermoset polymers [18, 19]. Yadav et al. stated that the stiffness of hyper branched polyurethane nanocomposites' was improved with different amount of MWCNT. They reported that homogeneous dispersion of MWCNT in addition to well interaction with matrix restricted their chain movement, as a result decreased breaking strain of that material [20]. Besides, MWCNT

Correspondence to: A.K.M. Moshiul Alam; e-mail: almoshiul@gmail.com or M.D.H. Beg; e-mail: dhbeg@yahoo.com
DOI 10.1002/pc.23911
Published online in Wiley Online Library (wileyonlinelibrary.com).

J Nanopart Res (2015) 17:53
DOI 10.1007/s11051-014-2846-8

RESEARCH PAPER

Improvement of interaction between pre-dispersed multi-walled carbon nanotubes and unsaturated polyester resin

M. D. H. Beg · A. K. M. Moshiul Alam · R. M. Yunus · M. F. Mina

Received: 31 July 2014 / Accepted: 23 December 2014 / Published online: 22 January 2015

Abstract Efforts are being given to the development of well-dispersed nanoparticle-reinforced polymer nanocomposites in order to tailor the material properties. In this perspective, well dispersion of multi-walled carbon nanotubes (MWCNTs) in unsaturated polyester resin (UPR) was prepared using pre-dispersed MWCNTs in tetrahydrofuran solvent with ultrasonication method. Then the well-dispersed MWCNTs reinforced UPR nanocomposites were fabricated through solvent evaporation. Fourier-transform infrared spectroscopy indicates a good interaction between matrix and MWCNTs. This along with improvement in the crystallinity of UPR from 14 to 21 % after MWCNTs inclusion was observed by X-ray diffractometry. The mechanical properties, such as tensile strength, tensile modulus, impact strength, and elongation-at-break, of nanocomposite were found to be increased to 22, 20, 28, and 87 %, respectively. The estimated melting enthalpy per gram for composites as analyzed by differential scanning calorimetry is higher than that of UPR. The onset temperature of thermal decomposition in the nanocomposites as monitored by thermogravimetric analysis is found higher than that of UPR. Correlations among MWCNTs dispersion,

Influence of Carbon Nano Tubes on the Thermo-Mechanical Properties of Unsaturated Polyester Nanocomposite

A K M Moshiul Alam, M D H Beg, Rosli Mohd Yunus

Faculty of Chemical and natural Resources Engineering, University Malaysia Pahang, 26300, Gambang, Kuantan, Pahang, Malaysia

akmmalam@gmail.com

Abstract. To date nano fillers are renowned reinforcing agent for polymer materials. In this work, unsaturated polyester (UPR) nanocomposites were fabricated by 0.1, 0.3 and 0.5 wt% multi walled carbon nanotubes (MWCNTs) through solution dispersion and casting method. The influence of MWCNT content was investigated by thermo-mechanical properties. Dispersion of nanotubes was observed by fracture morphology. The strength of nanocomposites rose with raising the CNT content. Moreover, DSC thermograms of nanocomposites represent noticeable improvement of glass transition temperature (T_g), melting temperature (T_m) and enthalpy (ΔH_m). Micro-crystallinity of nanocomposites increased with increasing the CNT content. Moreover, the stiffness increased with increasing the CNT content.

Key word: Solvent dispersion, Nanocomposites, Characterization

1. Introduction

The unsaturated polyester resins (UPRs) are common thermosetting resins and steadily increasing their applications for several purposes because of their sound properties, cost effectiveness as well as simple handling. However, cross-linked UPRs have limited structural reliability, therefore , before cross-linking they are often mixed with reinforcing materials such as natural fibers, synthetic fibers, nanofillers as well as mineral fillers and so on [1,2,3,4] . The reinforced composites are devoted for construction, marine and automotive industries due to their light weight and durability.

The carbon nanotubes (CNTs) are more attractive fillers in the vicinity of polymer composites because of their outstanding properties therefore they are substitute of conventional macro and micro fillers [5,6,7]. CNTs are geometrically distinctive to their surface area, provide an immense resources of interaction with any continuous phase giving rise to great opportunity for effective load transfer [8].Moreover, small amount of CNT with efficient dispersion in matrix exhibit considerable enhancement of different properties [9].The significant improvement of properties are determined by the degree of CNTs dispersion and interfacial adhesion into the composite system [10]. Conversely, several phenomena restrict carbon nanotube dispersions, such as nanotube morphology and Van der Waal's forces between nanotube surfaces. Not only that but also the high aspect ratios together with the high flexibilities noticeably increase the possibilities for entanglements. These entangled aggregates are very complicated to separate into individual nanotubes [11].The interaction of CNTs reveal high potential energy which naturally making them more difficult to separate as individuals nanotubes [12,13].Therefore, different physical and chemical methods are demonstrated for control dispersion of individual nano tubes in matrix. Physical methods consider for direct mixing through mechanical force. Chemical methods are carried out by surfactants action, functionalization of carbon nanotube surface modification and polymer wrapping technology [14,15]. For instance studies

World Academy of Science, Engineering and Technology
International Journal of Materials and Metallurgical Engineering Vol:2, No:3, 2015

Effect of Multi Walled Carbon Nanotubes on Pyrolysis Behavior of Unsaturated Polyester Resin

Authors : Rosli Mohd Yunus, A. K. M. Moshiul Alam, Mohammad Dalour Beg

Abstract : In the case of advance polymeric materials reinforcement and thermal stability of matrix is a focused arena of researchers. The distribution of carbon nanotubes (CNTs) in polymer matrix influences material properties. In this study, multi-walled carbon nanotubes (MWCNTs) have been dispersed in unsaturated polyester resin (UPR) through solution mixing and sonication techniques using tetra hydro furan (THF) solvent. Nanocomposites have been fabricated with solution mixing and without solution mixing. Viscosity, Fourier-transform infrared spectroscopy, Field emission scanning electron microscopy (FESEM) investigations have been conducted to study the distribution as well as interaction between matrix and MWCNT. The differential scanning calorimetry (DSC), thermogravimetric analyses (TGA) and pyrolysis behavior have been conducted to study the thermal degradation and stability of nanocomposites. In addition, the SEM micrographs of nanocomposite residual chars were exhibited more packed together. Incorporation of CNT enhances crystallinity and mechanical and thermal properties of the nanocomposites. Correlations among MWCNTs dispersion, nucleation, fracture morphology and various properties have been made.

Keywords : char, multiwall carbon nanotubes, nano composite, pyrolysis
Conference Title : ICNMN 2015 : 17th International Conference on Nanostructured Materials and Nanotechnology
Conference Location : Miami, USA
Conference Dates : March 09-10, 2015